1995-09

Strut and wall interference on jet-induced ground effects of a STOVL aircraft in hover

Kristy, Michael H.

Monterey, California. Naval Postgraduate School

NAVAL POSTGRADUATE SCHOOL
MONTEREY, CALIFORNIA

THESIS

STRUT AND WALL INTERFERENCE ON JET-INDUCED GROUND EFFECTS OF A STOVL AIRCRAFT IN HOVER

by

Michael H. Kristy

September 1995

Thesis Advisor: S.K. Hebbar

Approved for public release; distribution is unlimited

REPORT DOCUMENTATION PAGE

Form Approved OMB Np. 0704-0188

1. AGENCY USE ONLY *(Leave blank)*	2. REPORT DATE **September 1995**	3. REPORT TYPE AND DATES COVERED Master's Thesis

4. TITLE AND SUBTITLE STRUT AND WALL INTERFERENCE ON JET-INDUCED GROUND EFFECTS OF A STOVL AIRCRAFT IN HOVER

5. FUNDING NUMBERS

6. AUTHOR(S) Kristy, Michael H.

7. PERFORMING ORGANIZATION NAME(S) AND ADDRESS(ES)
Naval Postgraduate School
Monterey CA 93943-5000

8. PERFORMING ORGANIZATION REPORT NUMBER

9. SPONSORING/MONITORING AGENCY NAME(S) AND ADDRESS(ES)

10. SPONSORING/MONITORING AGENCY REPORT NUMBER

11. SUPPLEMENTARY NOTES The views expressed in this thesis are those of the author and do not reflect the official policy or position of the Department of Defense or the U.S. Government.

12a. DISTRIBUTION/AVAILABILITY STATEMENT
Approved for public release; distribution is unlimited.

12b. DISTRIBUTION CODE

13. ABSTRACT *(maximum 200 words)*

A small scale ground effect test rig was used to study the ground plane flow field generated by a STOVL aircraft in hover. The objective of the research was to support NASA-Ames Research Center planning for the Large Scale Powered Model (LSPM) test for the ARPA-sponsored ASTOVL program. Specifically, small scale oil flow visualization studies were conducted to make a relative assessment of the aerodynamic interference of a proposed strut configuration and a wall configuration on the ground plane stagnation line. A simplified flat plate model representative of a generic jet-powered STOVL aircraft was used to simulate the LSPM. Cold air jets were used to simulate both the lift fan and the twin rear engines. Nozzle Pressure Ratios were used that closely represented those used on the LSPM tests. The flow visualization data clearly identified a shift in the stagnation line location for both the strut and the wall configuration. Considering the experimental uncertainty, it was concluded that either the strut configuration or the wall configuration caused only a minor aerodynamic interference.

14. SUBJECT TERMS STOVL Configuration in Hover, CALF Program, Jet-Induced Ground Effects, Ground-Plane Flow, Stagnation Streamline, Oil Flow Visualization, Strut and Wall Interference

15. NUMBER OF PAGES 93

16. PRICE CODE

17. SECURITY CLASSIFICATION OF REPORT	18. SECURITY CLASSIFICATION OF THIS PAGE	19. SECURITY CLASSIFICATION OF ABSTRACT	20. LIMITATION OF ABSTRACT
Unclassified	Unclassified	Unclassified	UL

NSN 7540-01-280-5500 Standard Form 298 (Rev. 2-89)
Prescribed by ANSI Std. 239-18

Approved for public release; distribution is unlimited.

STRUT AND WALL INTERFERENCE ON JET-INDUCED GROUND EFFECTS OF A STOVL AIRCRAFT IN HOVER

Michael H. Kristy
Lieutenant, United States Naval Reserves
B.S.A.A.E., University of Illinois, 1987

Submitted in partial fulfillment
of the requirements for the degree

MASTER OF SCIENCE IN AERONAUTICAL ENGINEERING

from the

NAVAL POSTGRADUATE SCHOOL

September 1995

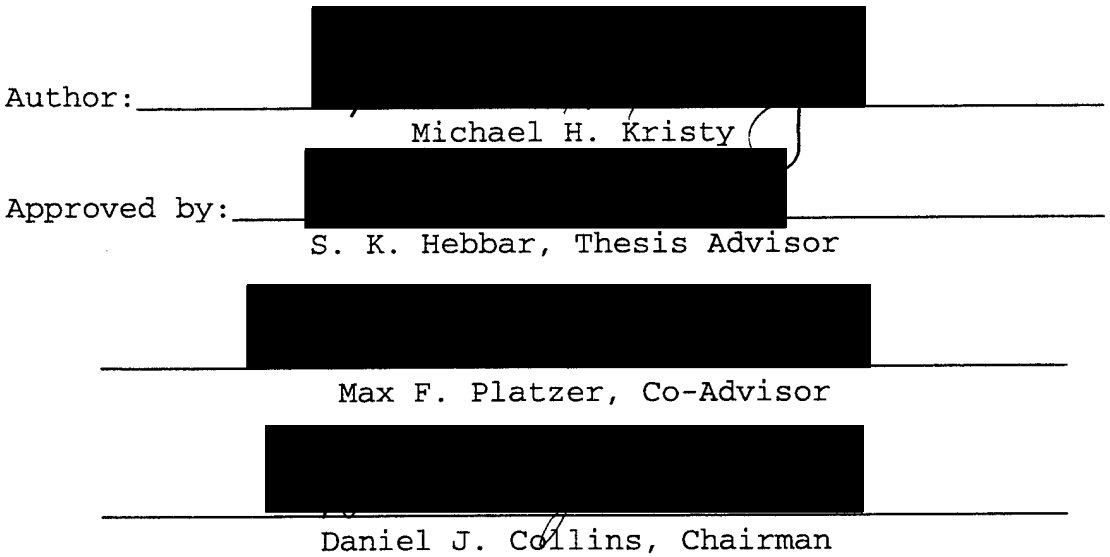

ABSTRACT

A small scale ground effect test rig was used to study the ground plane flow field generated by a STOVL aircraft in hover. The objective of the research was to support NASA-Ames Research Center planning for the Large Scale Powered Model (LSPM) test for the ARPA-sponsored ASTOVL program. Specifically, small scale oil flow visualization studies were conducted to make a relative assessment of the aerodynamic interference of a proposed strut configuration and a wall configuration on the ground plane stagnation line. A simplified flat plate model representative of a generic jet-powered STOVL aircraft was used to simulate the LSPM. Cold air jets were used to simulate both the lift fan and the twin rear engines. Nozzle Pressure Ratios were used that closely represented those used on the LSPM tests. The flow visualization data clearly identified a shift in the stagnation line location for both the strut and the wall configuration. Considering the experimental uncertainty, it was concluded that either the strut configuration or the wall configuration caused only a minor aerodynamic interference.

TABLE OF CONTENTS

ACKNOWLEDGMENT

This thesis was funded by NASA Ames Research Center in support of the ongoing, ARPA sponsored, Common Affordable Lightweight Fighter Program. The NASA support in the form of hardware and technical assistance is greatly acknowledged. In particular, the technical assistance by Rich Margason was instrumental to the successful completion of this study.

My deeper gratitude is extended to Professor S. K. Hebbar for his continuing guidance, persistent help, and unending patience. I would also wish to extend my appreciation to Professor M. F. Platzer for his direction and assistance

A very hearty acknowledgment goes out to Mr. Rick Still and Mr. Thaddeus Best. Without their day to day help and keen insight in solving problems, this undertaking could not have been completed. Thanks also goes out to Mr. Pat Hickey, Mr. Don Harvey, and Mr. Ron Ramaker for their help in the design and fabrication of the precision tooled nozzles and test models.

My absolute greatest appreciation goes out to my Ursula and my family for being so patient and understanding.

I. INTRODUCTION

A. BACKGROUND

For the past few years, the Department of Defense (DoD) has been investigating the possibility of providing the next generation of air superiority fighter with a Short Take-Off and Vertical Landing (STOVL) capability. These studies have led to the formulation and funding of the Advanced Short Take-Off and Vertical Landing (ASTOVL) aircraft program. Therefore, the Advanced Research Project Agency (ARPA) has invited the Lockheed Advanced Development Company (LADC), McDonnell Douglas Company (MD), The Boeing Company, and Northrop-Grumman (NG) corporation to submit design proposals [Ref. 1]. In March 1993, contracts were awarded to LADC and MD for the technology validation phase. Boeing and NG are also participating in the technology validation phase.

NASA Ames will test the Large Scale Powered Models (LSPM) in their 80' x 120' wind tunnel for the forward flight phase and the hover phase of the flight. Additional hover tests will be conducted at NASA's Outdoor Aerodynamic Research Facility (OARF). The prototype will be supported by struts to allow testing of the ground effects of the ASTOVL in hover. The placement of the struts is of great importance. It is desired to place the struts where they will not interfere with the flow of the test model in hover.

A small scale visualization of the flow field on the ground plane can give a quick, qualitative comparison of the model flowfield with the struts and without the struts. These data can confirm a favorable placement of the struts to minimize the aerodynamic interference.

NASA is considering the construction of walls to partially enclose the OARF for noise abatement reasons. Economy dictates that a smaller wall closer to the model test area will reduce costs. No money is saved if the wall interferes with the test and produces questionable data. It is reasonable to expect that obstructions such as the wall will have

no effect if placed far enough from the test model. Testing conducted using a small-scale flow visualization test rig can yield data to determine how close the wall can be placed to the LSPM so it does not interfere with the ground plane flow field.

B. JET-INDUCED GROUND EFFECTS

As discussed, for example, by Platzer and Margason [Ref. 2], depending on the height of the aircraft above the ground, the aircraft will produce a fountain effect that can increase the net lift of the aircraft or produce an entrainment of air that can lead to a suckdown effect reducing the net lift on the aircraft. Therefore, unlike conventional aircraft, the STOVL aircraft can actually lose lift due to the ground effects.

The ground effects for a STOVL aircraft can be seen in Figure 1. The main component of lift is provided by the exhaust of the front and rear nozzles. The fountain effect is produced when the impinging exhausts of the two engines interact on the ground

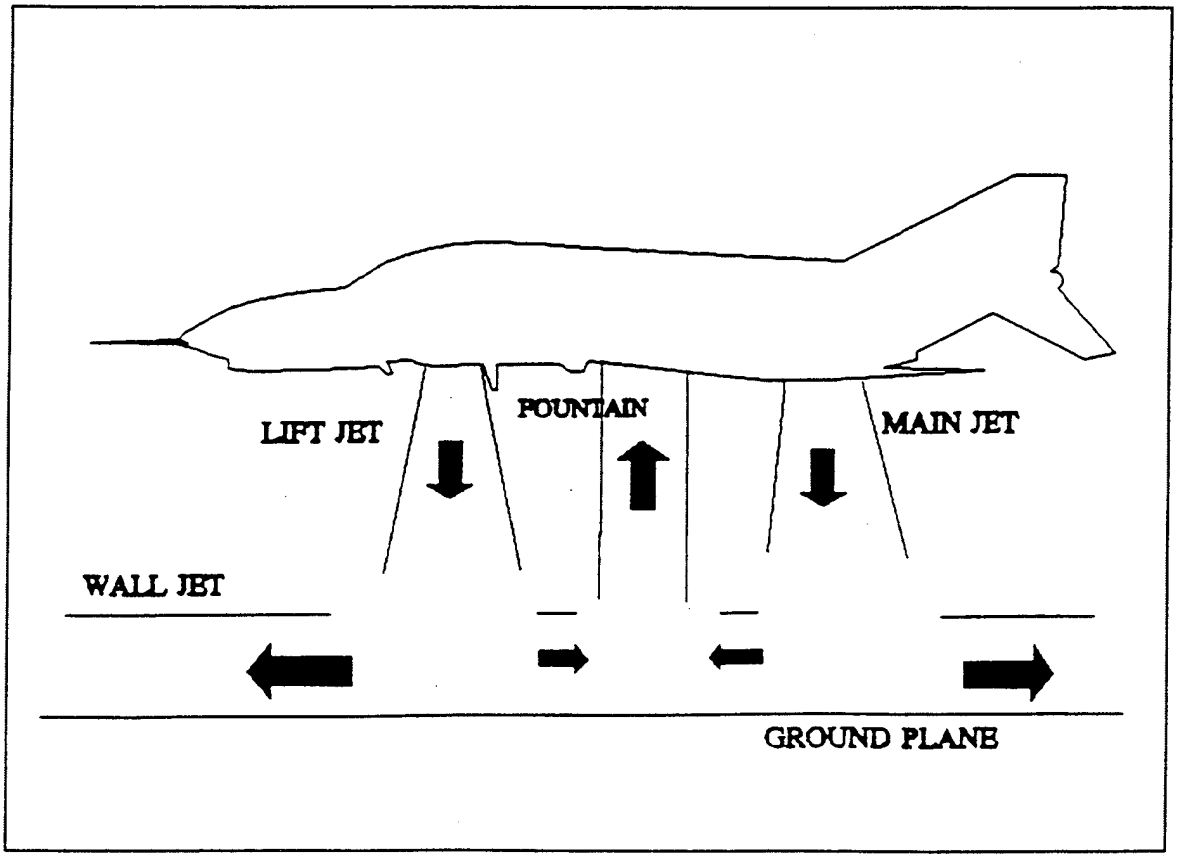

Figure 1 Flow Field for STOVL Aircraft Hovering in Ground Effect

and the resulting flow is diverted up, causing additional lift on the aircraft. A reduction in lift is produced when the airflow is entrained by the exhaust jets inducing air flow on the bottom of the wing and aircraft. The fountain effect is more prevalent at the higher heights of hover and the suckdown is more prevalent at the lower heights. It is important to determine at all heights if there is any interference from the struts that could change the fountain effect or the suckdown effect on the test model. The effect of the wall on the ground-plane flow field must also be determined prior to the construction of the wall for any testing at the OARF.

C. SCOPE OF THESIS

The aim of this thesis is to support NASA Ames Research Center's planning for LSPM hover tests for the ARPA sponsored Common Affordable Lightweight Fighter (CALF) program. Specifically, it was aimed at conducting small-scale flow visualization studies in the Naval Postgraduate School (NPS) Monterey, CA ground-effect test rig on a simplified flat-plate configuration representative of a generic jet-powered STOVL aircraft in hover. The support-strut and wall interference on jet-induced ground effects was determined by the oil-flow technique on the ground-plane.

The general procedure followed here consists of comparing the ground-flow oil pattern and stagnation line produced by the model without the walls and the struts (baseline model) to those produced by the model with the struts and those with the struts and walls. The strut location was chosen based on the proposed strut location for the NASA Ames OARF tests. The wall location was chosen primarily because of the dimension of the ground-effect test rig. This distance was very close to the closest proposed wall location at the OARF A total of seven ground-plane heights and three nozzle thrust ratios were used to cover the anticipated operating conditions in the OARF.

II. EXPERIMENTAL APPARATUS

A. MODEL

1. Scaling

The major consideration for the model sizing was the relative size of the model's nozzles to the LSPM's nozzles [Ref. 3]. An effective diameter was computed from the exit area of the forward nozzle of the LSPM. The forward nozzle of the model has a diameter of one inch and the scaling factor was determined from the ratio of the effective diameter to the model's forward nozzle diameter. From that ratio, each of the two rear nozzles of the model was determined to be 0.39 inches in diameter. The model and nozzle configurations are shown in Figure 2. An appropriately scaled generic model was installed with the nozzle setup.

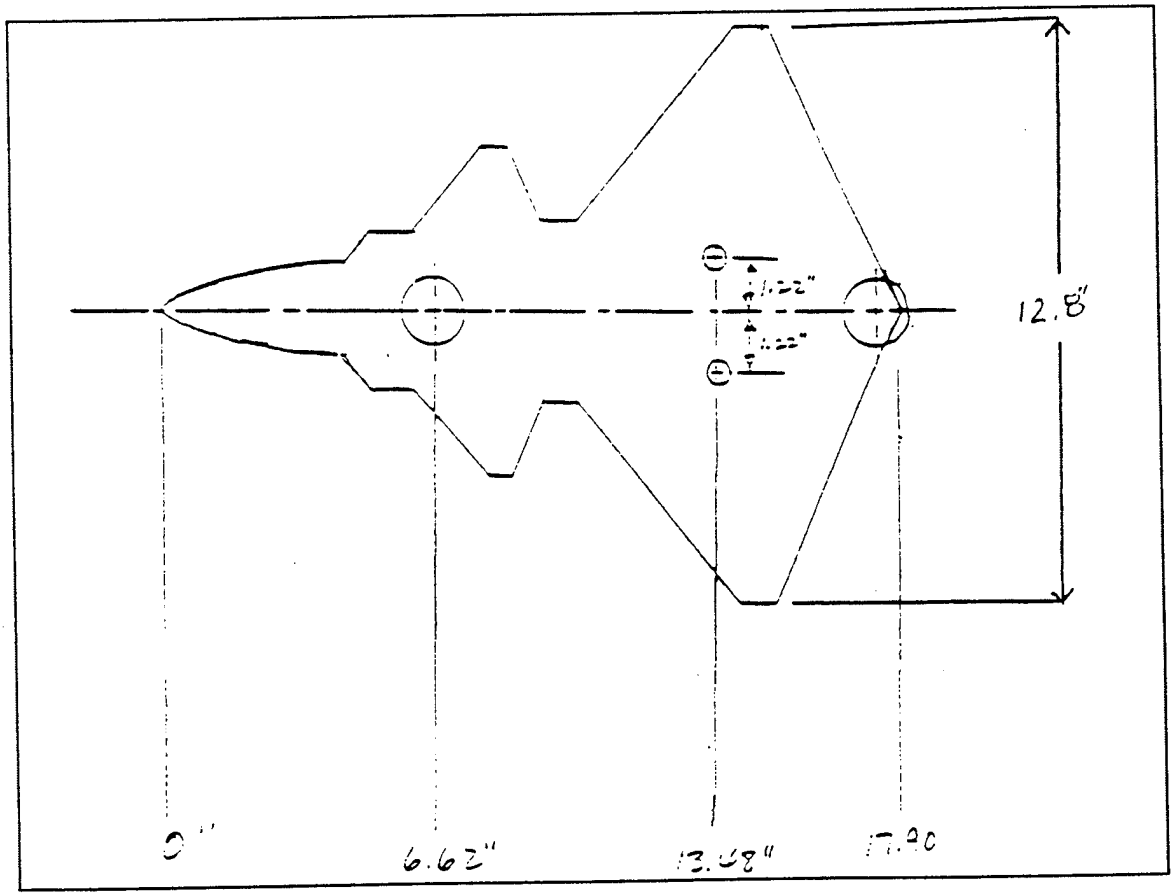

Figure 2 Nozzle and Model Configuration

2. Nozzles

The nozzles used were a simple converging passage fit flush to the model. The diameters were chosen to represent the exit area for the given scaling factor. The nozzles were fitted to the scale model at the appropriate distance corresponding to the scaling factor and attached to the two-inch feed pipes that supplied the high-pressure air. An access was provided at the entrance of each nozzle configuration to mount a pitot tube for pressure measurement. The nozzle designs are shown in Figure 3.

3. Model Construction

A generic model was used for the aircraft model to avoid any proprietary design information. The model design can be seen in Figure 2. Because the nozzle sizing determines the overall size of the model and LADC and MD used two different nozzle sizes, the models were similar in shape but different in size. The model was constructed from Plexiglas with flat edges. It was determined that the flat edges would have little effect on the ground plane flow [Ref. 3].

B. SUPPLY AIR AND TEST RIG

The air was supplied by the existing facilities at the Naval Postgraduate School Gas Dynamics Laboratory. The supply air provided up to 300 psi of air. The tests were carried out in the NPS ground-effect test rig used in the previous investigation [Ref. 4]. Two modifications were required to the test rig for this study: installing the new nozzle sizes on the feed pipes and fitting the new model to the nozzles.

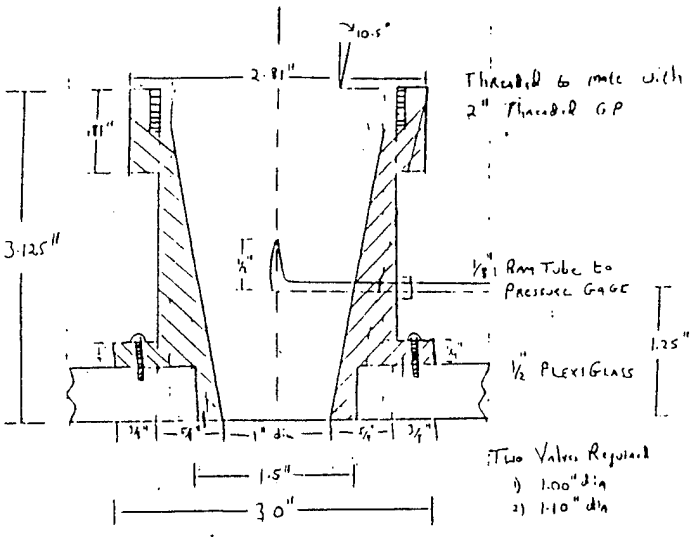

Front

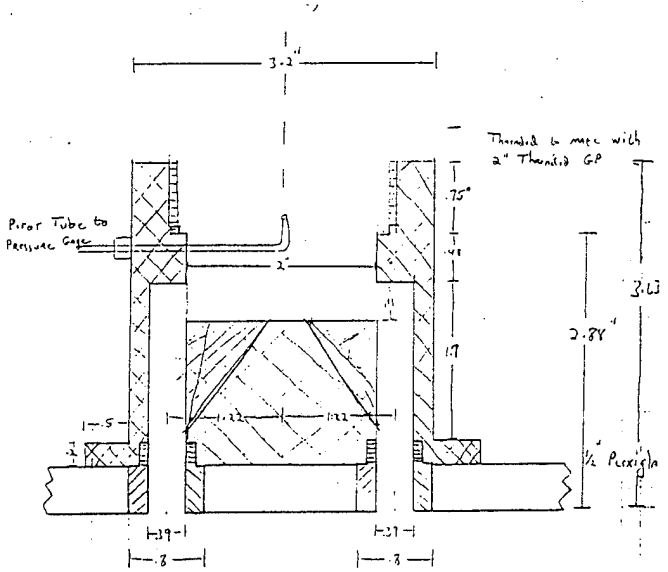

Aft

Figure 3 0.39" and 1" Nozzle Design

C. GROUND PLANE

1. Surface Platform

The 46-inch square wooden frame used in the previous investigation was adequate for the current experiment. Since the strut locations for the current model were different, the reverse side of the frame was used with a new sheet of aluminum to accommodate the new strut locations.

2. Lift Mechanism

The aircraft model was not movable and to change the relative height of the model aircraft to the ground plane, the height of the ground-plane was changed. The ground plane was placed on a hydraulic lift to change the relative heights of the ground plane. The existing facility was improved for this study. A new hydraulic lift was purchased to replace the previous hydraulic lift on loan. The new lift is of the same precision as the previous lift and did not increase or decrease the accuracy of the measurements. The ground plane was leveled to the exit nozzle plane.

D. STRUTS

NASA originally was going to construct a crane and support system for the LSPM. This would have an advantage of not interfering with the ground-plane flow. The associated cost and time penalties made the strut configuration a more attractive alternative. The struts in the 80' x 120' wind tunnel could be used in the OARF. The struts are arranged in a triangular configuration with two main mounts and a nose support. A similar configuration was used in the previous study [Ref. 4].

The strut size and placement was scaled for the present model configuration, shown in Figure 4. The struts in this study are wooden dowels. The main struts have a diameter of 1.33 inches with a separation of 26.67 inches. The nose support strut is a

wooden dowel of diameter 1.00 inch with a separation from the main strut centerline of 16.67 inches.

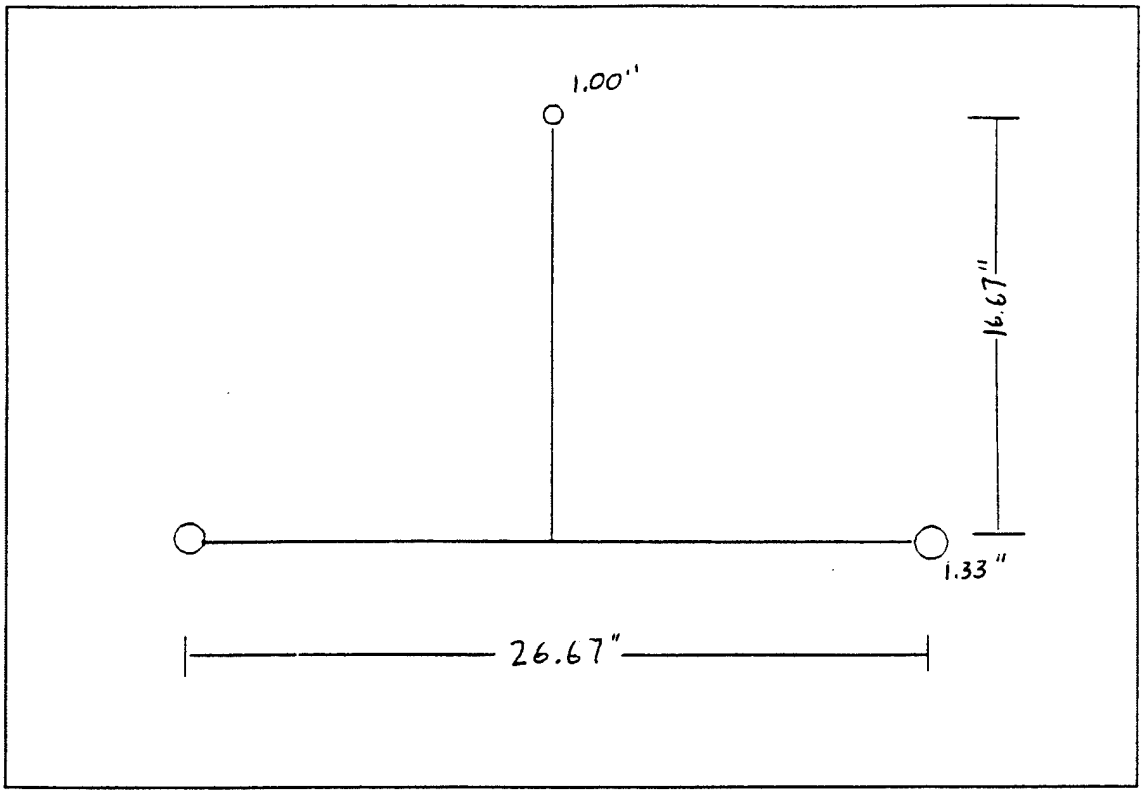

Figure 4 Strut Position Configuration

E. WALLS

The testing of an ASTOVL aircraft in hover is a noisy undertaking. The engines are at or near maximum thrust conditions for long periods of time. Due to safety and environmental concerns NASA is studying the idea of placing noise abatement walls around the OARF. To minimize costs, walls will be placed only on the most critical sides of the OARF. The sides considered for the walls corresponded to the sides of the OARF where the nose and right side of the LSPM will be located (See Figure 5). Further reduction in cost can be realized by placing a smaller wall closer to the OARF. But the placement of the wall cannot be too close or this will interfere with the ground-plane flow.

Of the many wall configurations which were proposed, the configuration with the wall closest to the model was tested because, if any effect would be detected, it would be with this configuration. Wall modeling was accomplished by placing a large piece of one inch plywood adjacent to the left side of the ground-plane test platform. The placement of the wall was on the left side of the model, even though the NASA proposed wall was on the right side of the LSPM. Due to the supply air lines, it was a difficult task to place the wall on the right side of the model. The wall near the nose section was modeled by placing two office dividers adjacent to the ground plane test section. This arrangement allowed the wall to be tested at all the anticipated heights of the LSPM. The walls were chosen to model the proposed noise abatement walls and for ease of assembling the wall configuration.

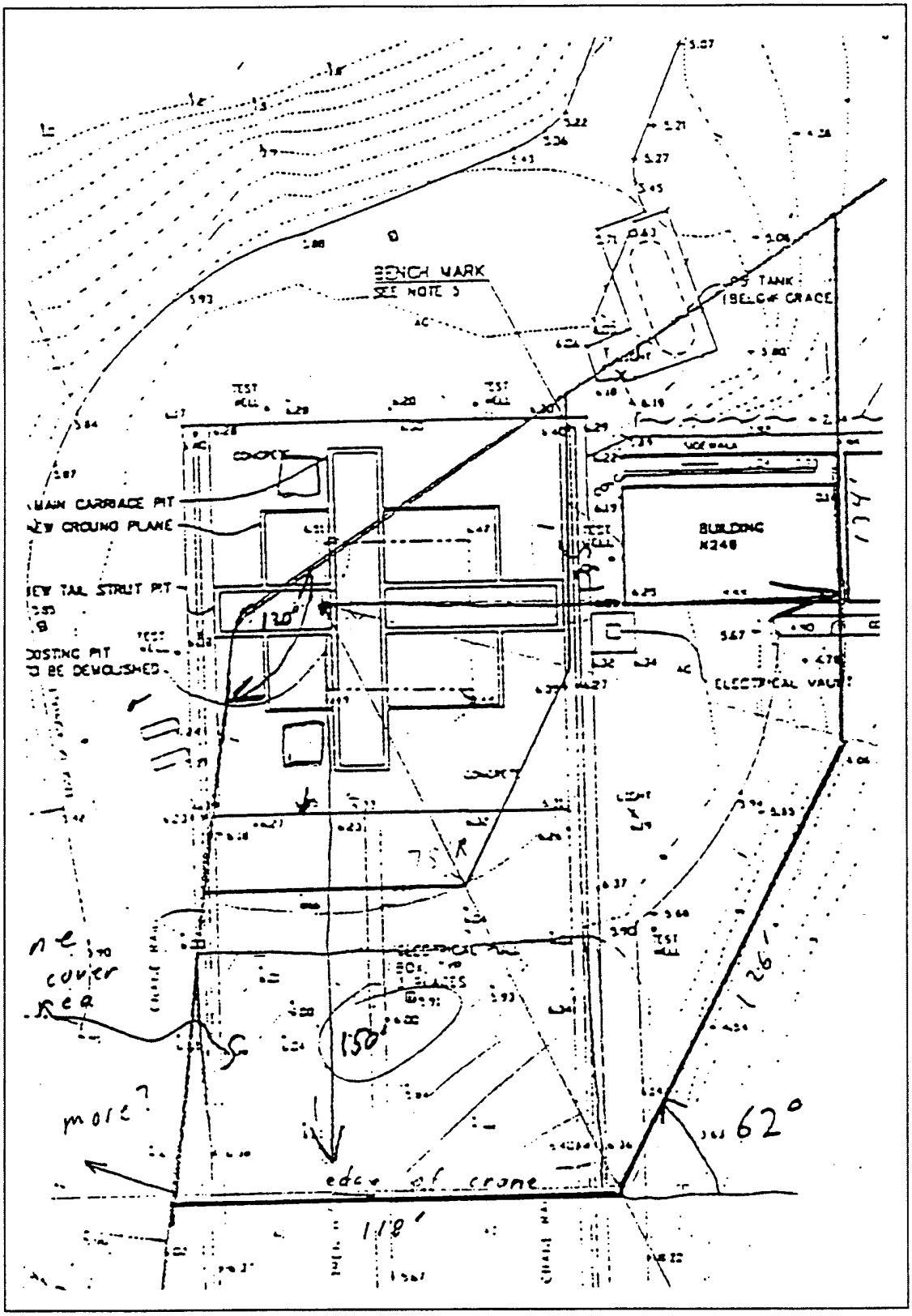

Figure 5 Proposed Wall Configuration at NASA's OARF

III. EXPERIMENTAL PROCEDURE

A. OIL-DOT TECHNIQUE

The general procedure for obtaining the ground-plane oil-flow visualization was to apply the oil to the ground plane using a wooden template, adjust the height of the ground plane, and turn the jets on for approximately five minutes. Photographs and measurements could be taken and the process could be repeated after cleaning the ground plane. For more details see Ref. 4.

1. Composition Of Oil

The composition of the oil was of vital importance for good results. Earlier research [Ref. 4] suggested mixing Pennzoil 10W-40 with STP oil treatment. Some test runs were conducted to confirm that the 5:1 oil to STP mixture was ideal. Measurements and photographs were improved by using color pigments. The amount of pigment added was subjective and not measured. Four colors (rocket red, aurora pink, blaze orange, and saturn yellow) were provided by the Day-Glo Color Corporation of Cleveland, Ohio.

2. Application

The oil-dot technique was chosen over a brush-type application to study the local surface streamline pattern. For consistency and ease of applying the oil dots, a wooden template was constructed. The template consisted of a matrix of 17 x 17 holes with a diameter of 0.25". Additional oil drops could be applied manually when it was deemed necessary.

B. NOZZLE THRUST RATIO

1. Pressure Ratio

Three nozzle thrust ratios (NTR's) were tested during this investigation: 0.92, 1.5, and 4.9. The nozzle thrust ratio is the ratio of the thrust produced from the rear nozzles to the thrust produced from the front nozzle. The thrust ratios were provided by NASA Ames. Using NASA Ames methods [See Appendix A], the nozzle thrust ratios were

converted to nozzle pressure ratios (NPR's) so that pressure gauges could be used to set the proper NTR.

2. Setting The Pressure Ratio

Pressure was controlled by an independent pressure regulator valve attached to each of the feed pipes that were connected to the nozzles. Inside each nozzle was a pitot tube. The pitot tubes were connected to large pressure gauges with a precision of ± 0.5 psi. The atmospheric pressure was obtained every day so the proper NPR's could be set. Once the NPR's were set, periodic checks of the atmospheric pressure and the nozzle pressures were conducted.

C. GROUND-PLANE HEIGHT

1. Specification

The preferred manner of referencing the ground-plane height is to measure the height of the model above the ground plane and divide it by the equivalent diameter of the total exit area (h/De) of the nozzles. The nondimensional heights that were measured in the NPS Ground Effect Test Rig were 1,2,4,6,8,10,15. These were chosen to coincide with the expected test height in the OARF and earlier research.

2. Setting The Height

Before any runs were conducted, the ground plane was leveled by placing shims under the hydraulic lift. Several measurements were taken of the ground plane and the nozzles. These measurements were taken at different heights to ensure they were level as the heights were changed. When the ground plane was adjusted for the proper position of the model in relation to the struts, C-clamps were applied to protect against large movements. Periodic checks to ensure proper alignment were conducted.

D. PHOTOGRAPHY

Photographs were taken of every run to record the flow visualization effects of each run. The camera used was a Minolta 5000i with a 50/1.4 lens. Initially, many

variations of lighting and exposure times were tried. After many different trials it was determined that photos taken in black light with an F-stop of 5.6 and an exposure time of two seconds gave satisfactory results. Black and White ASA 400 film was used.

The camera was mounted on a tripod to capture the entire flow field in the photograph. The tripod was also necessary because of the long exposure time. Two new fluorescent blacklights were purchased to improve the lighting of the flow field. This inexpensive improvement increased the quality of the photographs. One portable blacklight was also used to increase the amount of light.

E. MEASUREMENTS

The primary record of the test results was the photographs. In order to quantify the results for comparison, measurements of the stagnation line were made. The stagnation line is the loci of points where the ground-plane flow velocities from the front and rear nozzles cancel each other, leaving a buildup of oil. Usually this buildup is small allowing for accurate measurements. In an extreme case, a stagnation line of approximately 0.15 inches wide was observed. Determining the exact stagnation line was somewhat subjective, decreasing the precision of the measurement.

Due to the large range of NTR's and heights used, the stagnation line varied in its shape. At some lower heights, a discontinuous line was observed (See Figure 6). These extra areas of interest were recorded. Depending on the pressure ratio and height, the stagnation line was observed to "bend" forward or "bend" backwards. The method used to locate the stagnation line was to measure the distance from the stagnation line to the centerline of the two main mounts. Measurements were taken at three points; the center of the stagnation line, and the two points of the stagnation line that coincided with the wingtip extensions (See Figure 6).

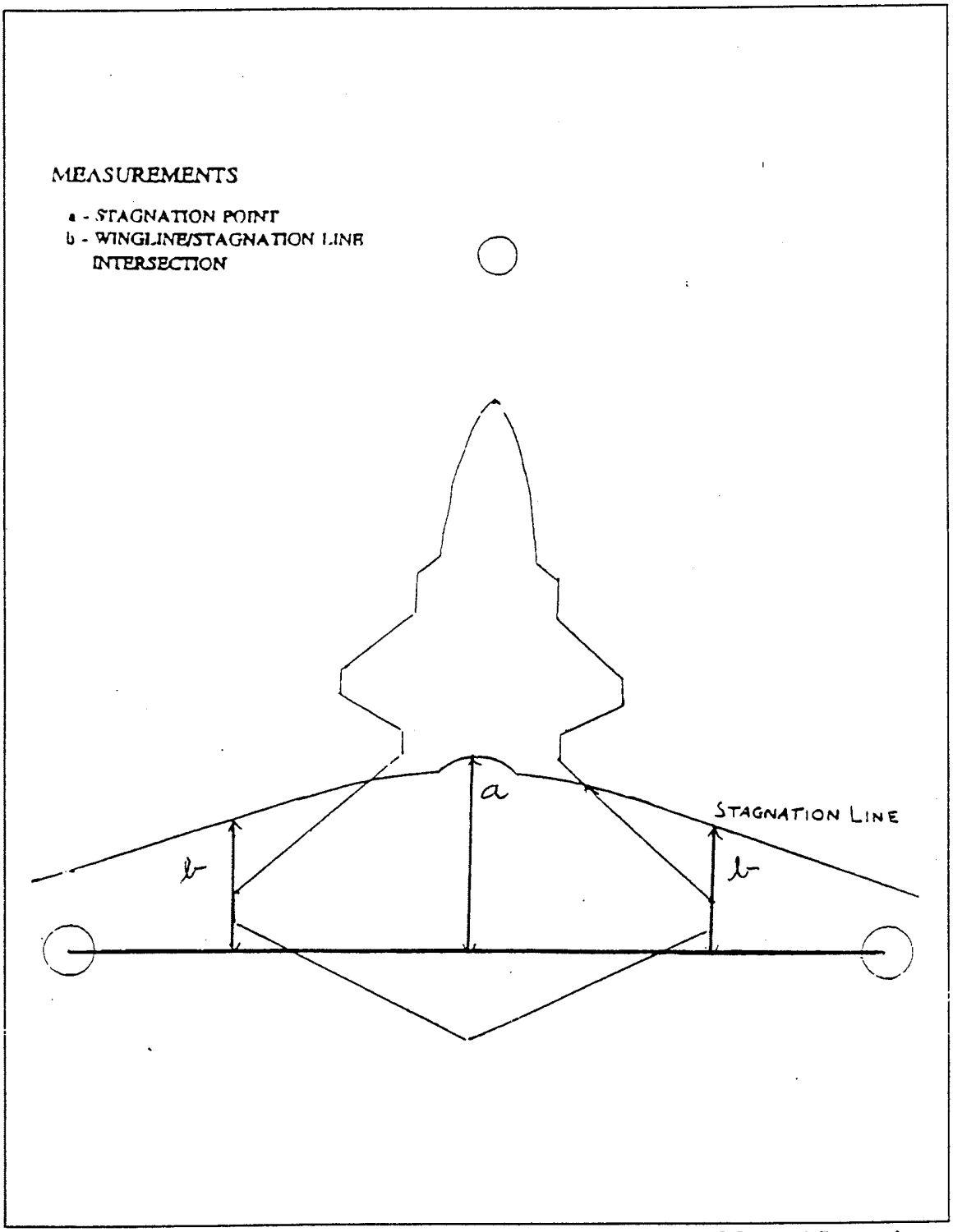

Figure 6 Discontinuous Stagnation Line and Measurements of Ground Stagnation Line

IV. RESULTS AND DISCUSSION

A. EXPERIMENTAL ACCURACY

1. Measurements

The ground-plane measurements of the stagnation line were made using a steel ruler with graduations every 0.02 inches. The stagnation line was in all cases thicker than 0.02 inches, in some cases as thick as 0.15 inches. The determination of the location of the stagnation line in these cases was done in a subjective manner. The measurement uncertainty was estimated to be $\pm$0.05 inches.

A complete uncertainty analysis would consist of numerous runs and determining some statistical error for each test condition. Due to time constraints, only three runs were conducted for one test condition to check for repeatability. In order to quantify the location of the stagnation line, measurements were taken at three points on the line. All distances were measured from the stagnation line to the centerline of the two main struts. One measurement specified the stagnation point (i.e. center point of the stagnation line). The other two measurements represented the points on the stagnation line that coincided with the intersection of the wingtip extension lines (See Figure 6). When graphing, these distances were transformed to represent the corresponding distances from the nose of the model to the stagnation line.

2. Test Conditions

It is recognized that reproducing the NTR's, heights, and other parameters exactly from day-to-day was not possible. The test conditions were kept as uniform as possible between the runs for different configurations to minimize errors as much as possible.

B. REPEATABILITY

To assess repeatability of the test data, three repeat runs were conducted. The configuration chosen corresponded to NTR = 0.92, with struts and no walls. The distances were averaged together and the individual runs were compared to the mean value.

1. Stagnation Point Measurements

The results of the three test runs and the mean are shown in Figure 7. The largest difference from the mean was 0.15 inches and occurred at h/De = 10. The overall average difference from the mean was 0.05 inches.

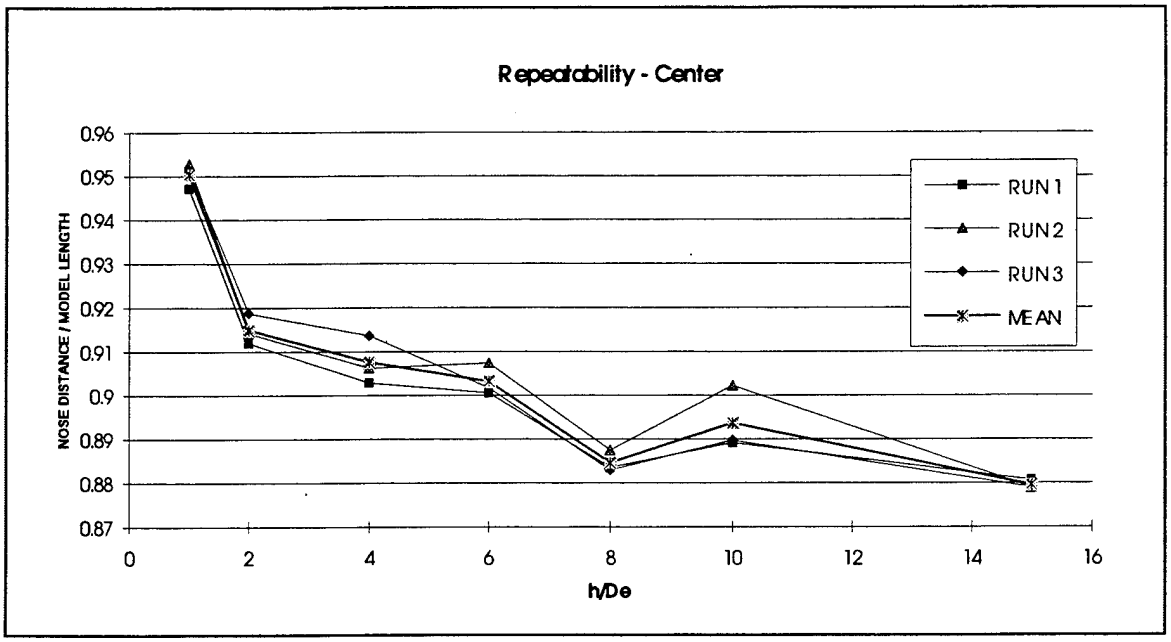

Figure 7 Repeatability of Stagnation Point Measurements

2. Left Wingtip Extension Line and Stagnation Line Intersection

Due to the presence of a small asymmetry in the flow pattern, the left and right measurements will be discussed separately. The results of the three runs and their mean are shown in Figure 8. The largest difference from the mean, which occurred at h/De = 2, was 0.30 inches. The overall average difference from the mean was 0.12 inches.

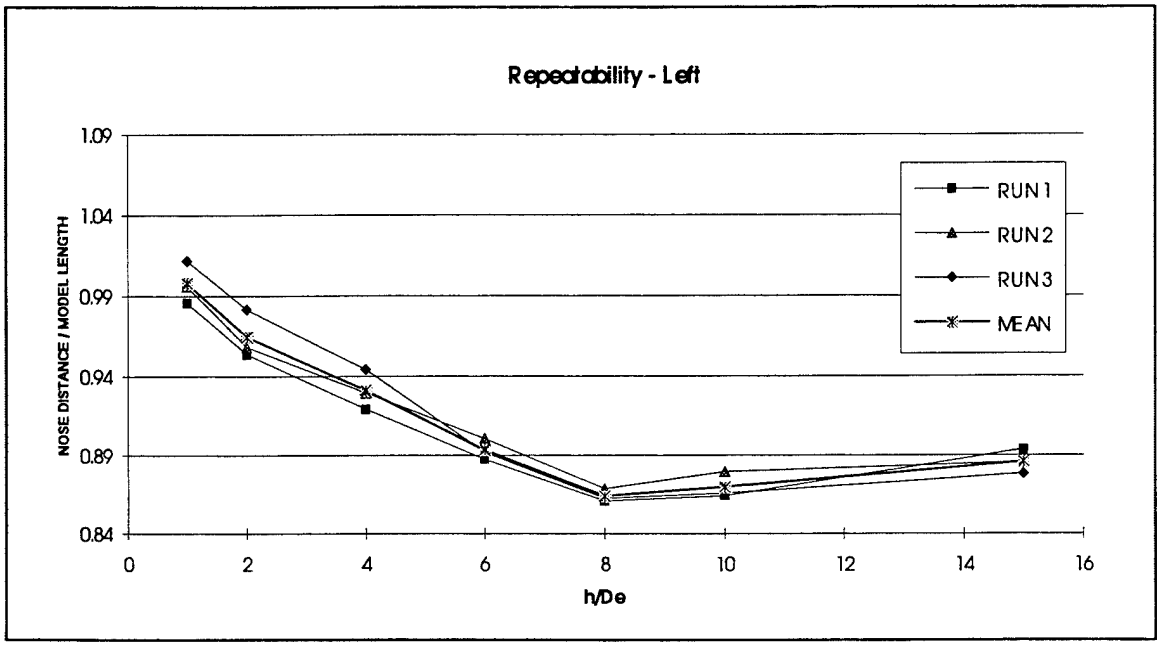

Figure 8 Repeatability of Left Wingtip Extension Line and Stagnation Line Intersection

3. Right Wingtip Extension Line and Stagnation Line Intersection

Figure 9 shows the results of the three runs and their mean. At h/De = 2, the largest difference from the mean was recorded. This difference was 0.42 inches. The overall average difference from the mean was 0.13 inches.

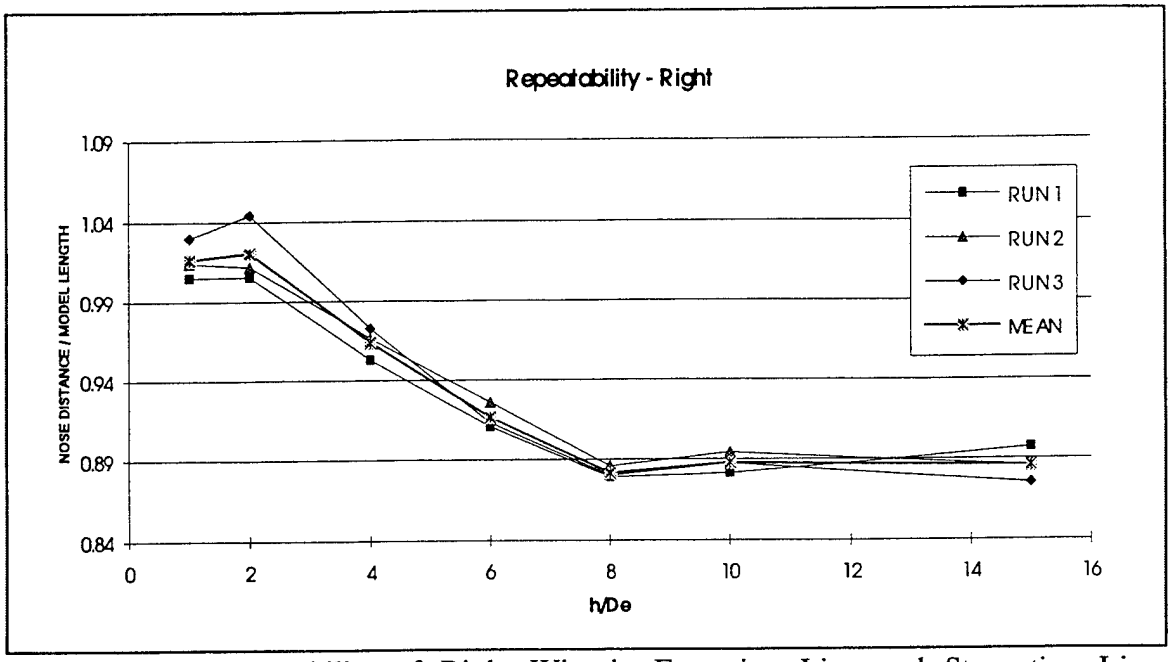

Figure 9 Repeatability of Right Wingtip Extension Line and Stagnation Line Intersection

C. GROUND - PLANE FLOW FIELD VISUALIZATION

The ground-plane flow-field visualization was photographed and recorded. The changes noted in the stagnation line were due to the different NTR's used and the changing height of the model. The most dramatic shift was due to a large variation of the NTR's. At the lowest NTR (= 0.92), the stagnation line was convex with respect to the nose of the model for the lower heights tested (Figure 10). With an NTR = 1.5, the stagnation line was relatively straight and perpendicular to the longitudinal axis of the aircraft for h/D_e = 4.0 (Figure 11). At the highest NPR (= 4.9), the stagnation line was concave with respect to the nose of the model for all heights (Figure 12).

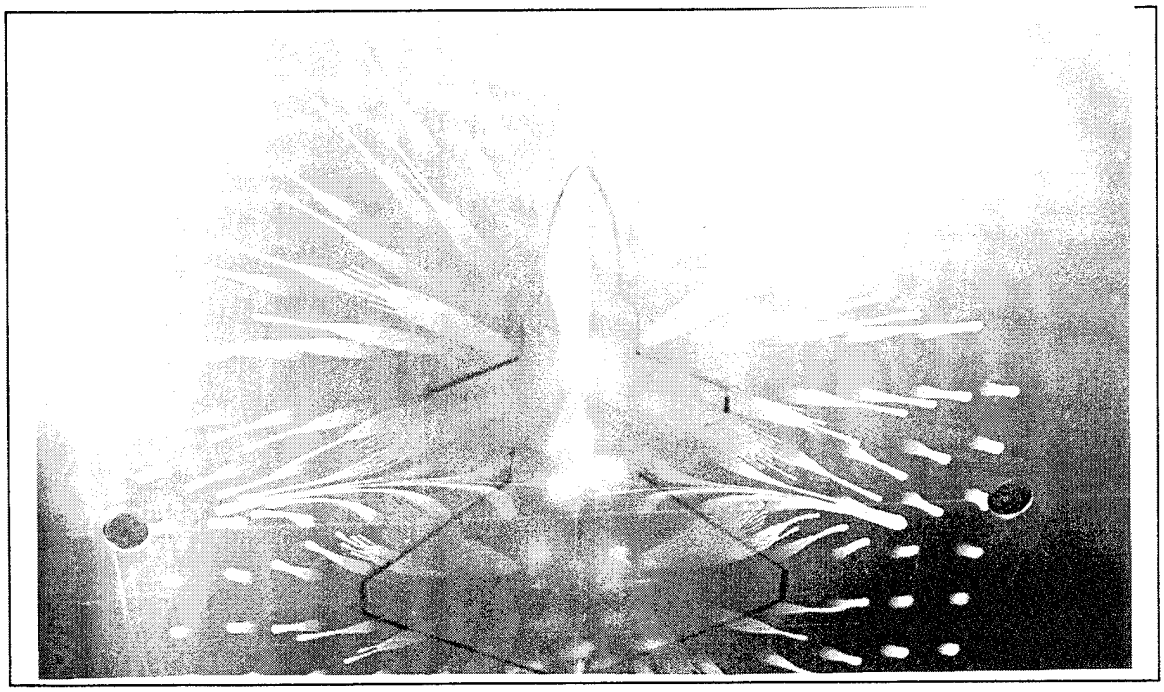

Figure 10 Convex Stagnation Line (NTR = 0.92 h/De = 4)

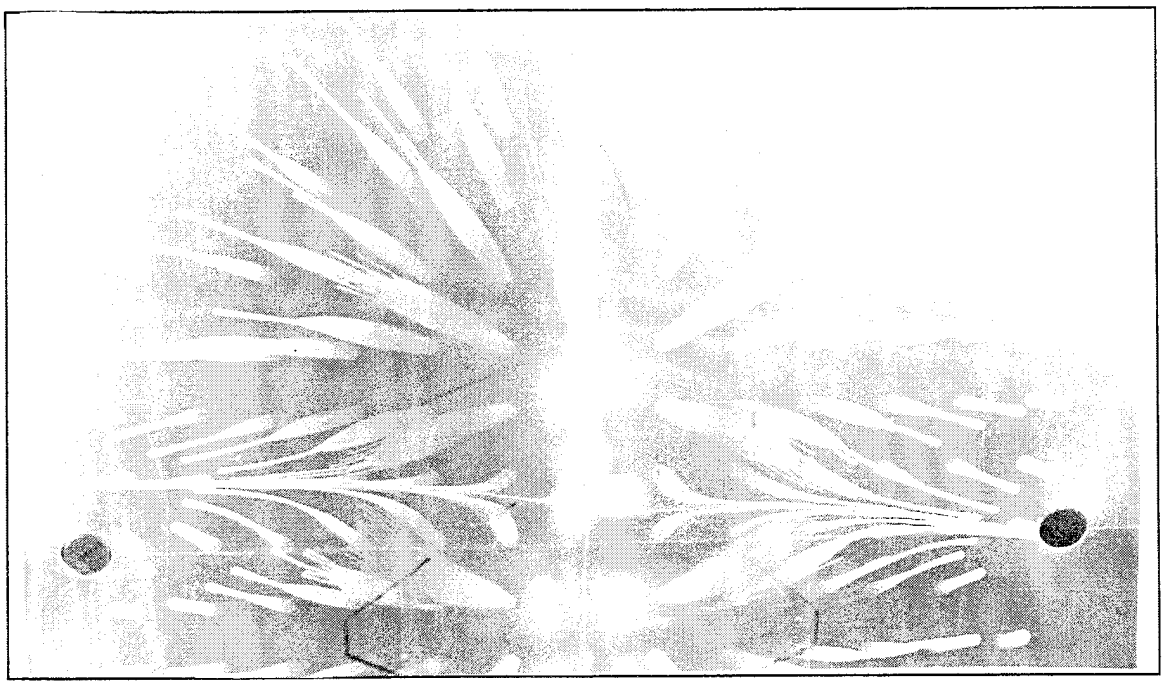

Figure 11 Straight Stagnation Line (NTR = 1.5 h/De = 4)

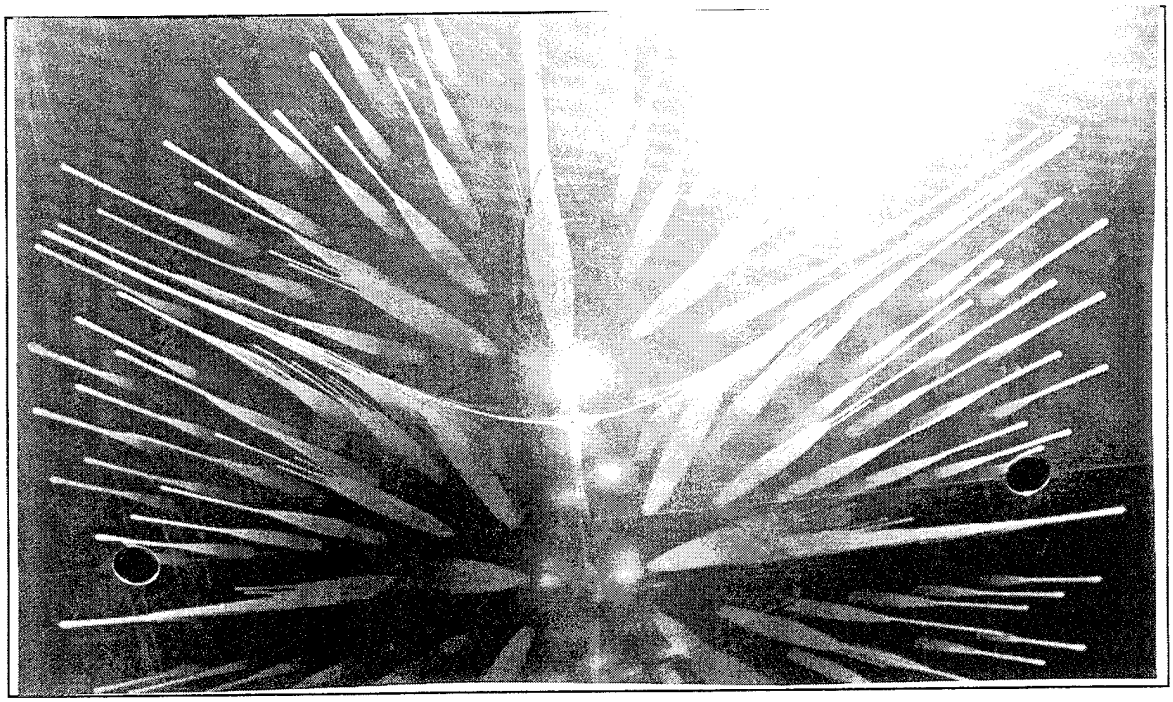

Figure 12 Concave Stagnation Line (NTR = 4.9 h/De =10)

The stagnation line changed shape with the changing height of the model. The most visible change was the appearance of distinct corners as seen in Figure 13. These were recorded at lower heights. At the higher heights, the two small jets in the aft section of the model effectively behave like a single jet before impingement and their presence does not individually affect the stagnation line. At the lower heights, however, the individual effect of the two small aft jets is felt on the stagnation line.

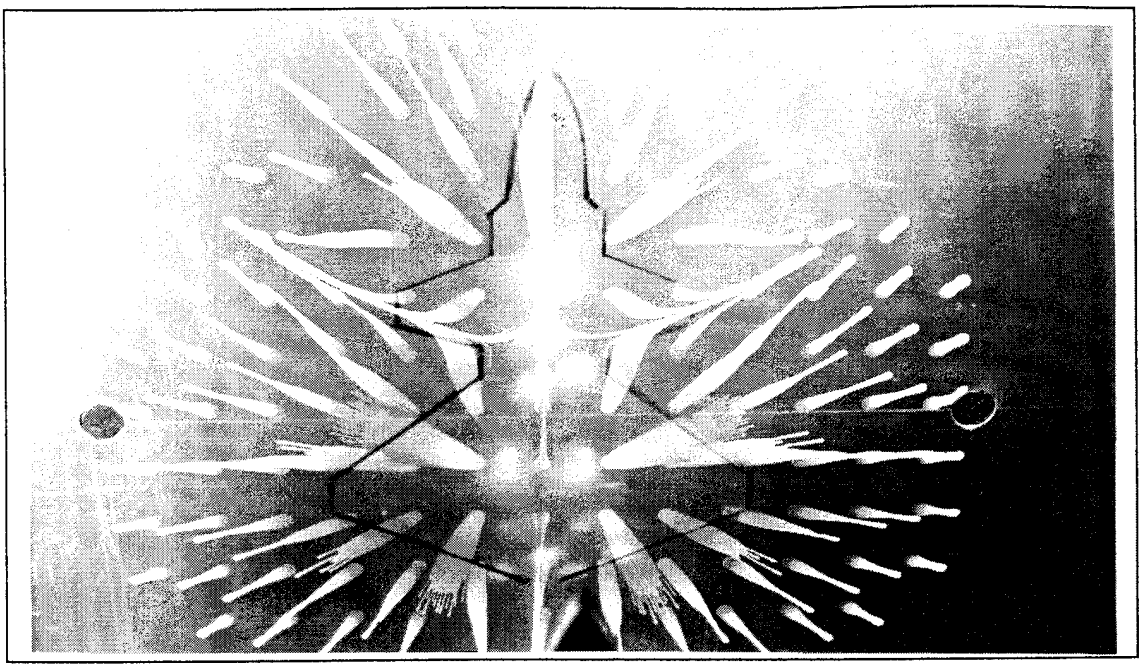

Figure 13 Additional Stagnation Points (NTR = 4.9 h/De = 4)

D. STRUT VS. NO STRUTS

The results of the stagnation line measurements for the configuration with the struts were compared to those for the configuration without the struts (baseline model). There was a shift in the stagnation line that seemed to be dependent on the NTR. An NTR less than unity (0.92) produced a forward shift and NTR's greater than unity (1.5 and 4.9) produced an aft shift of the stagnation line.

1. Stagnation Point Location

In some cases, the stagnation point was large and determining its exact location was difficult at best. The stagnation point could be as large as 1 inch in diameter (See Figure 14). To estimate where the stagnation point was, the stagnation lines were "followed" back to the center to give a better indication of the stagnation point. An NTR = 1.5 gave the least variation in the stagnation line and an NTR = 4.9 gave the largest shift in the stagnation line.

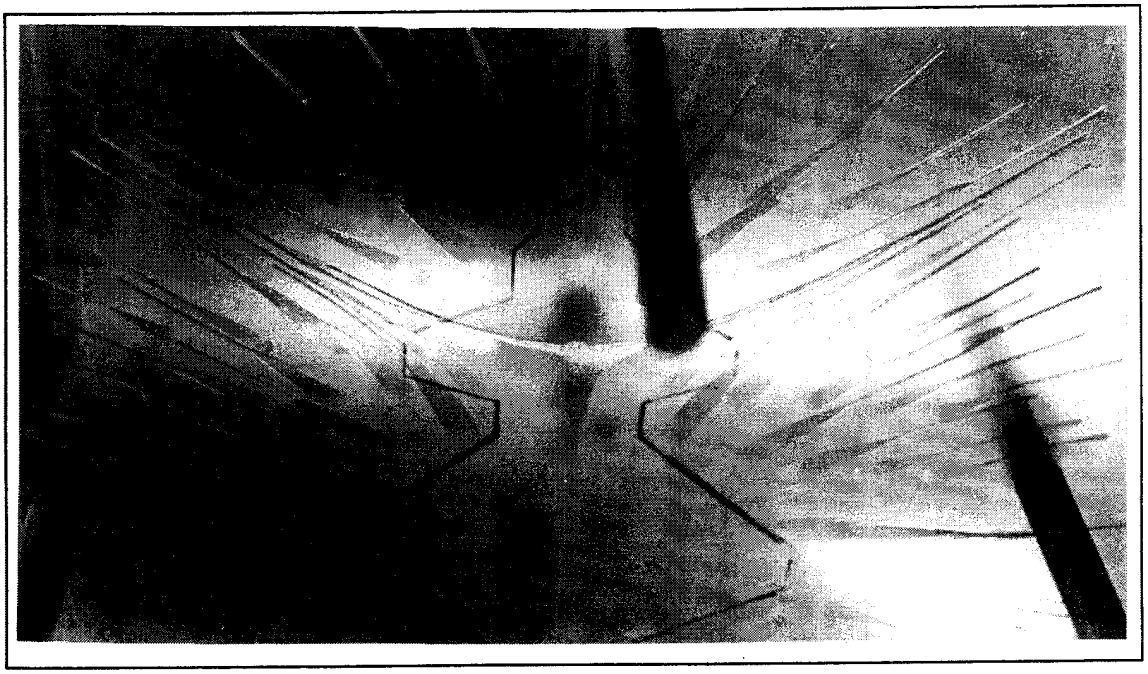

Figure 14 Large Stagnation Point (NTR = 4.9 h/De = 15)

a. NTR = 0.92

The stagnation point shifted slightly forward with the addition of the struts. The largest shift measured was at h/De = 6 and was 0.17 inches. The average forward shift was 0.08 inches. Figure 15 shows these results.

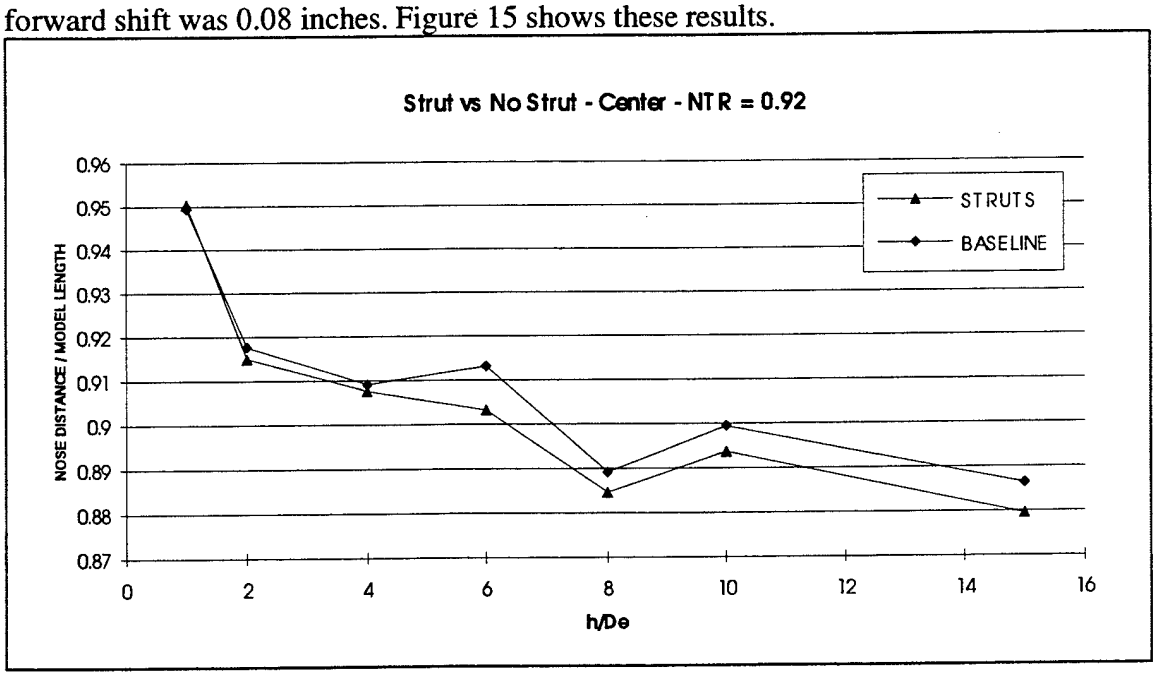

Figure 15 Stagnation Point Location for NTR = 0.92

b. NTR = 1.5

The results are shown in Figure 16. At h/De = 10, the largest shift of 0.38 inches was recorded. The average shift of the stagnation line with the addition of the struts was aft by 0.12 inches.

c. NTR = 4.9

The shift in the stagnation point with the struts in place was the largest for NTR = 4.9. The average shift was 0.18 inches. The largest shift occurred at h/De = 1 and was 0.28 inches and can be seen in Figure 17.

2. Wingtip Extension and Stagnation Line Intersections

The shifts in the left and right intersections of the wingtip extension lines with the stagnation line were not equal due to a small asymmetry condition noted

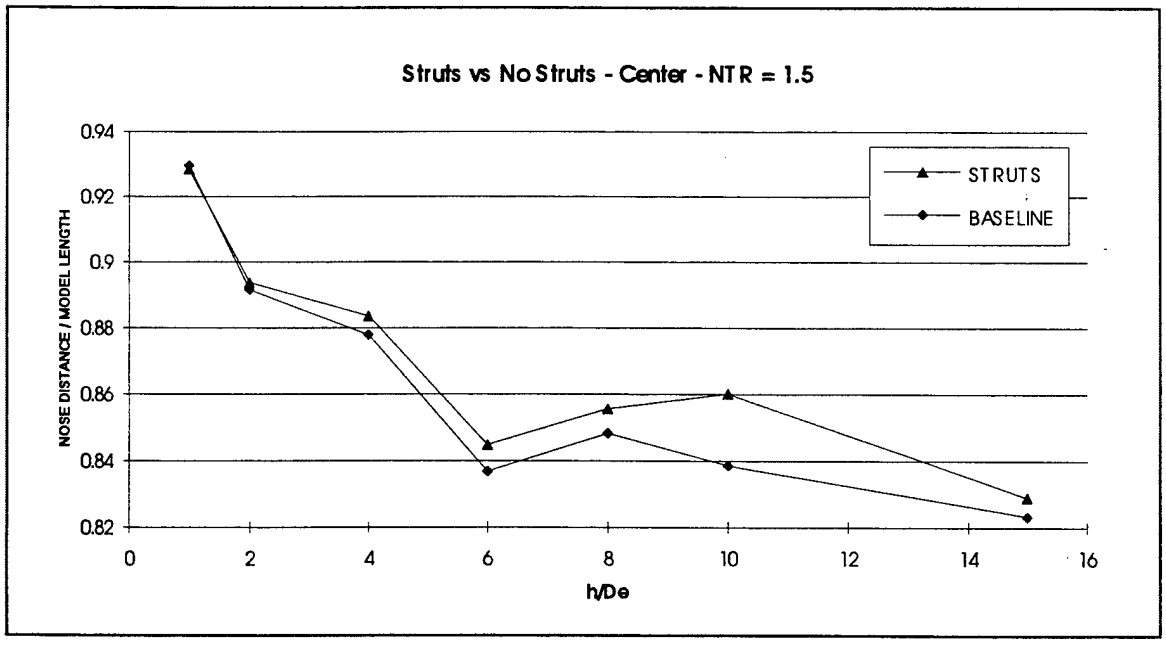

Figure 16 Stagnation Point Location for NTR = 1.5

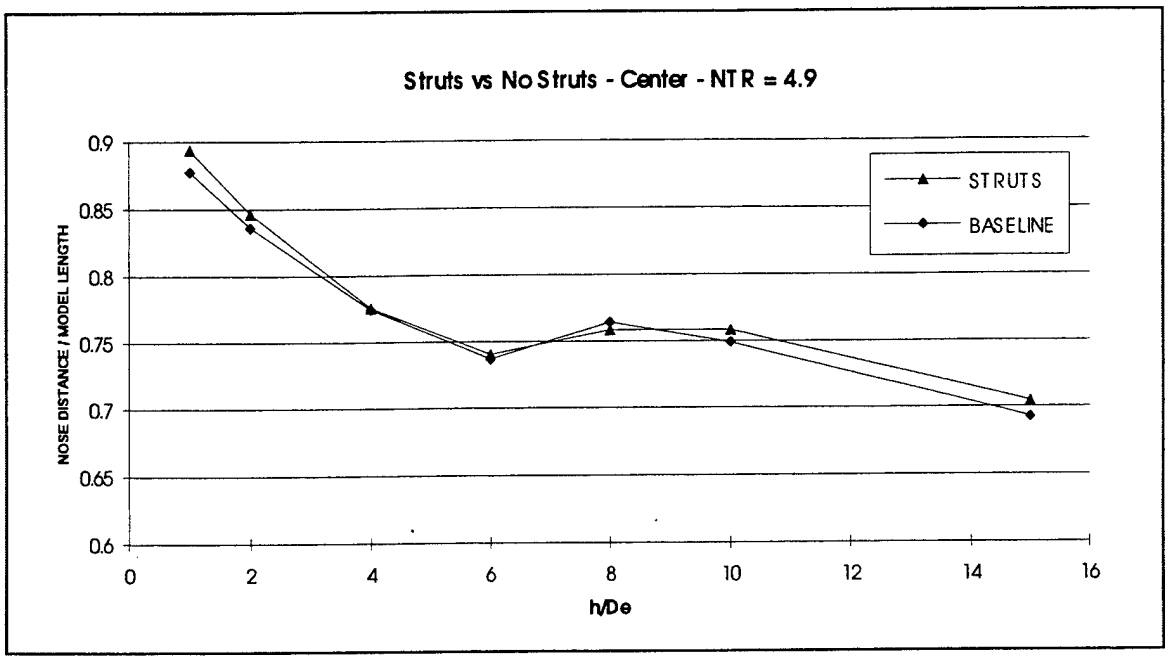

Figure 17 Stagnation Point Location for NTR = 4.9

throughout this experiment. For more information on the asymmetry see Ref. 4. The average shift of the intersection points on the stagnation line due to the struts was measurable but was less than the experimental uncertainty.

a. NTR = 0.92

As with the stagnation point at NTR = 0.92, the intersection of the wingtip extension line and the stagnation lines shifted forward with the addition of the struts. The left intersection shifted an average of 0.12 inches and the right intersection shifted an average of 0.18 inches. The maximum shifts occurred at h/De = 6 and 2, respectively, and are shown in Figures 18 and 19. These maximum values were 0.26 inches and 0.42 inches, respectively.

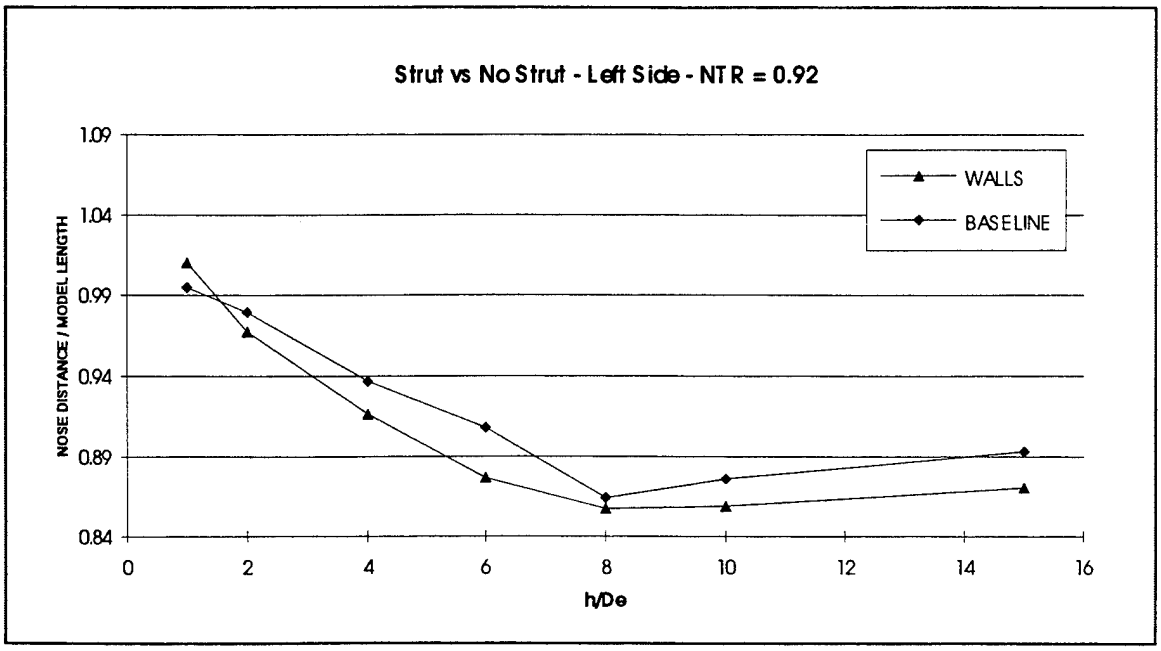

Figure 18 Wingtip Extension and Stagnation Line Intersection Distance for NTR = 0.92 (Left Side)

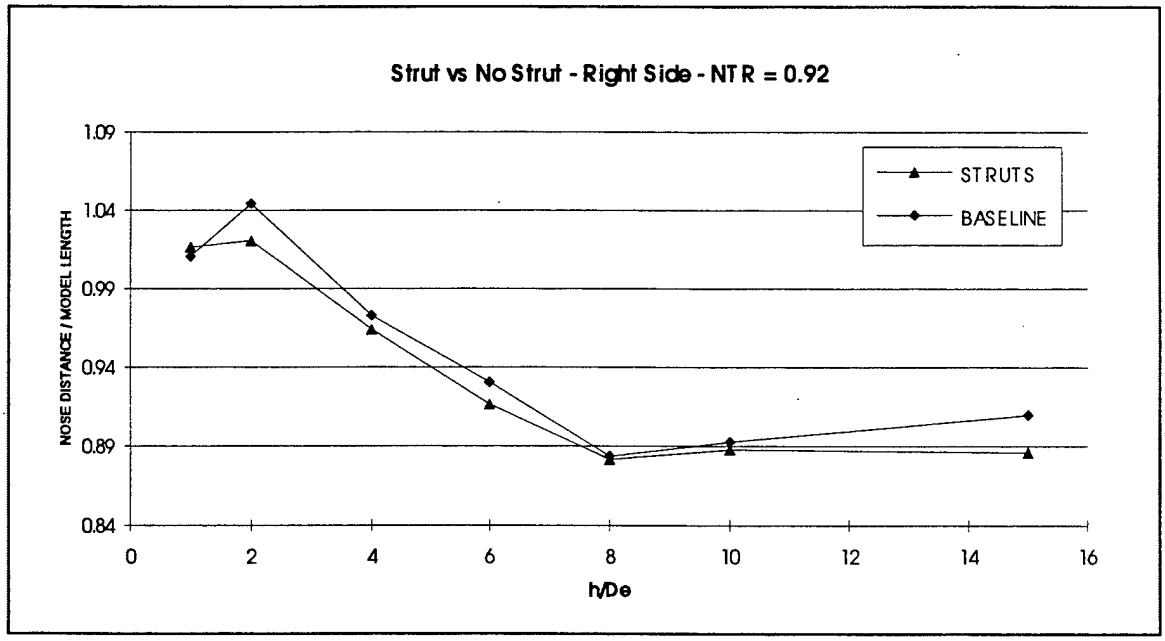

Figure 19 Wingtip Extension and Stagnation Line Intersection Distance for NTR = 0.92 (Right Side)

b. NTR = 1.5

There was an aft shift in both the right and the left intersections with the struts present. The average shift was 0.22 inches for the left and 0.07 inches for the right. The results are shown in Figures 20 and 21. The largest shift measured was 0.59 inches for the left and 0.34 inches for the right intersection, both occurring at h/De = 10.

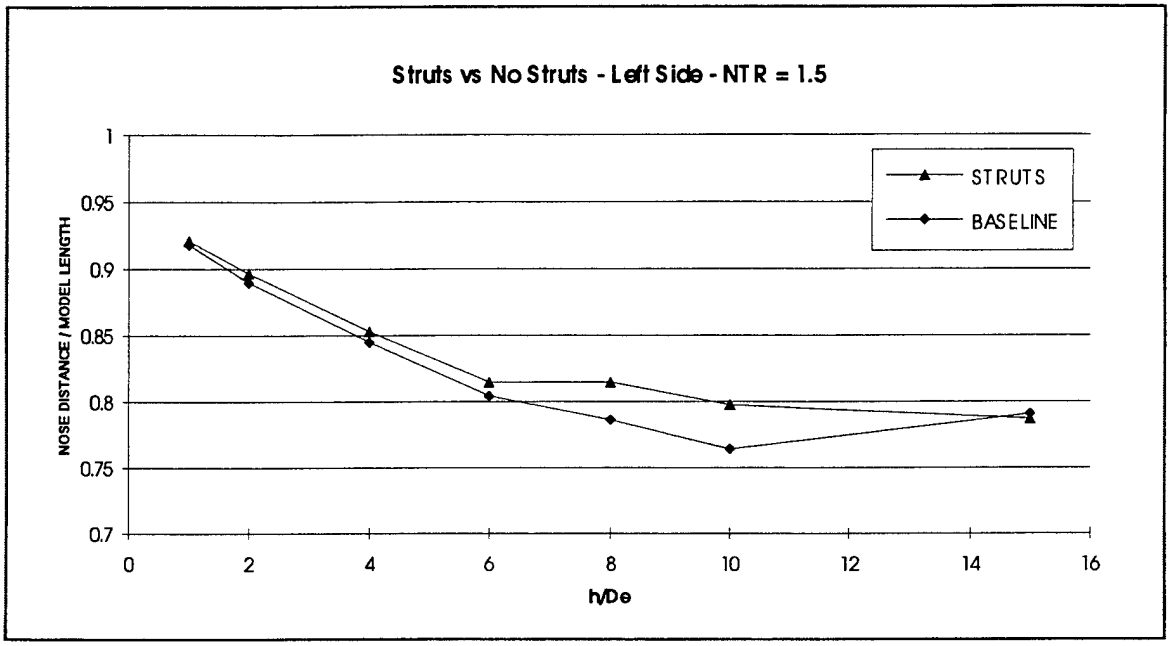

Figure 20 Wingtip Extension and Stagnation Line Intersection Distance for NTR = 1.5 (Left Side)

c. NTR = 4.9

The intersections of the wingtip extension lines with the stagnation line showed the largest average shift with NTR = 4.9. This average shift was 0.31 inches for the left side and 0.10 inches for the right side. The largest shift was 0.75 inches for both the right and left intersections. These shifts occurred at h/De = 1 and 15 respectively. The results are plotted in Figure 22 and Figure 23 for the left and right intersections, respectively.

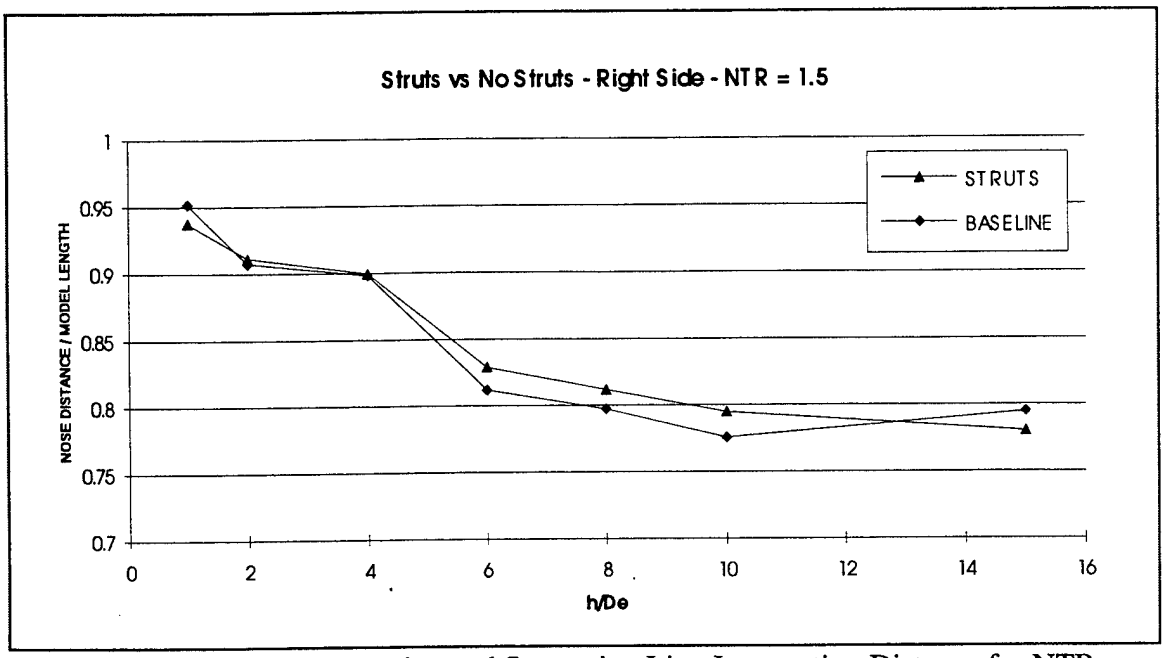

Figure 21 Wingtip Extension and Stagnation Line Intersection Distance for NTR = 1.5 (Right Side)

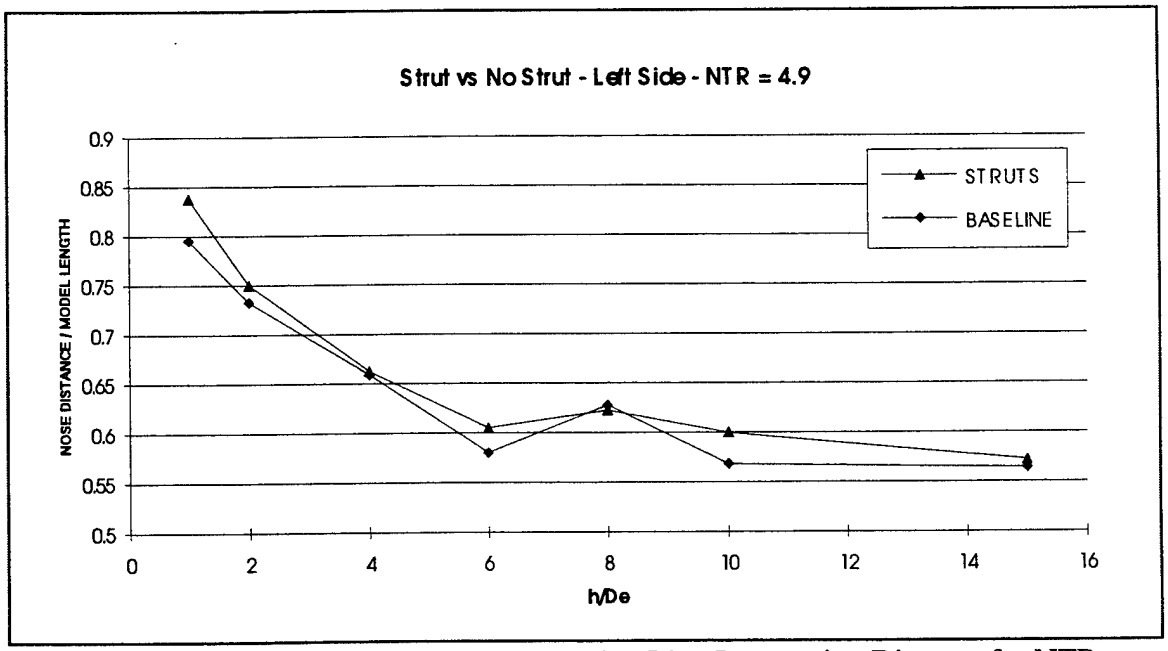

Figure 22 Wingtip Extension and Stagnation Line Intersection Distance for NTR = 4.9 (Left Side)

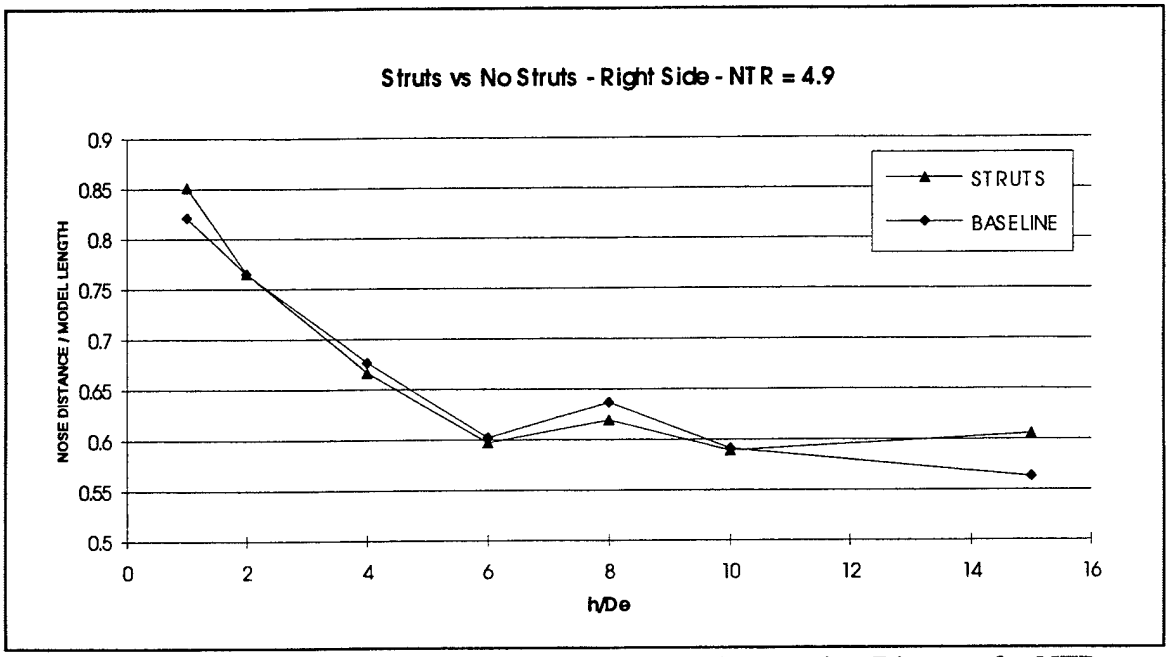

Figure 23 Wingtip Extension and Stagnation Line Intersection Distance for NTR = 4.9 (Right Side)

E. WALL VS. NO WALL

The wall configuration consisted of walls on two sides of the test rig and the struts described earlier. The measurements were compared to the baseline configuration. Similar to the strut situation, the shift in the stagnation line was different depending on the NTR. For an NTR less than unity (0.92), the presence of the walls shifted the stagnation line forward and for NTR's greater than unity (1.5 and 4.9) it shifted the stagnation line aft.

1. Stagnation Point Location

The measurement of the stagnation point had the same difficulties as in the previous configuration. The same general trends were noted while comparing the wall configuration to the baseline configuration.

a. NTR = 0.92

The stagnation point shifted aft with the addition of the walls. The largest error measured was at h/De = 6 and was 0.40 inches. The average aft shift was 0.03 inches. Figure 24 displays the results.

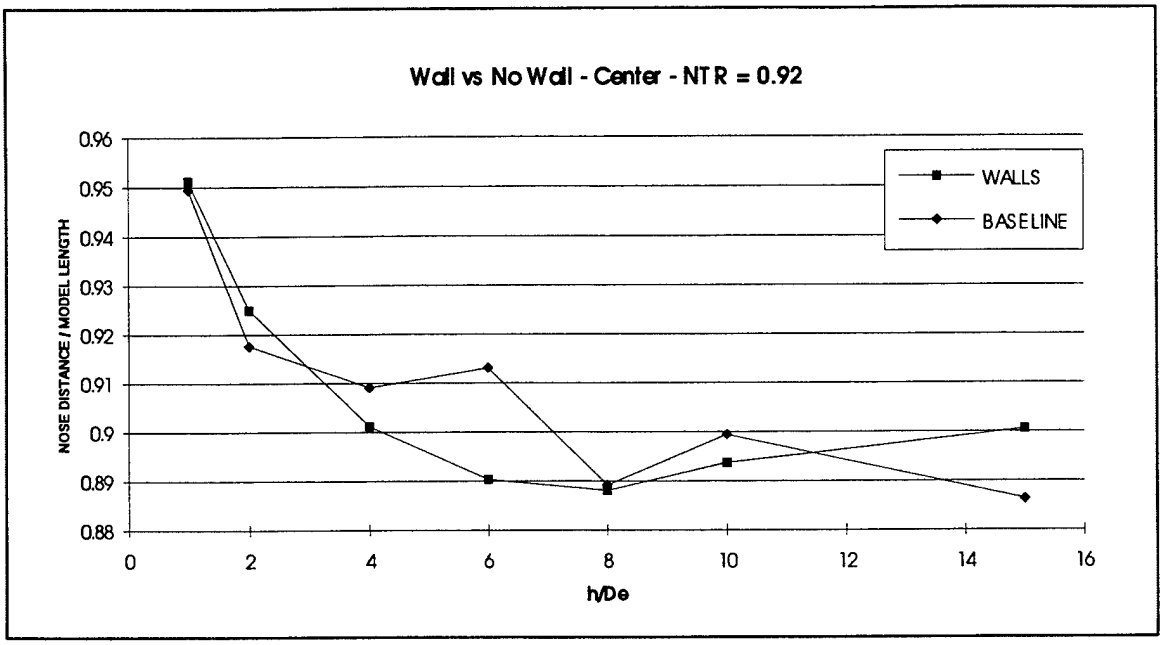

Figure 24 Stagnation Point Location for NTR = 0.92

b. NTR = 1.5

The results are shown in Figure 25. At h/De = 4, the largest error of 0.23 inches was recorded. The average forward shift of the stagnation line with the addition of the walls was 0.06 inches.

c. NTR = 4.9

The shift in the stagnation point with the walls in place was the largest for NTR = 4.9. The average shift was 0.21 inches. The largest shift occurred at h/De = 6 and was 0.72 inches and can be seen in Figure 26.

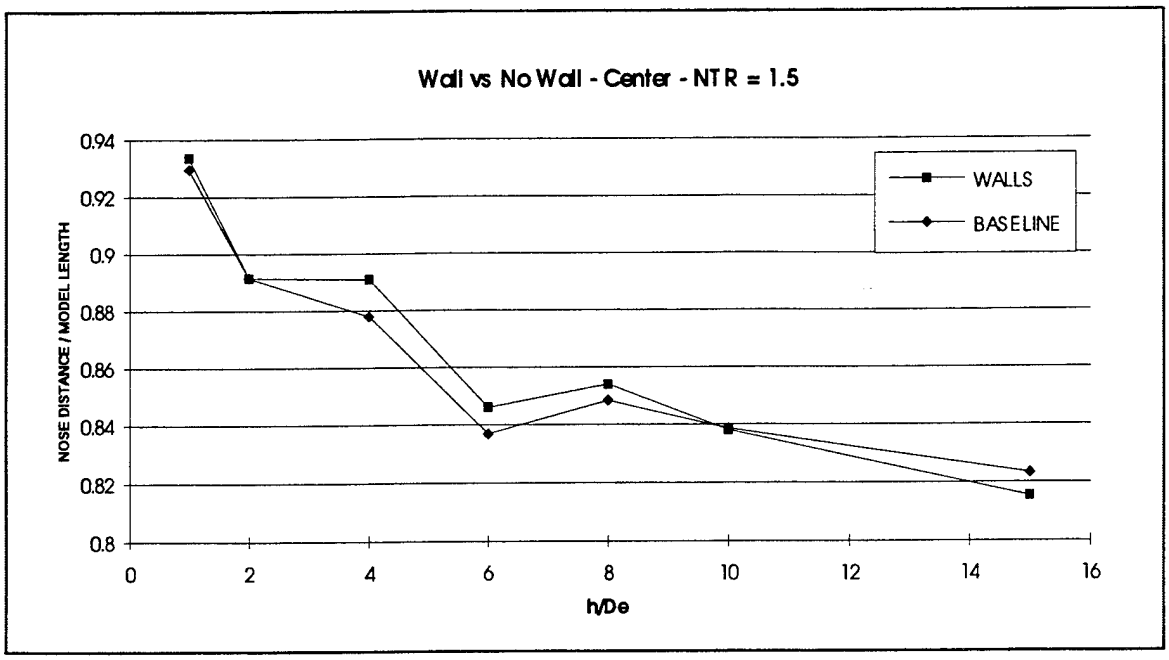

Figure 25 Stagnation Point Location for NTR = 1.5

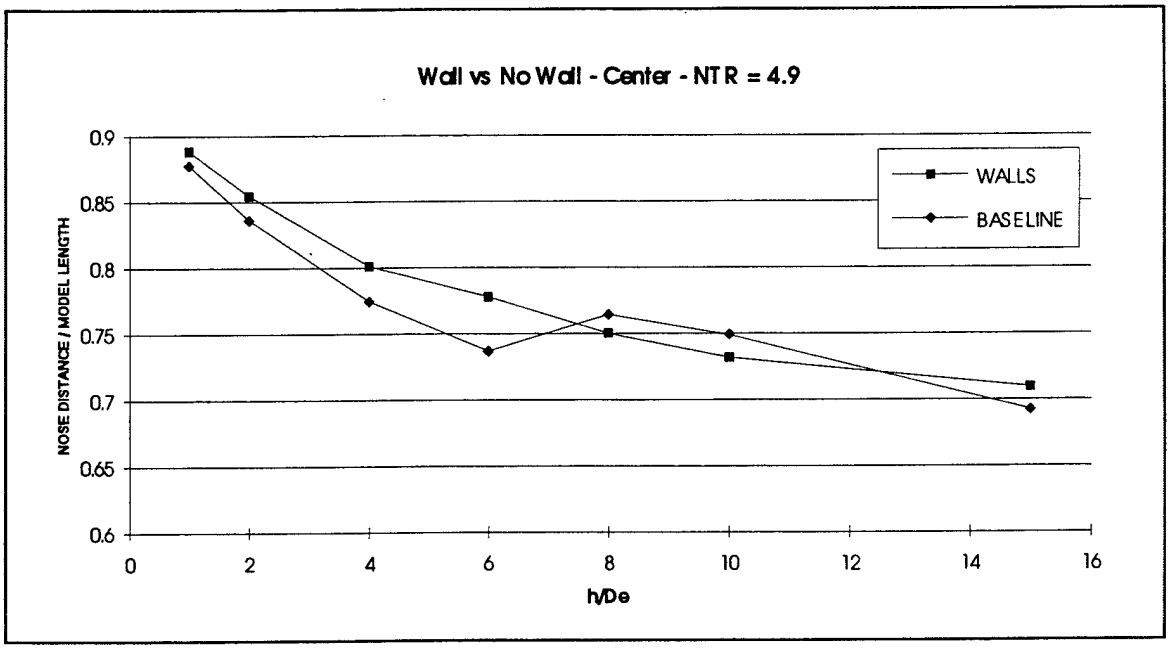

Figure 26 Stagnation Point Location for NTR = 4.9

2. Wingtip Extension Line and Stagnation Line Intersections

The asymmetric situation observed in the strut configuration was also present for the wall configuration. The larger shifts in the intersections were, in general, observed for the larger NTR's.

a. NTR = 0.92

As with the stagnation point at NTR = 0.92, the intersection of the wingtip extension lines and the stagnation line shifted forward with the addition of the walls. The left intersection shifted an average of 0.24 inches and the right shifted an average of 0.07 inches. The maximum shifts occurred at h/De = 6 and 15 and were 0.55 inches and 0.46 inches, respectively. The plots are shown in Figure 27 and 28.

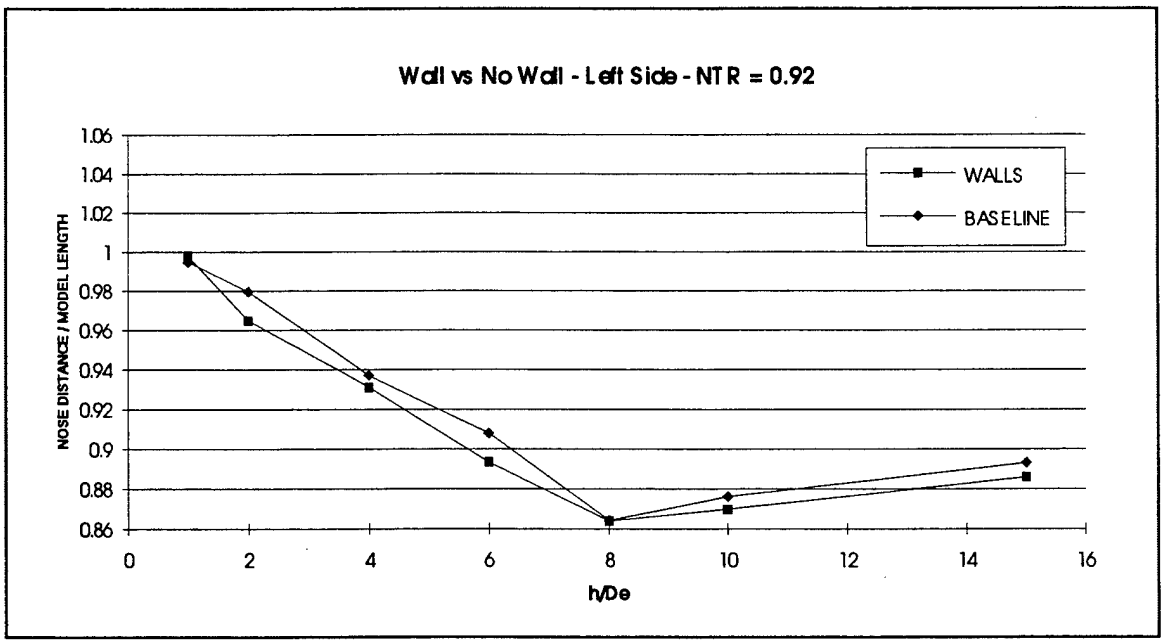

Figure 27 Wingtip Extension and Stagnation Line Intersection Distance for NTR = 0.92 (Left Side)

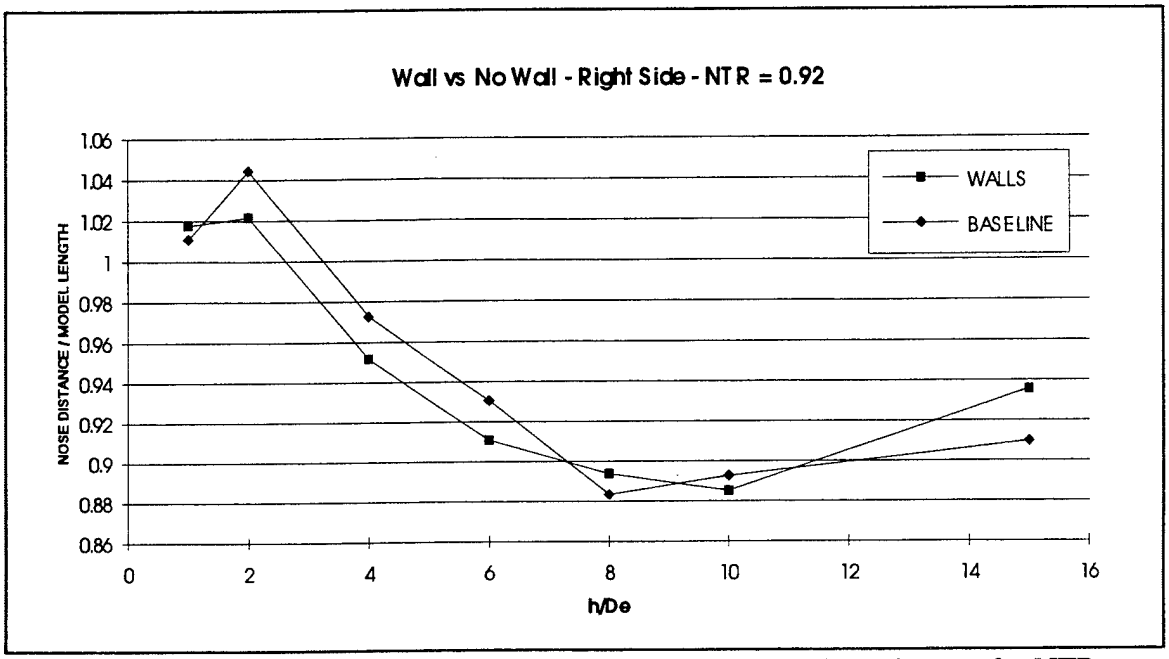

Figure 28 Wingtip Extension and Stagnation Line Intersection Distance for NTR = 0.92 (Right Side)

b. NTR = 1.5

There was an aft shift in both the right and the left intersections with the walls present. The average shift was 0.13 inches for the left and a 0.14 inches for the right. The results are shown in Figures 29 and 30. The largest shift measured for the left was 1.04 inches at h/De = 10, and 0.42 inches at h/De = 8 for the right.

c. NTR = 4.9

The intersections of the wingtip extension lines with the stagnation line showed the largest average shift with a NTR = 4.9. This average shift was 0.30 inches for the left and 0.26 inches for the right. The largest shift was 1.26 inches for the left and 1.08 inches for the right. These shifts both occurred at h/De = 6. The results are plotted in Figure 31 and Figure 32 for the left and right intersections, respectively

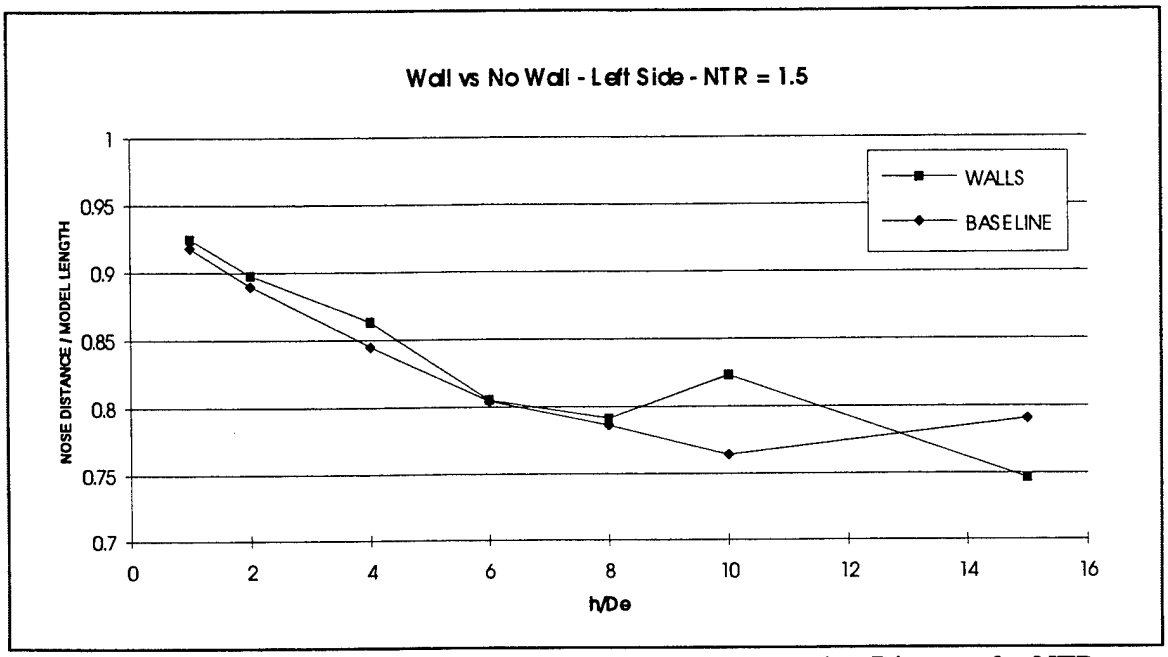

Figure 29 Wingtip Extension and Stagnation Line Intersection Distance for NTR = 1.5 (Left Side)

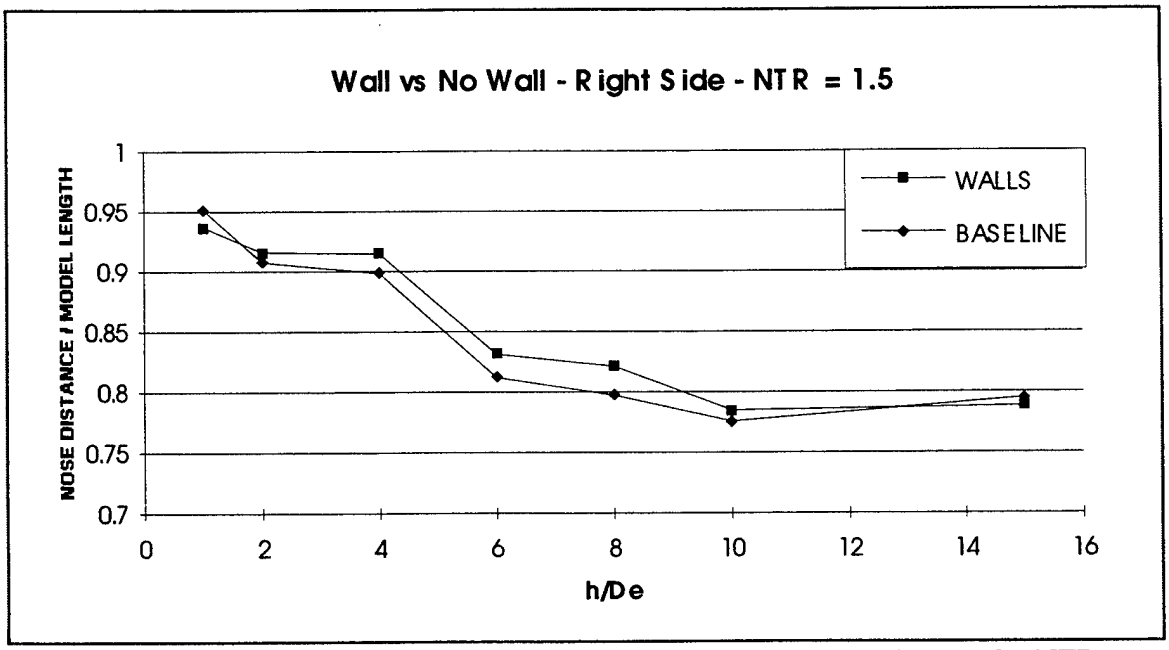

Figure 30 Wingtip Extension and Stagnation Line Intersection Distance for NTR = 1.5 (Right Side)

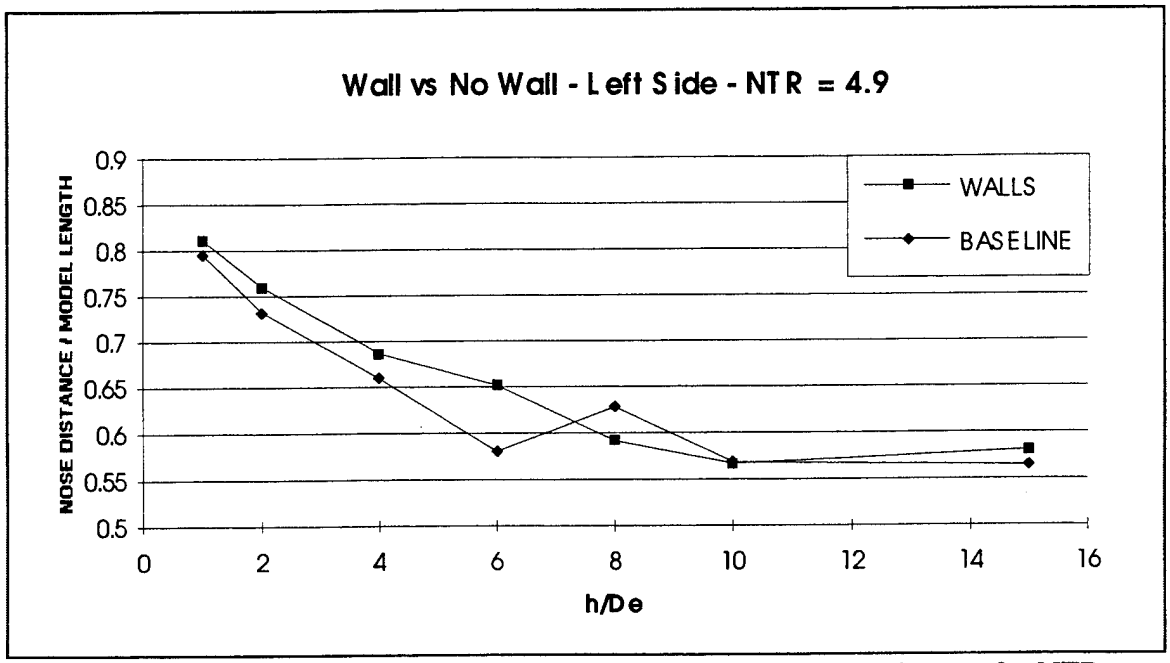

Figure 31 Wingtip Extension and Stagnation Line Intersection Distance for NTR = 4.9 (Right Side)

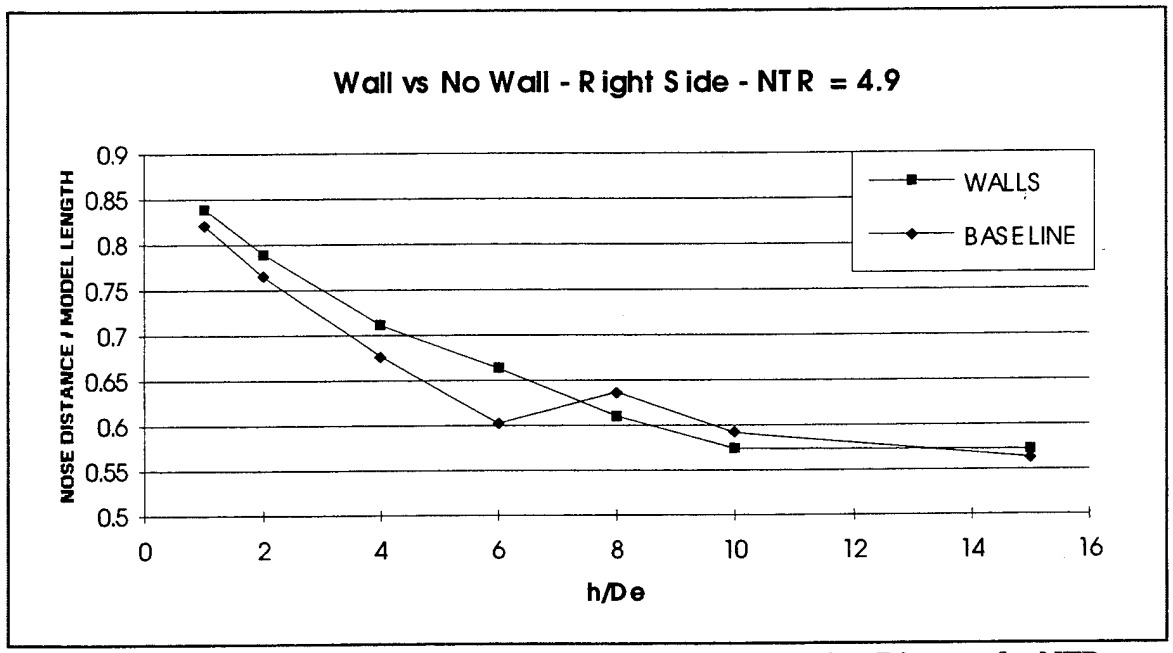

Figure 32 Wingtip Extension and Stagnation Line Intersection Distance for NTR = 4.9 (Right Side)

V. CONCLUSION AND RECOMMENDATIONS

A. CONCLUSION

At the request of NASA Ames, an investigation of strut and wall interference on the ground effects of a small scale model in hover was performed. This work differed from the earlier research in that it investigated a different model configuration and also studied the interference effect due to walls. An oil-flow visualization technique was used to record the ground-plane flow pattern including the stagnation line.

1. Small-Scale Model

The presence of the wooden dowels and the walls did affect the stagnation streamline. The shift in the stagnation line reversed in both the wall-configuration case and the strut-configuration case depending on whether the NTR was above or below unity. In the strut-configuration case, the stagnation line shifted forward when the NTR was less than unity but shifted aft when the NTR was greater than unity. In the wall configuration, the stagnation line also shifted forward when the NTR was less than unity, and shifted aft when the NTR was greater than unity. As the NTR was increased the average shift of the stagnation line also increased. A summary of the experimental data is shown in Appendix B. All values presented are the average taken over all heights tested. Negative values indicate a shift aft and positive values indicate a shift forward.

Although there was a definite trend noted in the stagnation streamline shift, the differences in the shifts were within the experimental uncertainty in most cases making a definite conclusion difficult.

B. RECOMMENDATIONS

1. Experimental Apparatus

Improvements such as a more precise lift mechanism or pressure gauges could be used to increase accuracy. It is doubtful that these improvements, however, would substantially increase the accuracy of the measurements of the stagnation line.

2. Experimental Procedure

In order to measure the difference in the stagnation line because of the change in configuration, similar types of run should ideally be carried out one after another to minimize the difference from other factors, such as not being able to set the pressure ratio exactly the same as the previous runs. In order to minimize these errors, many more runs should be conducted to get a statistical average. However, this could not be performed in view of the limited time available. An alternative method would be drilling pressure taps in the model and measuring the change in the pressure distribution on the model. A more accurate way would be to set up a force balance system that would directly measure the forces on the model. Both of these methods come with a cost of time and money.

APPENDIX A

NOZZLE PRESSURE RATIO CALCULATIONS

T	Thrust	A	Area
$\dot{m}$	Mass Flow Rate	ρ	Density
V	Velocity	M	Mach Number
P_e	Exit Pressure	a	Speed of Sound $a = (\gamma Rt)^{1/2}$
P_a	Ambient Pressure	R	Gas Constant
t	Temperature		

T_A/T_F Thrust Aft Nozzles / Thrust Forward Nozzle (Thrust Ratio)

THRUST EQUATION $T = \dot{m}V + (P_e - P_a) A$

For an underexpanded nozzle $P_e = P_a$

$T = \dot{m}V = \rho AV^2 = (P_e/Rt) A (aM)^2 = (P_e/Rt) A (\gamma Rt) M^2 = P_e A\gamma M^2 = P_a A\gamma M^2$

For an overexpanded nozzle

$T = P_e A\gamma M^2 + (P_e - P_a) A$

$P_e = 0.5283 * P_a * NPR$

$M = 1$ (all nozzles are convergent only and therefore choked)

Aft nozzles are overexpanded, and the Front nozzle is underexpanded therefore

$T_A / T_F = (P_e A_A \gamma + (P_e - P_a) A_A) / P_a A_F \gamma M_F^2$

where $P_e = \{ 0.5283 * P_a * NPR \} A$

Additional corrections were used to modify this equation to better match the operating conditions of NASA's LSPM. For more information, see Ref 5. Table 1 shows the nozzle pressure ratios used for the corresponding nozzle thrust ratios.

NTR	NPR (Forward)	NPR (Aft)
0.92	1.31	2.21
1.5	1.31	3.03
4.9	1.09	3.03

TABLE 1: Nozzle Thrust Ratios and Corresponding Nozzle Pressure Ratios.

APPENDIX B

EXPERIMENTAL RESULTS

Note 1:All measurements are in inches.
Note 2:Negative values indicate stagnation line aft of main strut centerline.

HEIGHT	1.14	2.28	4.57	6.85	9.14	11.42	17.13
NOSE	-0.06	0.50	0.65	0.58	1.00	0.82	1.05
LWING	-0.86	-0.59	0.16	0.67	1.44	1.23	0.93
RWING	-1.14	-1.73	-0.47	0.27	1.10	0.94	0.64

TABLE 2: NTR = 0.92 No Walls No Struts

HEIGHT	1.14	2.28	4.57	6.85	9.14	11.42	17.13
NOSE	-0.02	0.60	0.76	0.80	1.10	1.00	1.15
LWING	-0.70	-0.14	0.47	1.03	1.50	1.44	0.92
RWING	-1.04	-1.05	-0.12	0.62	1.18	1.14	0.86

TABLE 3: NTR = 0.92 No Walls Struts (Run 1)

HEIGHT	1.14	2.28	4.57	6.85	9.14	11.42	17.13
NOSE	-0.12	0.56	0.70	0.68	1.03	0.77	1.18
LWING	-0.88	-0.22	0.29	0.80	1.36	1.17	1.06
RWING	-1.20	-1.16	-0.36	0.35	1.06	0.91	1.06

TABLE 4: NTR = 0.92 No Walls Struts (Run 2)

HEIGHT	1.14	2.28	4.57	6.85	9.14	11.42	17.13
NOSE	-0.09	0.48	0.57	0.78	1.11	0.99	1.18
LWING	-1.16	-0.63	0.03	0.95	1.47	1.41	1.19
RWING	-1.48	-1.73	-0.47	0.58	1.16	1.03	1.25

TABLE 5: NTR = 0.92 No Walls Struts (Run 3)

HEIGHT	1.14	2.28	4.57	6.85	9.14	11.42	17.13
NOSE	-0.09	0.37	0.79	0.98	1.02	0.92	0.80
LWING	-1.13	-0.38	0.52	1.22	1.56	1.53	1.33
RWING	-1.26	-1.33	-0.10	0.62	0.92	1.07	0.18

TABLE 6: NTR = 0.92 Walls Struts

HEIGHT	1.14	2.28	4.57	6.85	9.14	11.42	17.13
NOSE	0.29	0.96	1.20	1.92	1.72	1.89	2.16
LWING	0.49	0.99	1.78	2.49	2.81	3.20	2.73
RWING	-0.10	0.68	0.84	2.36	2.62	3.00	2.66

TABLE 7: NTR = 1.5 No Walls No Struts

HEIGHT	1.14	2.28	4.57	6.85	9.14	11.42	17.13
NOSE	0.31	0.92	1.10	1.78	1.59	1.51	2.06
LWING	0.44	0.87	1.64	2.31	2.31	2.61	2.80
RWING	0.15	0.61	0.82	2.06	2.36	2.66	2.92

TABLE 8: NTR = 1.5 No Walls Struts

HEIGHT	1.14	2.28	4.57	6.85	9.14	11.42	17.13
NOSE	0.22	0.96	0.97	1.76	1.62	1.90	2.30
LWING	0.37	0.85	1.46	2.48	2.72	2.16	3.51
RWING	0.16	0.53	0.55	2.02	2.20	2.84	2.78

TABLE 9: NTR = 1.5 Walls Struts

HEIGHT	1.14	2.28	4.57	6.85	9.14	11.42	17.13
NOSE	1.20	1.93	3.02	3.68	3.20	3.47	4.46
LWING	2.65	3.76	5.05	6.44	5.60	6.65	6.72
RWING	2.20	3.19	4.74	6.05	5.44	6.24	6.74

TABLE 10: NTR = 4.9 No Walls No Struts

HEIGHT	1.14	2.28	4.57	6.85	9.14	11.42	17.13
NOSE	0.92	1.75	3.00	3.62	3.30	3.30	4.25
LWING	1.90	3.45	4.99	6.00	5.69	6.09	6.58
RWING	1.66	3.18	4.92	6.14	5.75	6.28	5.99

TABLE 11: NTR = 4.9 No Walls Struts

HEIGHT	1.14	2.28	4.57	6.85	9.14	11.42	17.13
NOSE	1.01	1.61	2.55	2.96	3.45	3.77	4.16
LWING	2.37	3.27	4.57	5.18	6.24	6.68	6.43
RWING	1.88	2.75	4.14	4.97	5.91	6.55	6.58

TABLE 12: NTR = 4.9 Walls Struts

APPENDIX C

PHOTOGRAPHIC RECORD OF TEST RUNS

I. NTR = 0.92 NO WALLS NO STRUTS

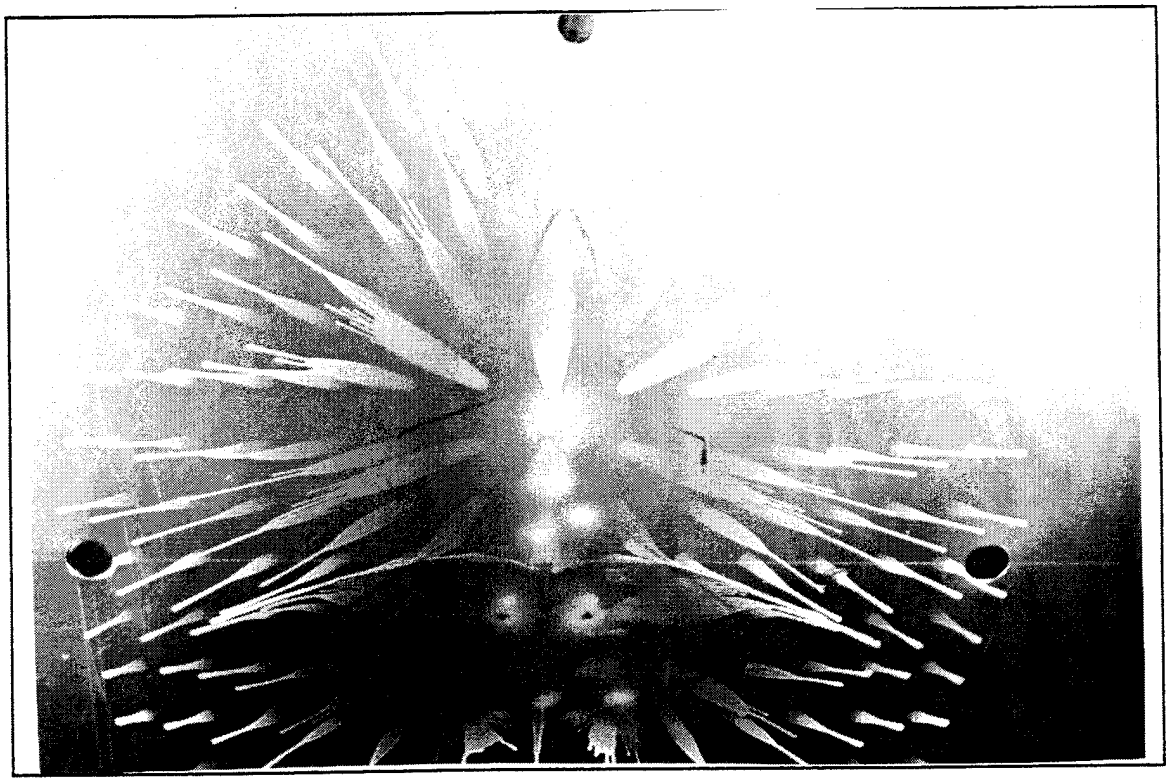

Figure 33 NTR = 0.92, Ground-Plane Height 1.14"

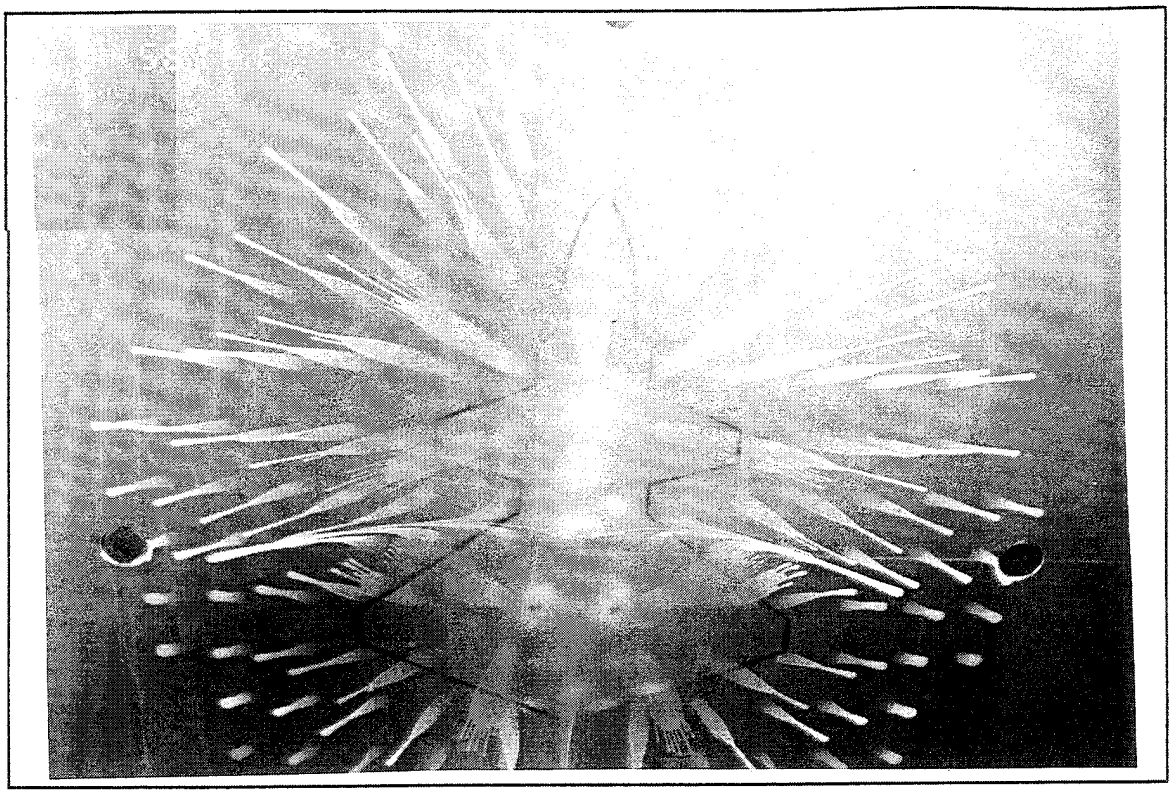

Figure 34 NTR = 0.92, Ground-Plane Height 2.28"

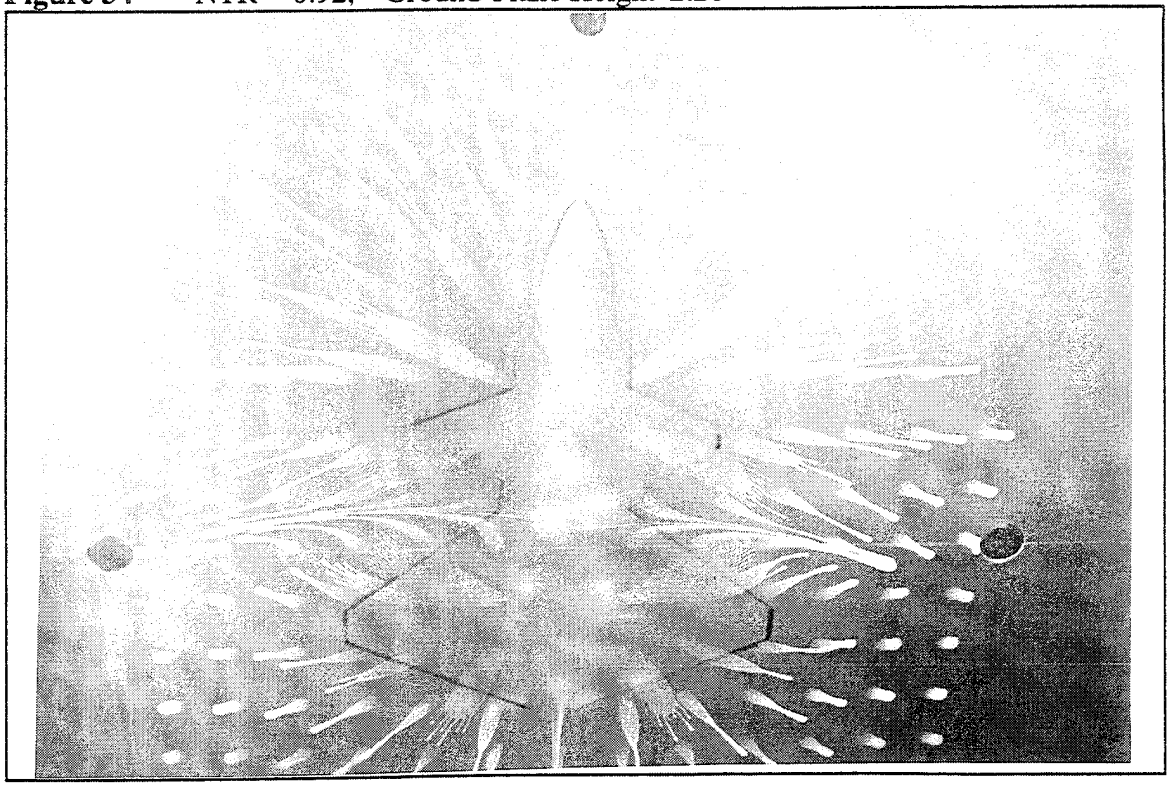

Figure 35 NTR = 0.92 Ground-Plane Height 4.57"

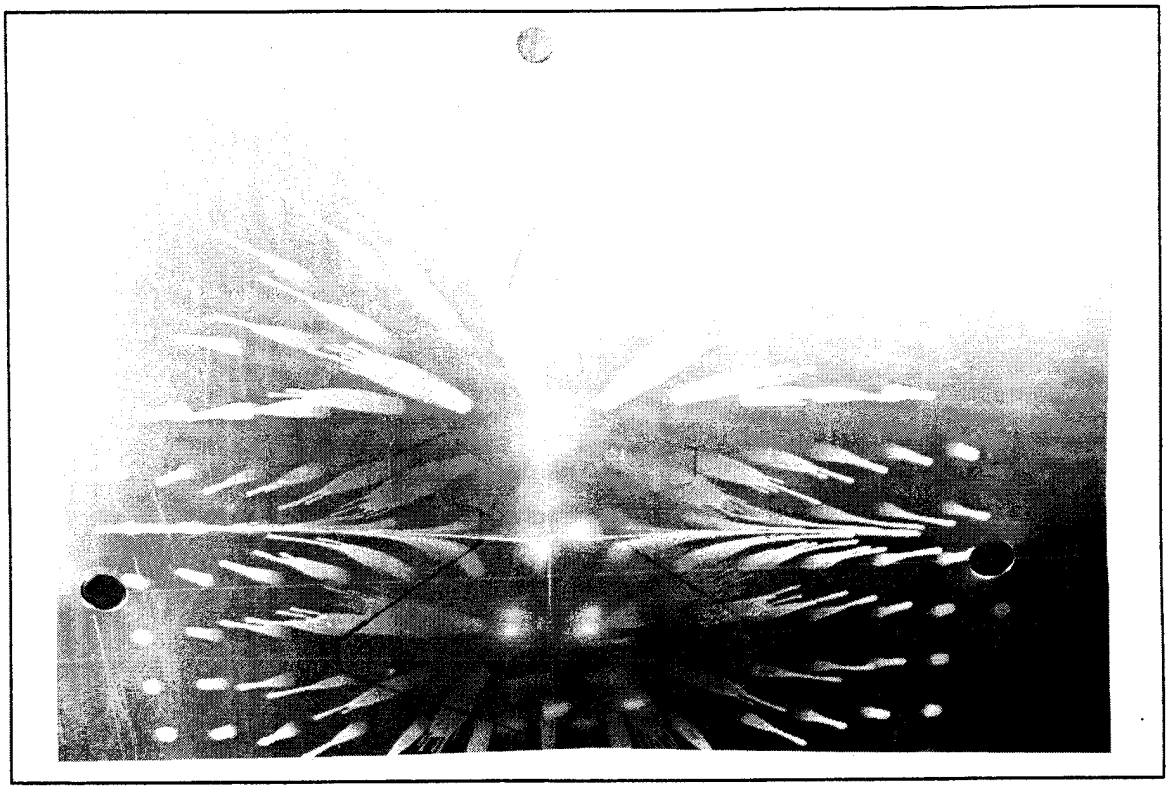

Figure 36 NTR = 0.92, Ground-Plane Height 6.85"

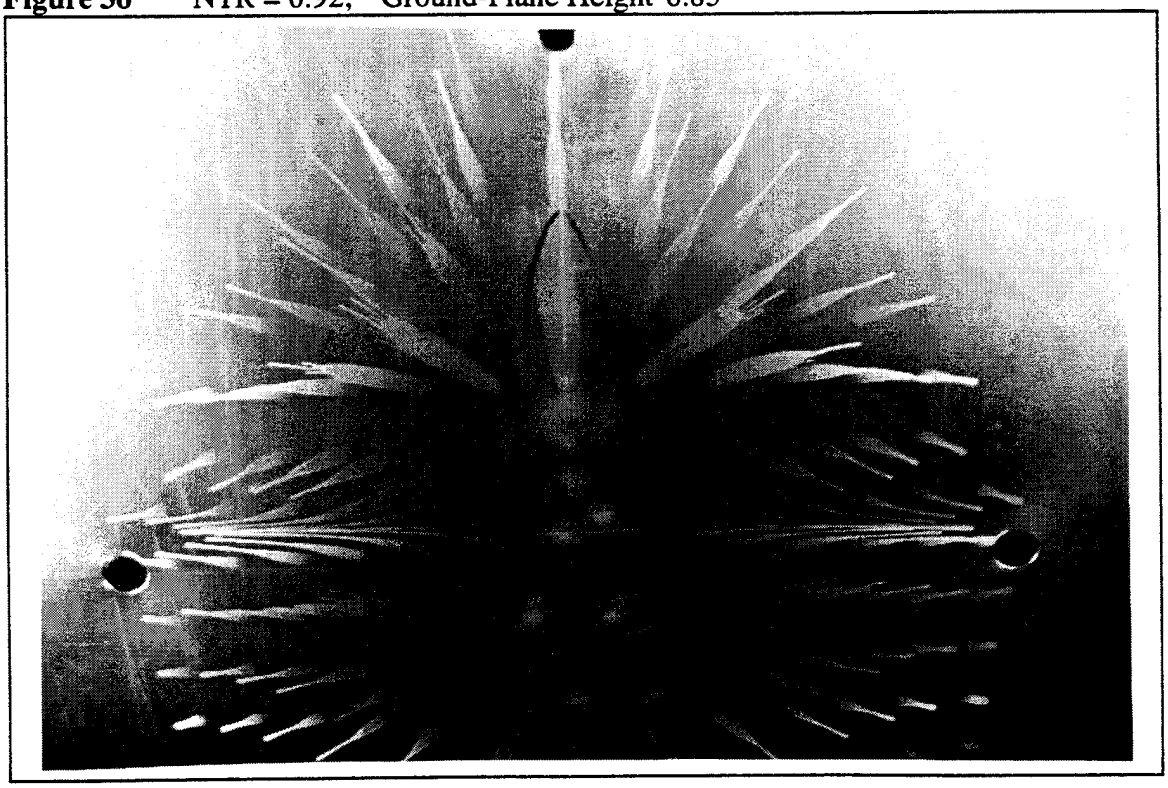

Figure 37 NTR = 0.92, Ground-Plane Height 9.14"

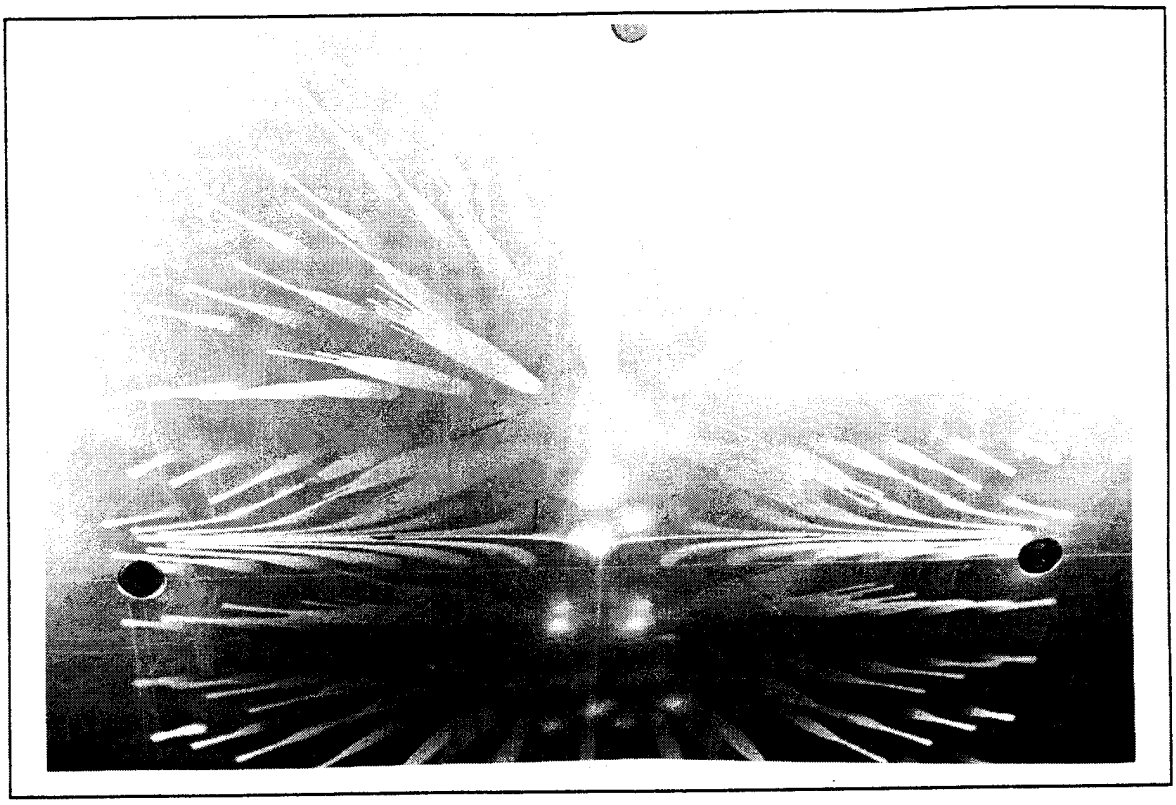

Figure 38 NTR = 0.92, Ground-Plane Height 11.42"

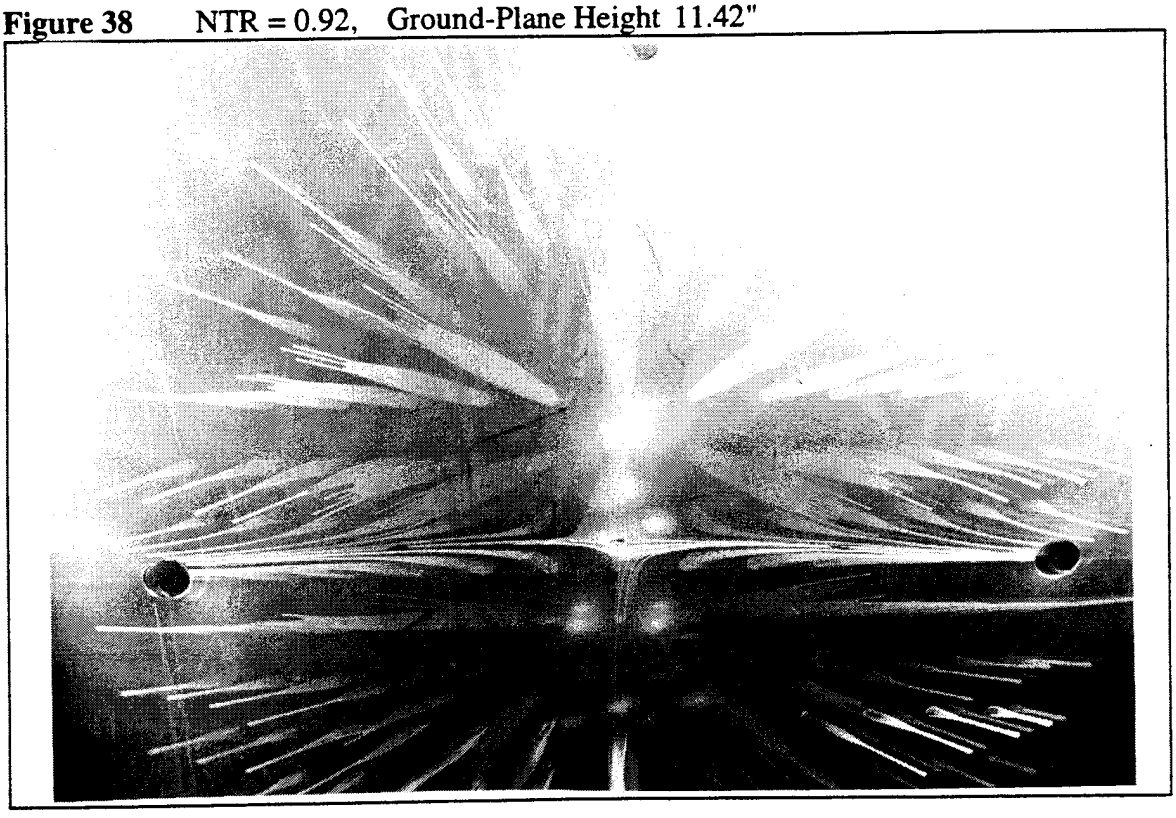

Figure 39 NTR = 0.92, Ground-Plane Height 17.13"

II. NTR = 0.92 WALLS STRUTS

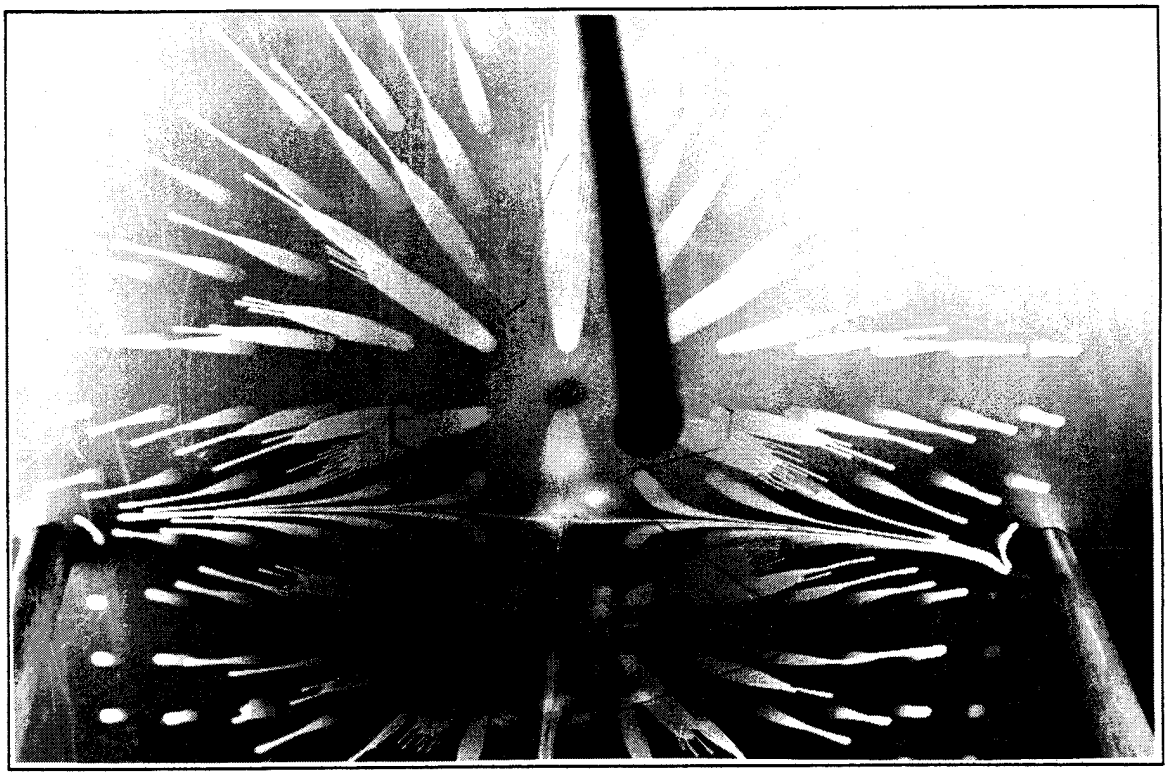

Figure 40 NTR = 0.92, Ground-Plane Height 6.85"

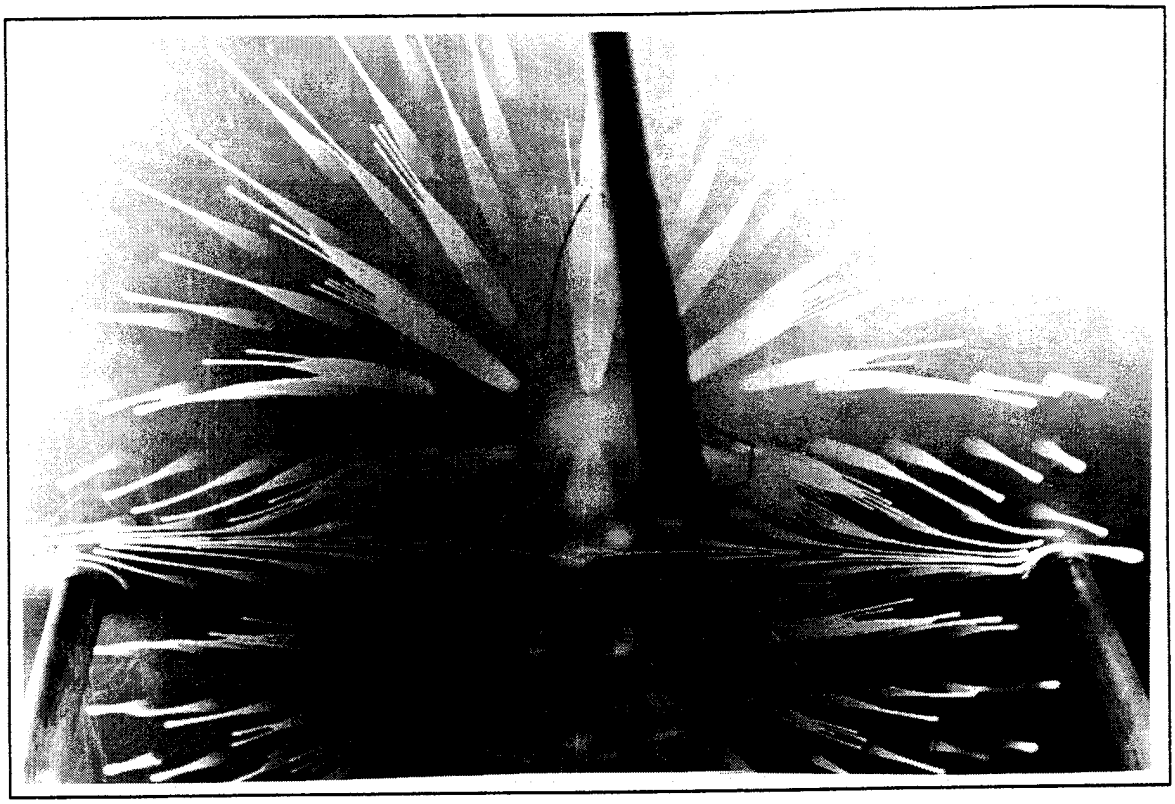

Figure 41 NTR = 0.92, Ground-Plane Height 9.14"

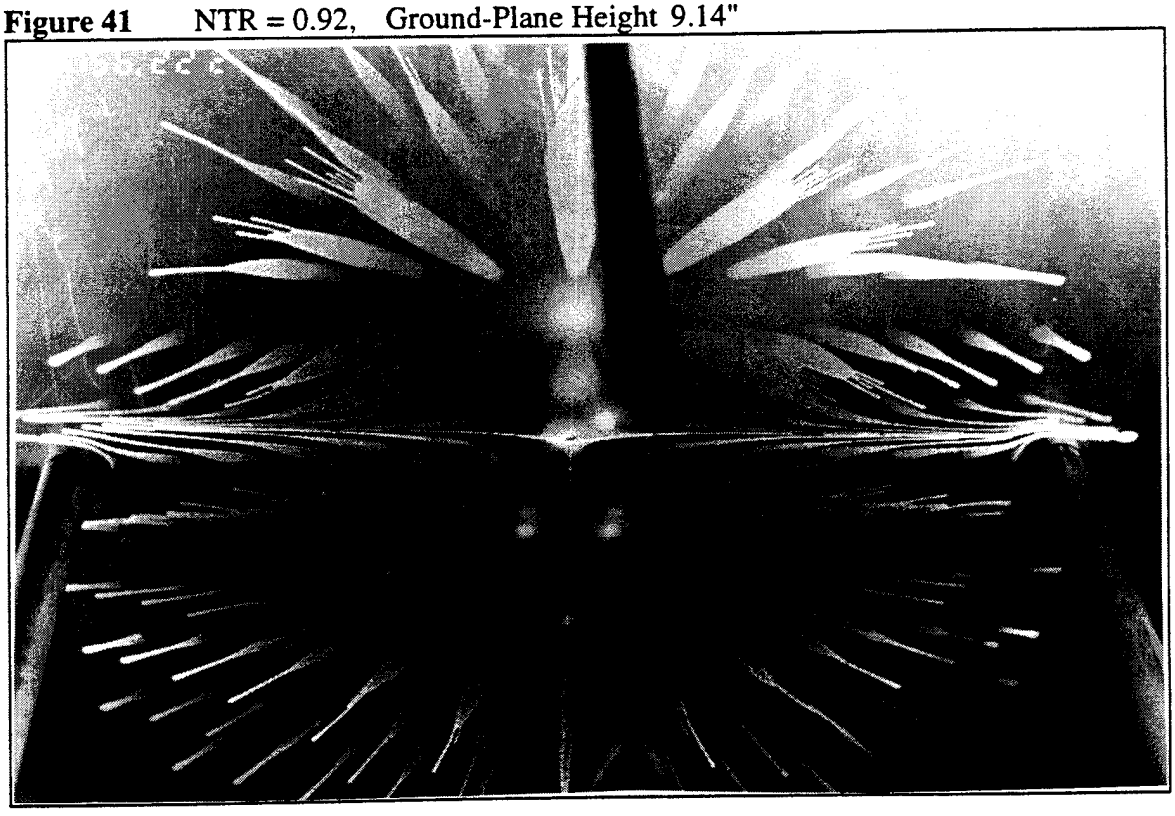

Figure 42 NTR = 0.92, Ground-Plane Height 11.42"

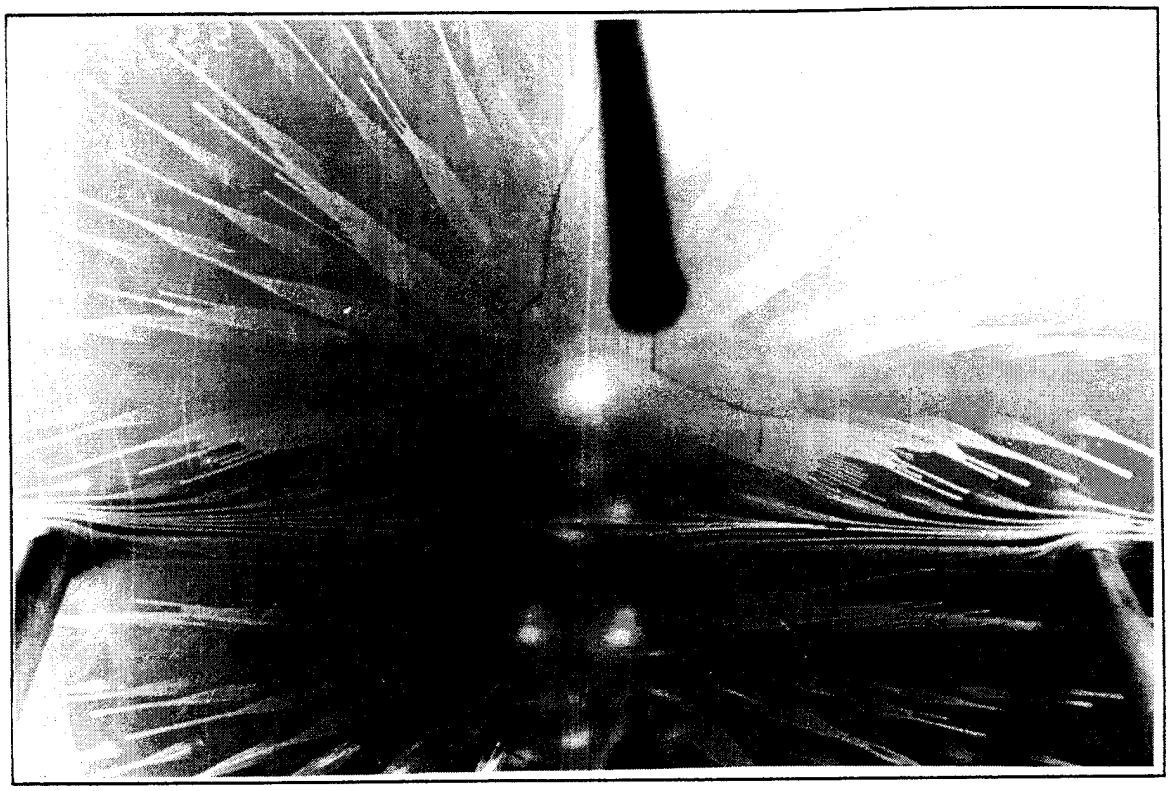

Figure 43 NTR = 0.92, Ground-Plane Height 17.13"

III. NTR = 0.92 NO WALLS STRUTS

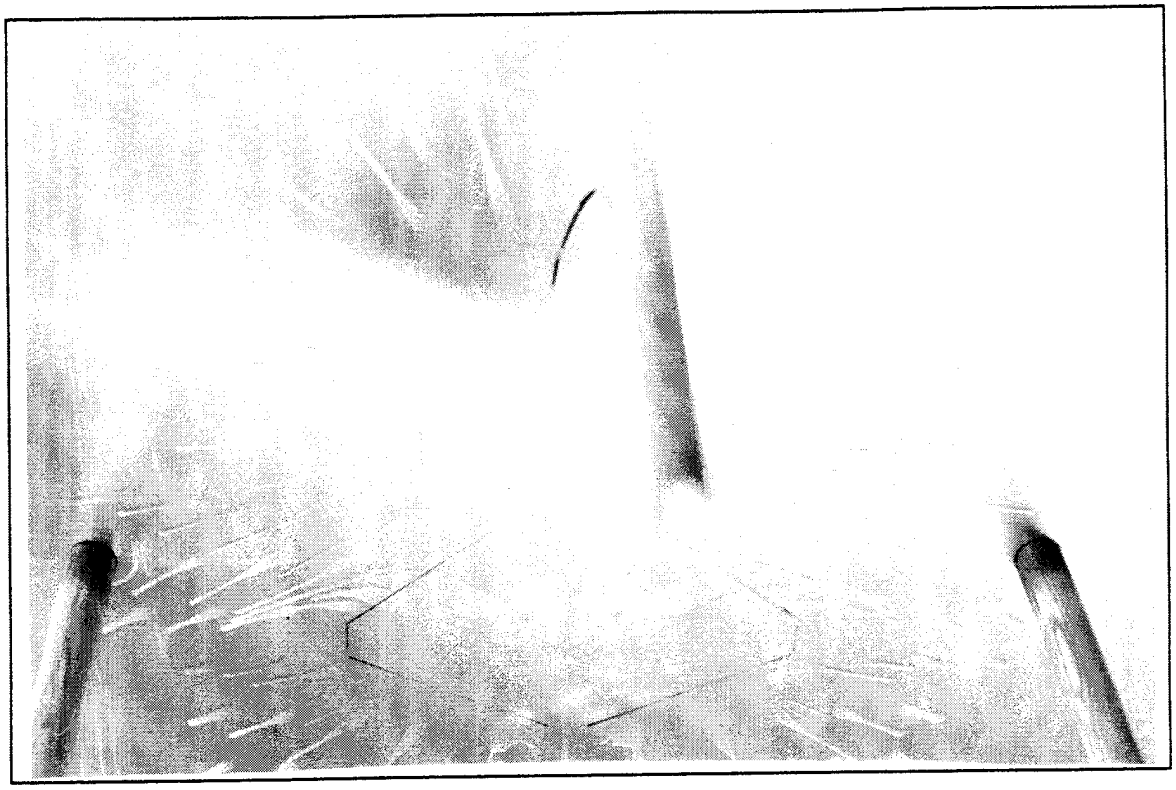

Figure 44 NTR = 0.92, Ground-Plane Height 1.14"

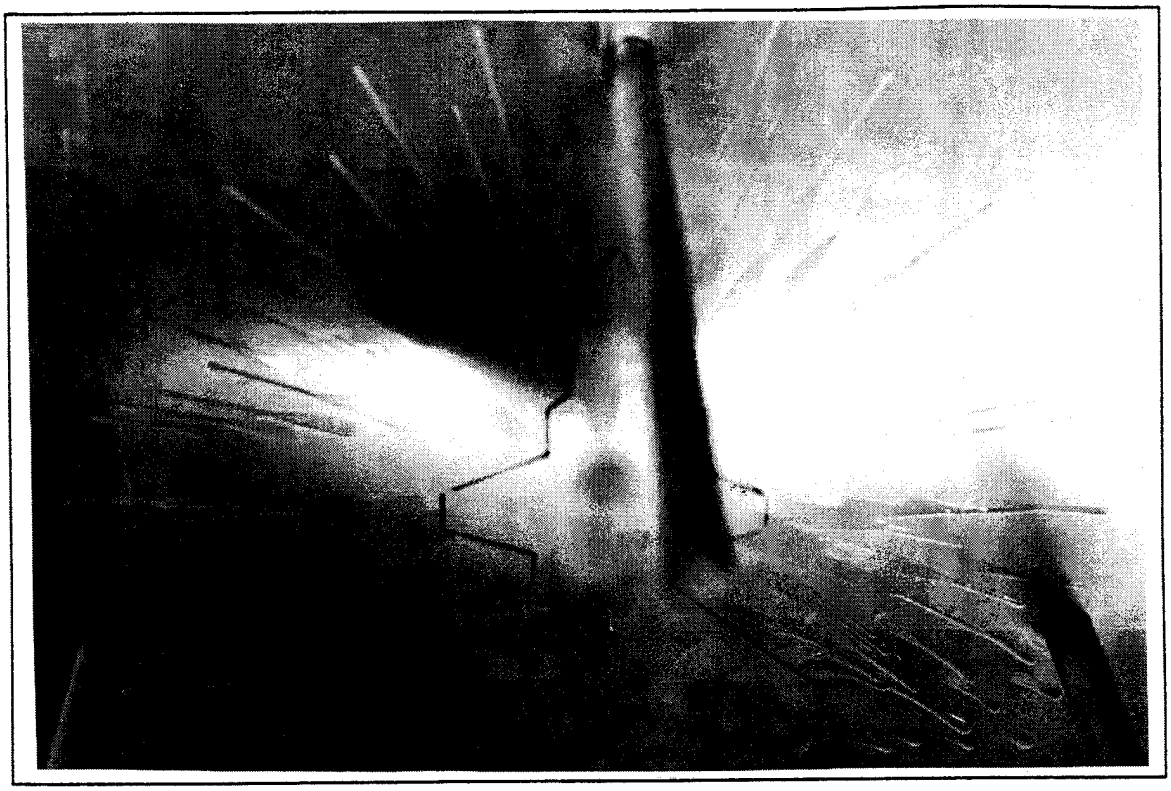

Figure 45 NTR = 0.92, Ground-Plane Height 2.28"

Figure 46 NTR = 0.92, Ground-Plane Height 4.57"

Figure 47 NTR = 0.92, Ground-Plane Height 6.85"

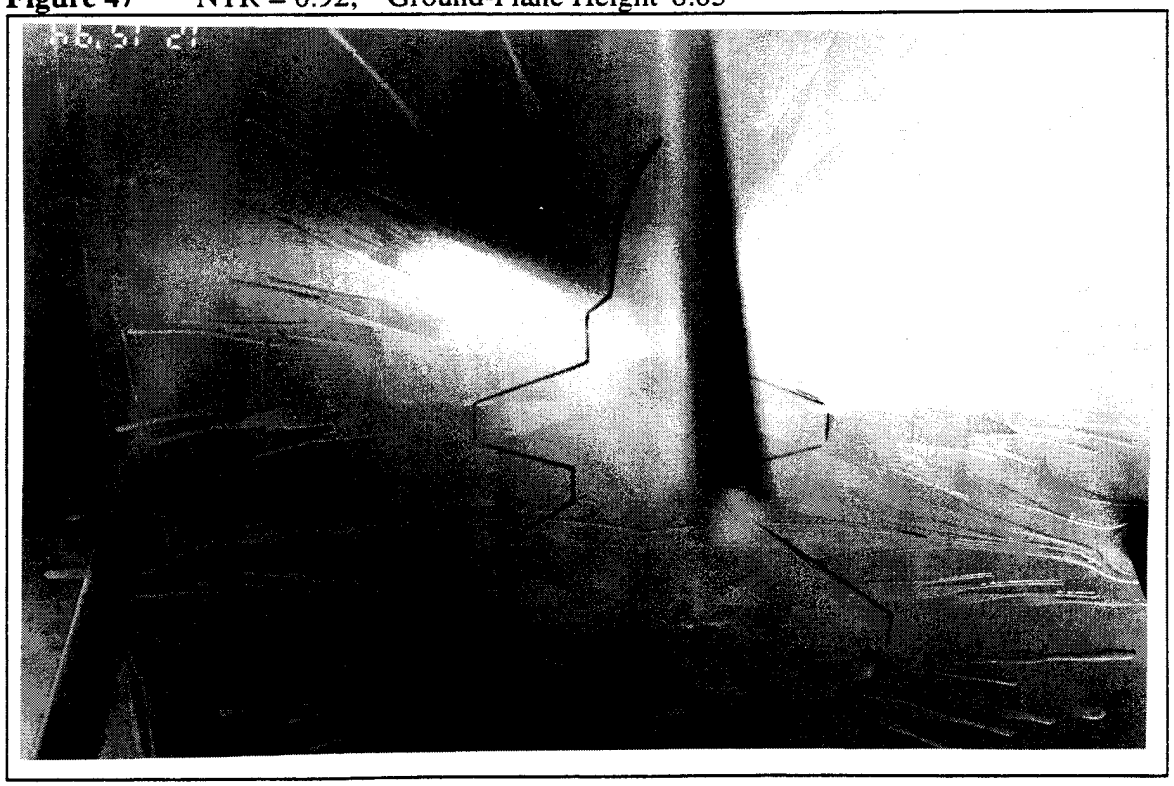

Figure 48 NTR = 0.92, Ground-Plane Height 9.14"

Figure 49 NTR = 0.92, Ground-Plane Height 11.42"

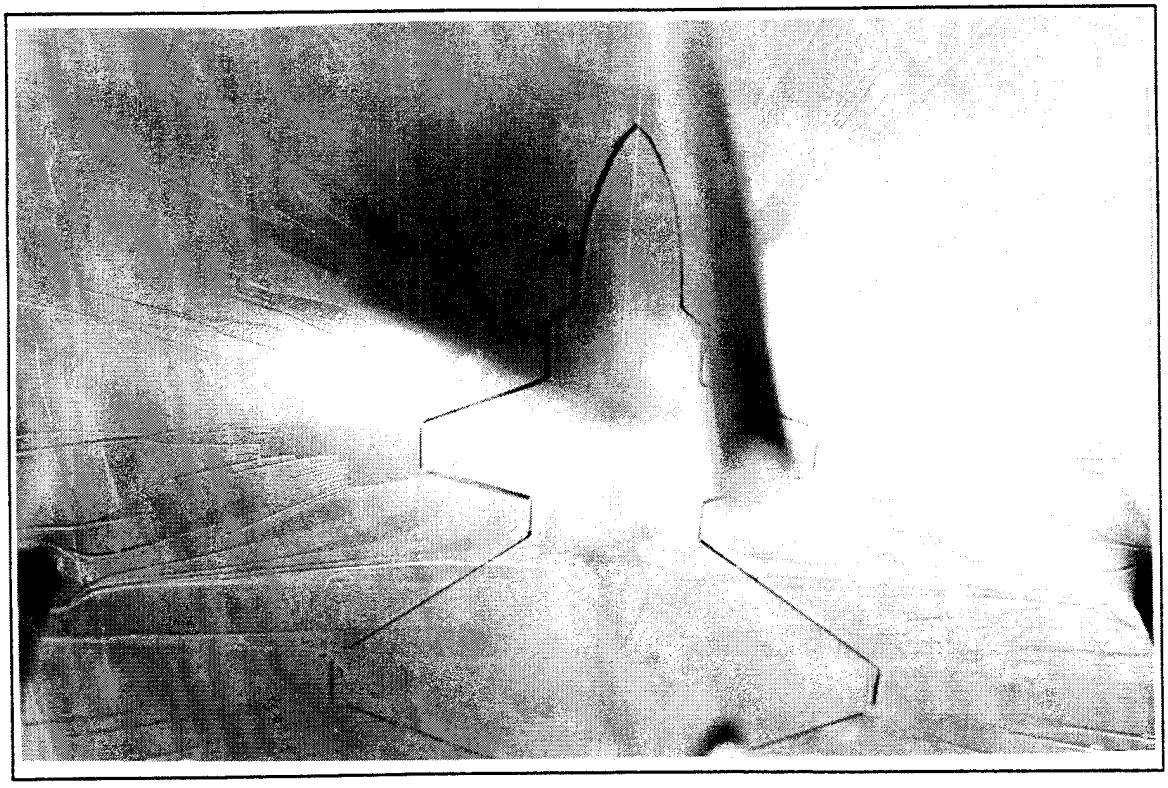

Figure 50 NTR = 0.92, Ground-Plane Height 17.13"

IV. NTR = 1.5 NO WALLS NO STRUTS

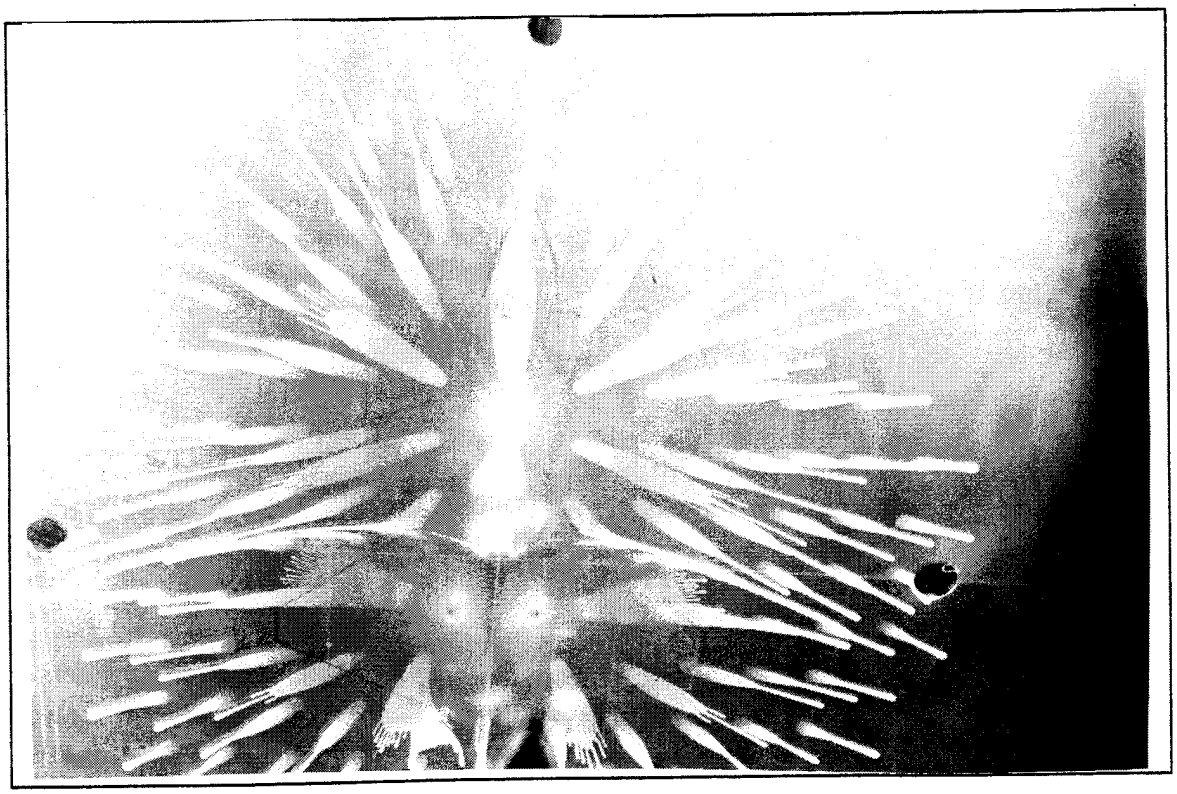

Figure 51 NTR = 1.5, Ground-Plane Height 1.14"

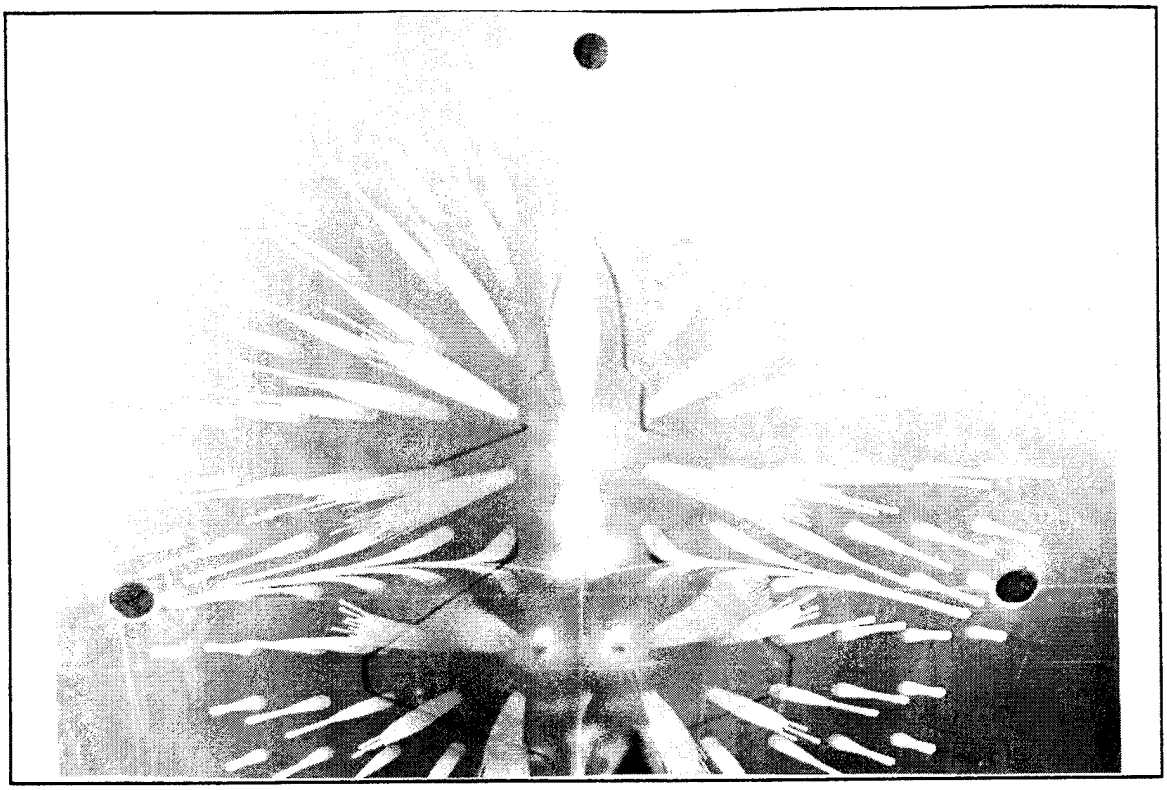

Figure 52 NTR = 1.5, Ground-Plane Height 2.28"

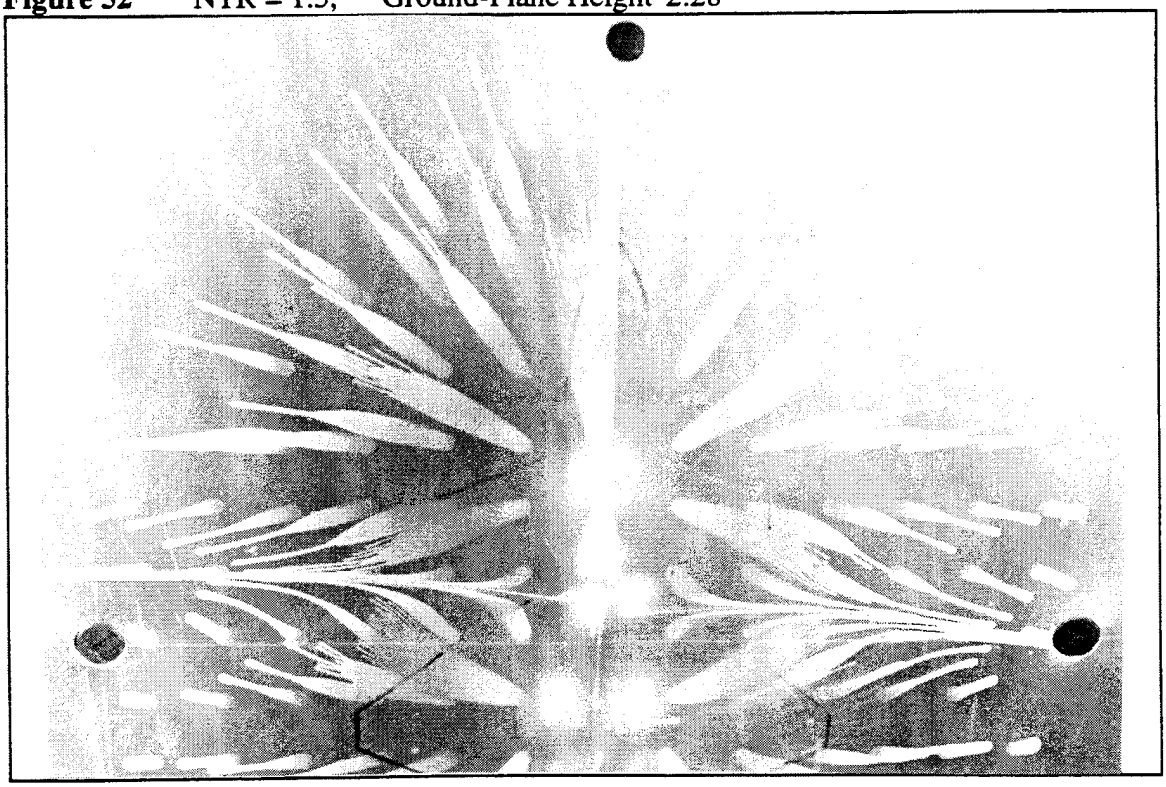

Figure 53 NTR = 1.5, Ground-Plane Height 4.57"

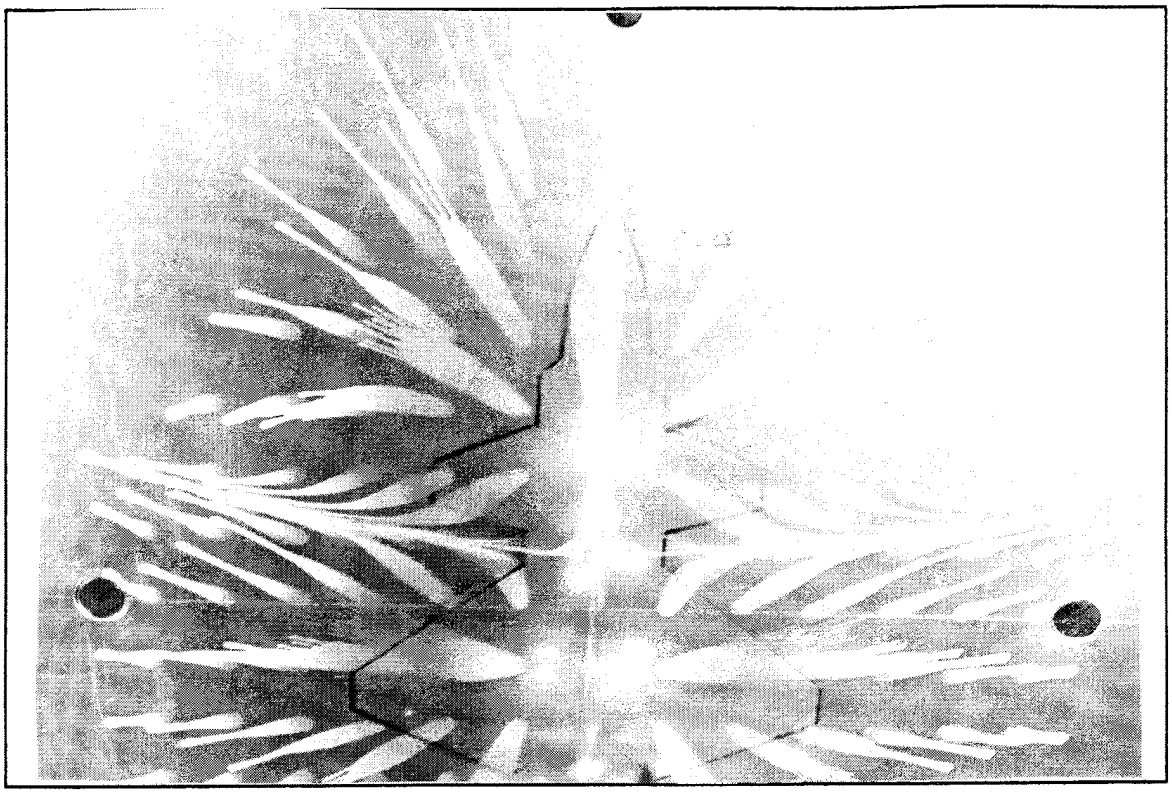

Figure 54 NTR = 1.5, Ground-Plane Height 6.85"

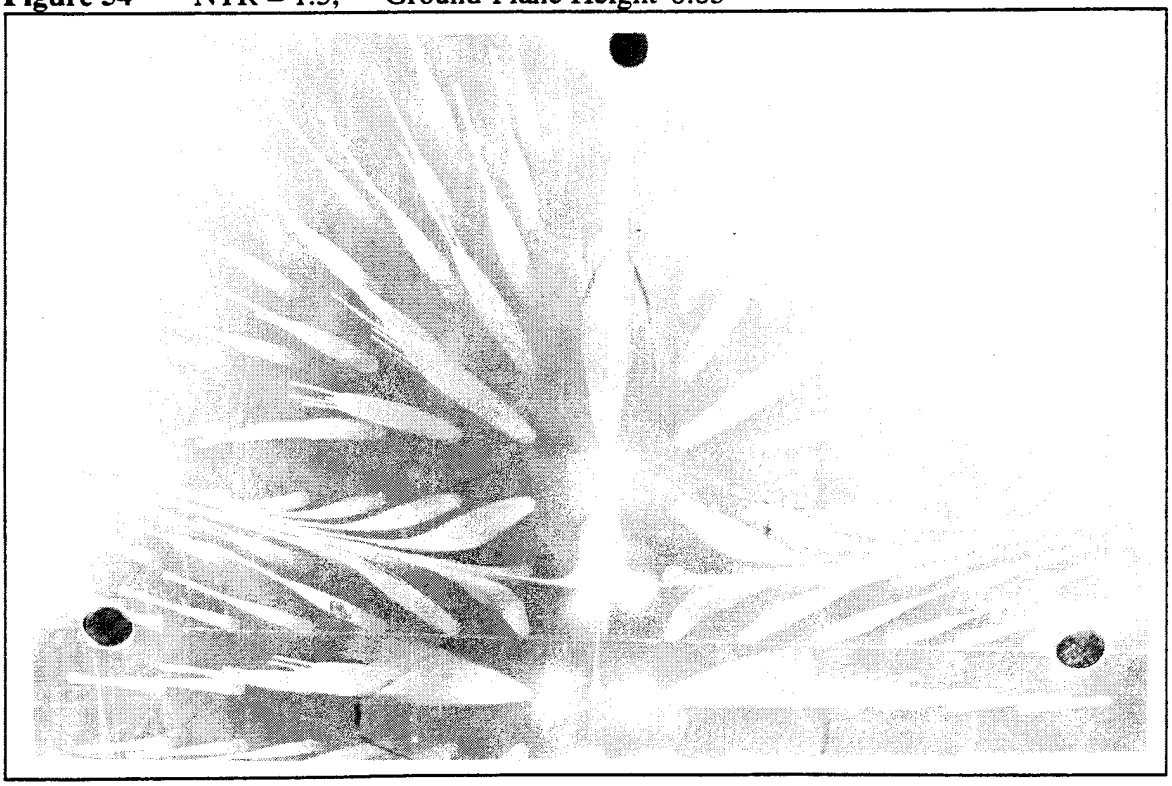

Figure 55 NTR = 1.5, Ground-Plane Height 9.14"

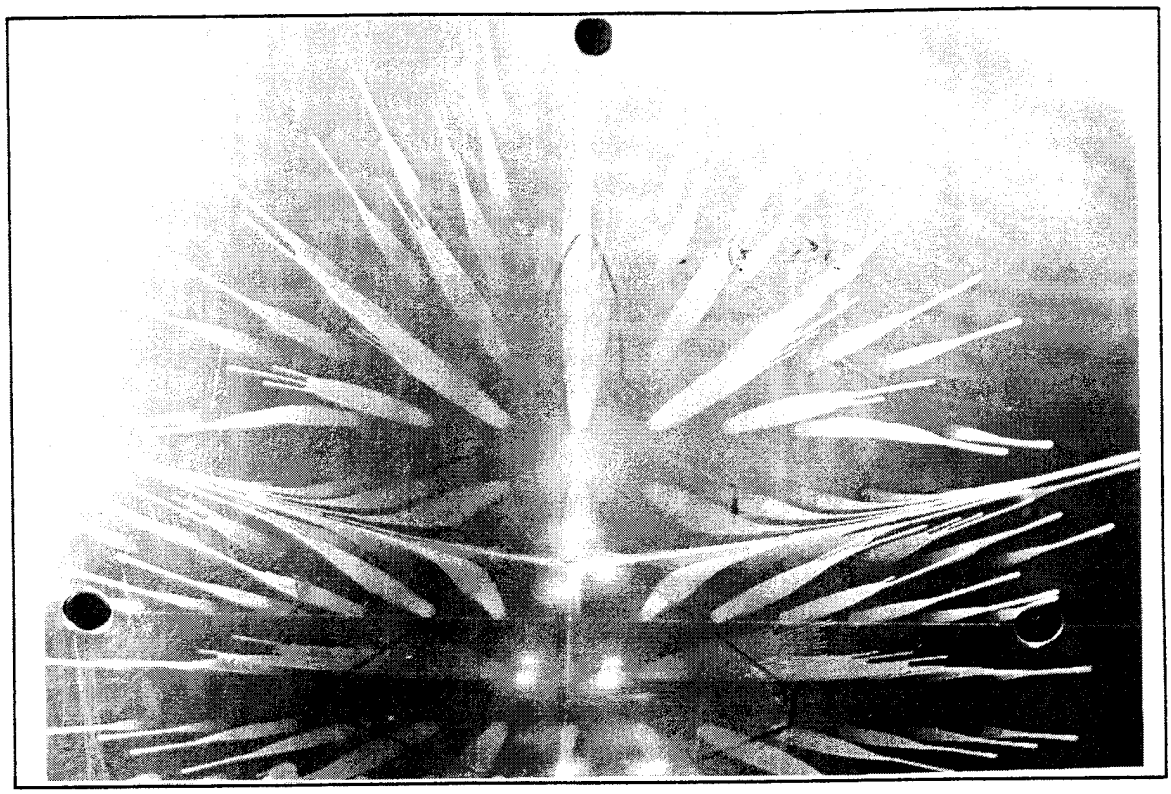

Figure 56 NTR = 1.5, Ground-Plane Height 11.42"

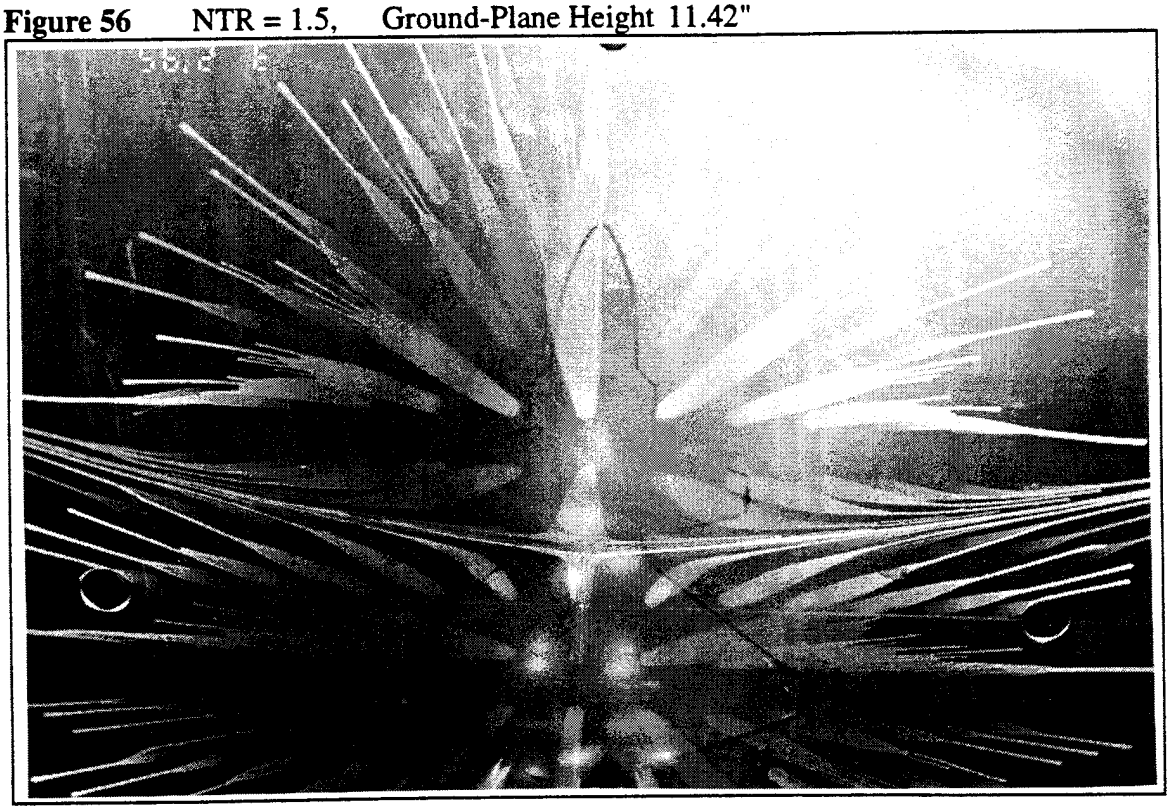

Figure 57 NTR = 1.5, Ground-Plane Height 17.13"

V. NTR = 1.5 WALLS STRUTS

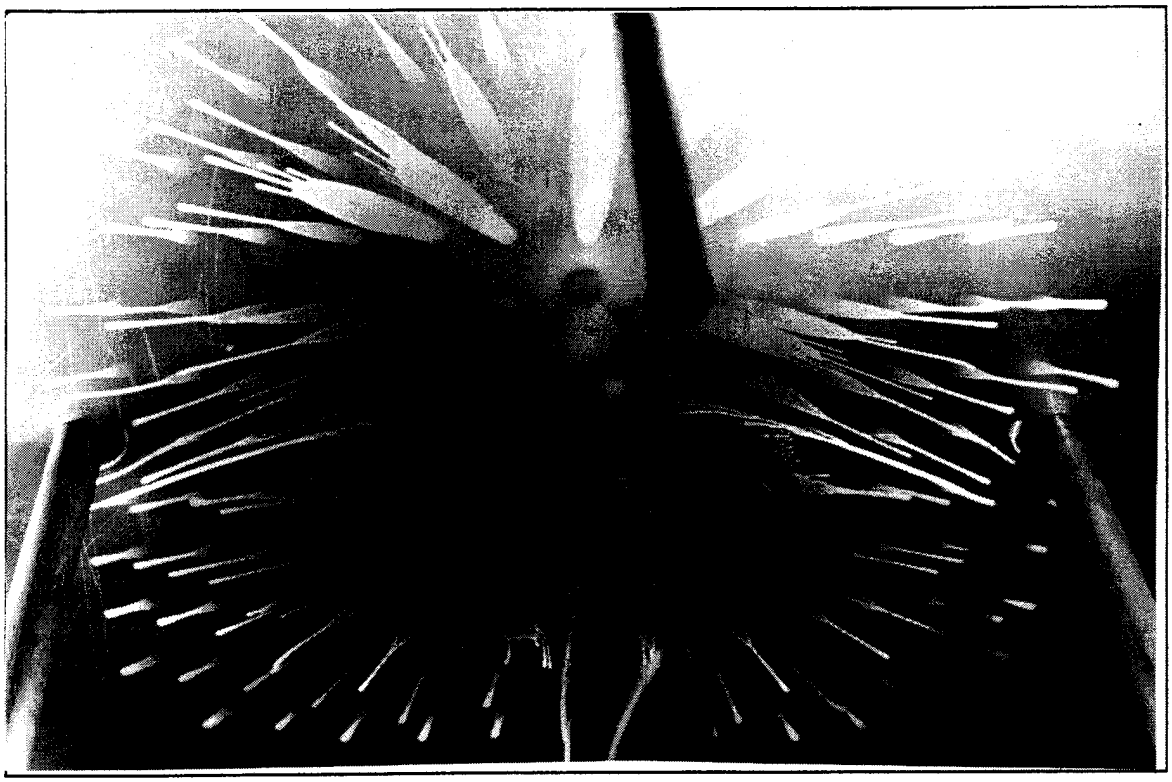

Figure 58 NTR = 1.5, Ground-Plane Height 1.14"

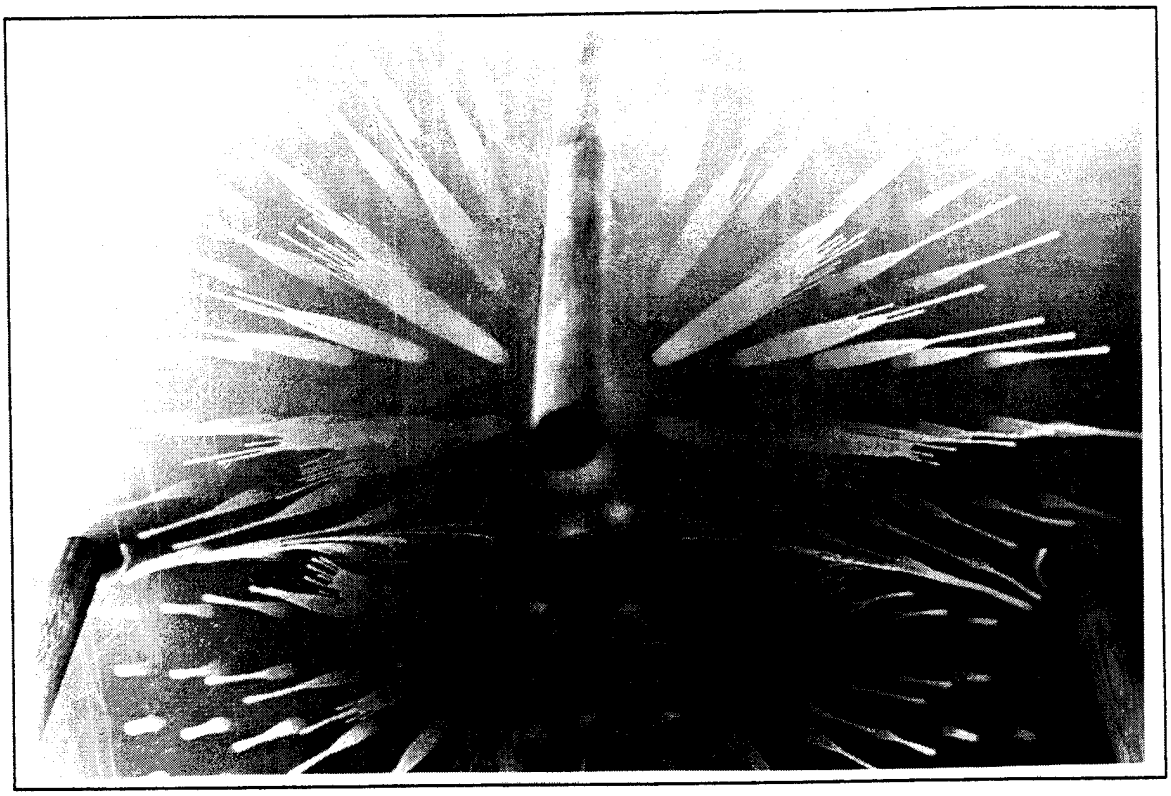

Figure 59 NTR = 1.5, Ground-Plane Height 2.28"

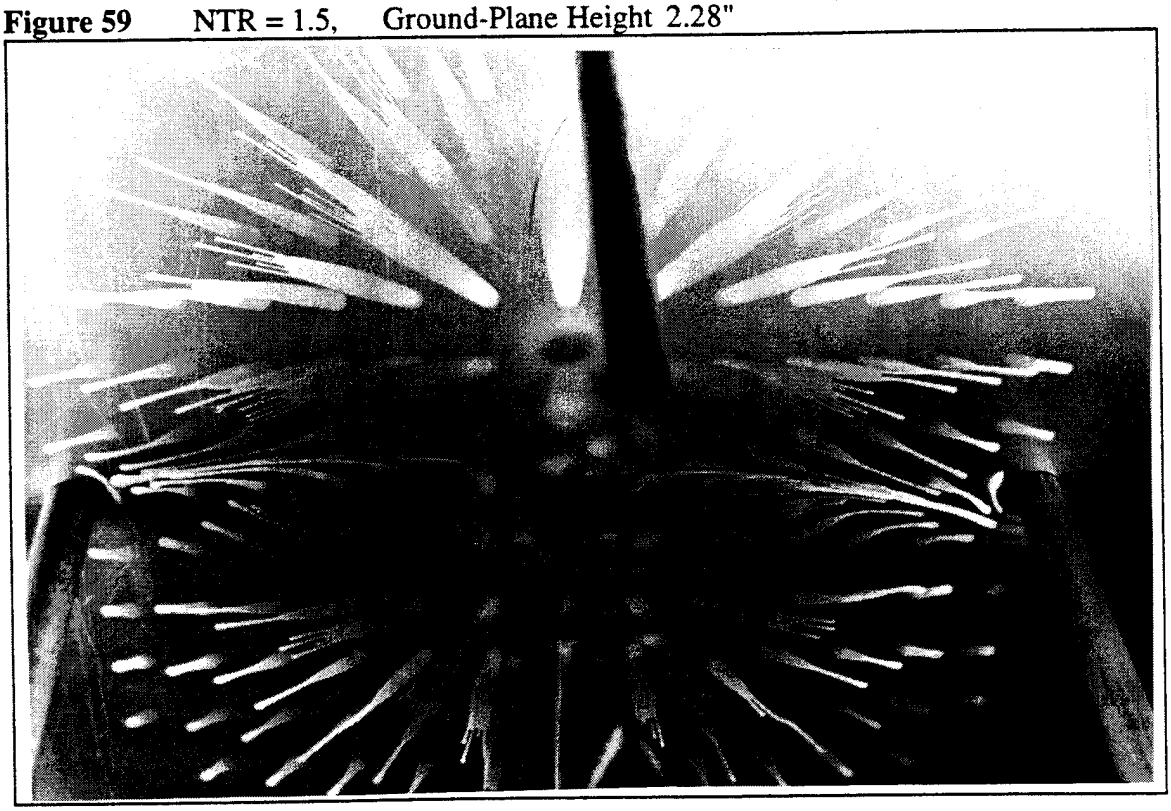

Figure 60 NTR = 1.5, Ground-Plane Height 4.57"

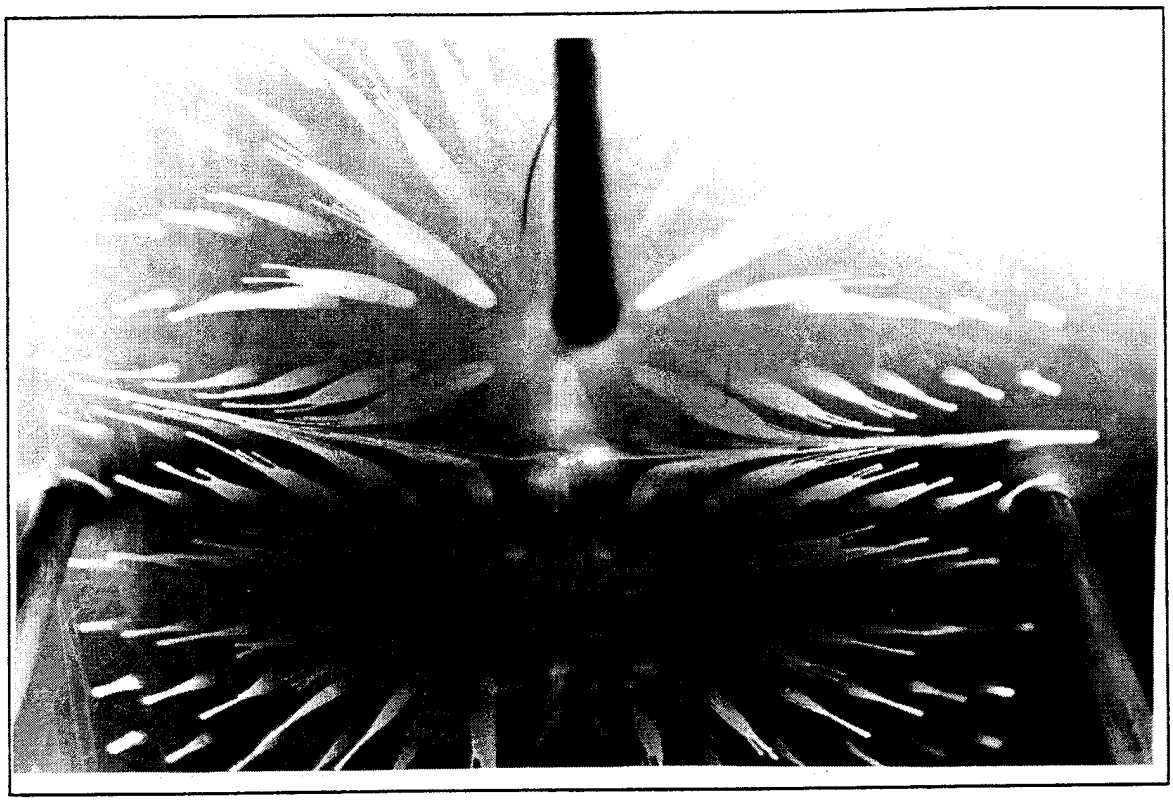

Figure 61 NTR = 1.5, Ground-Plane Height 6.85"

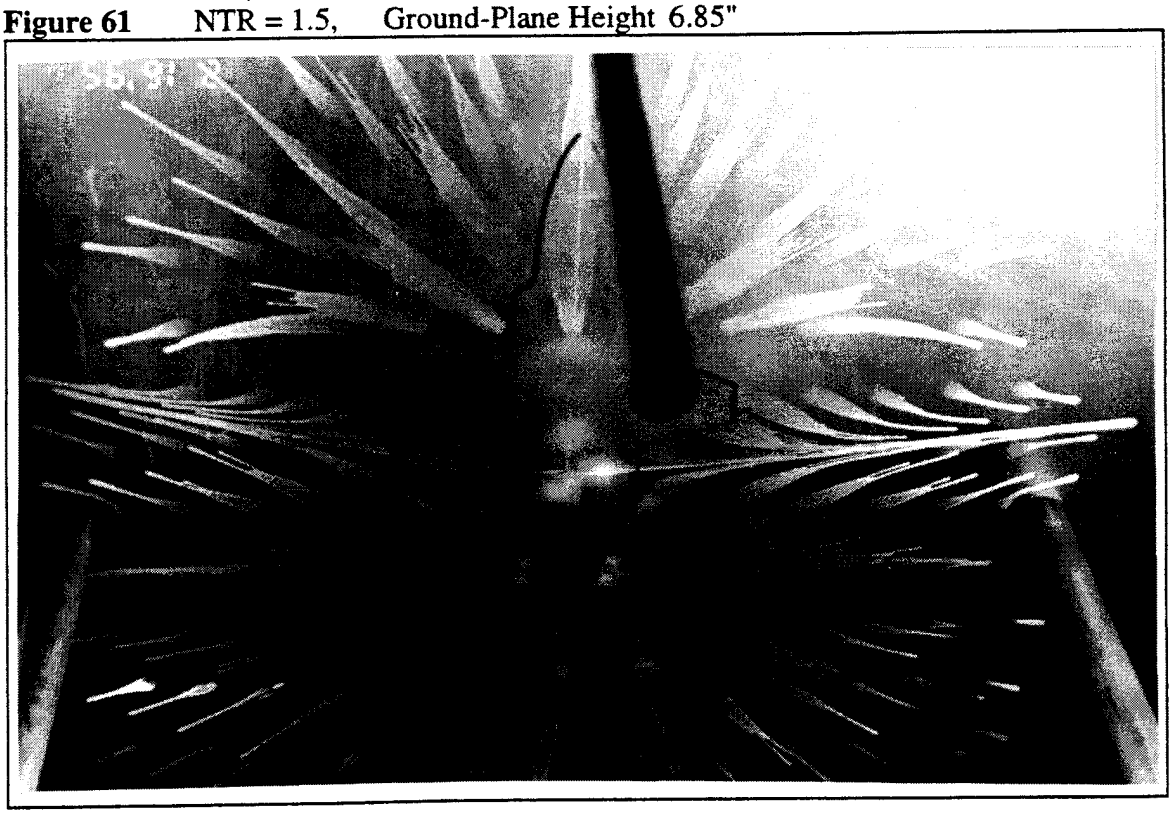

Figure 62 NTR = 1.5, Ground-Plane Height 9.14"

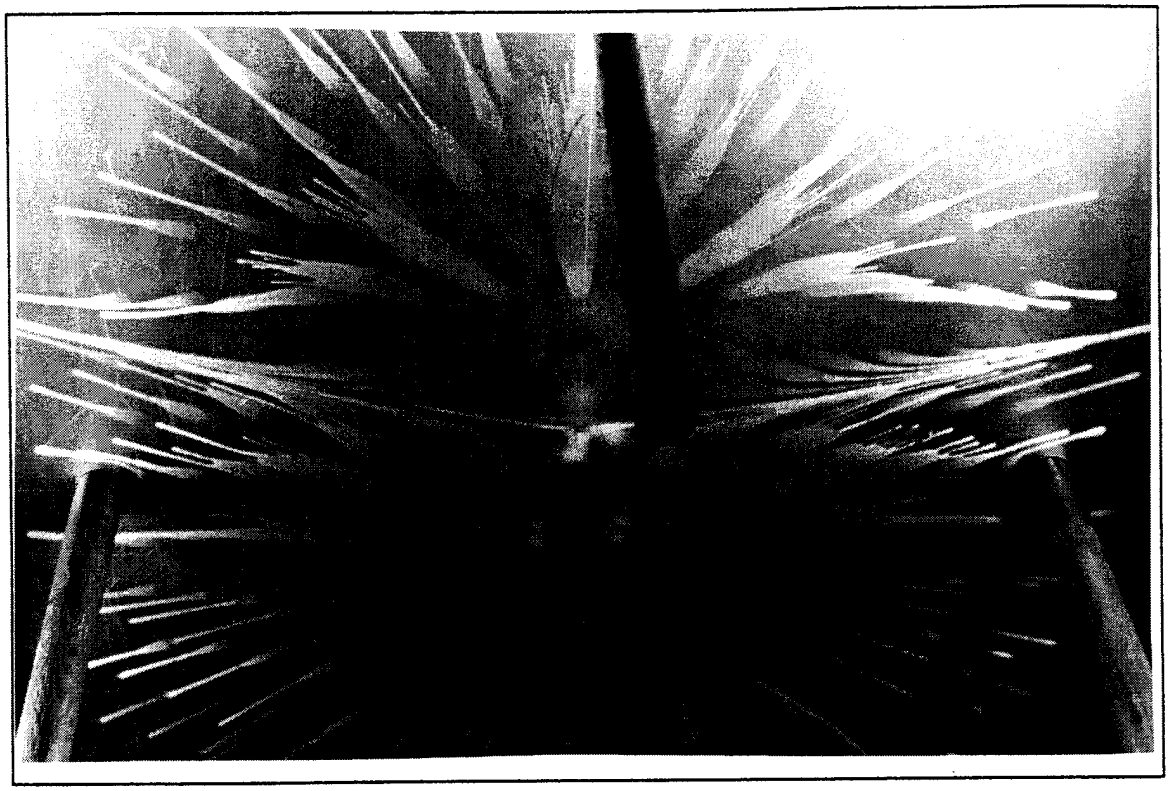

Figure 63 NTR = 1.5, Ground-Plane Height 11.42"

VI. NTR = 1.5 NO WALLS STRUTS

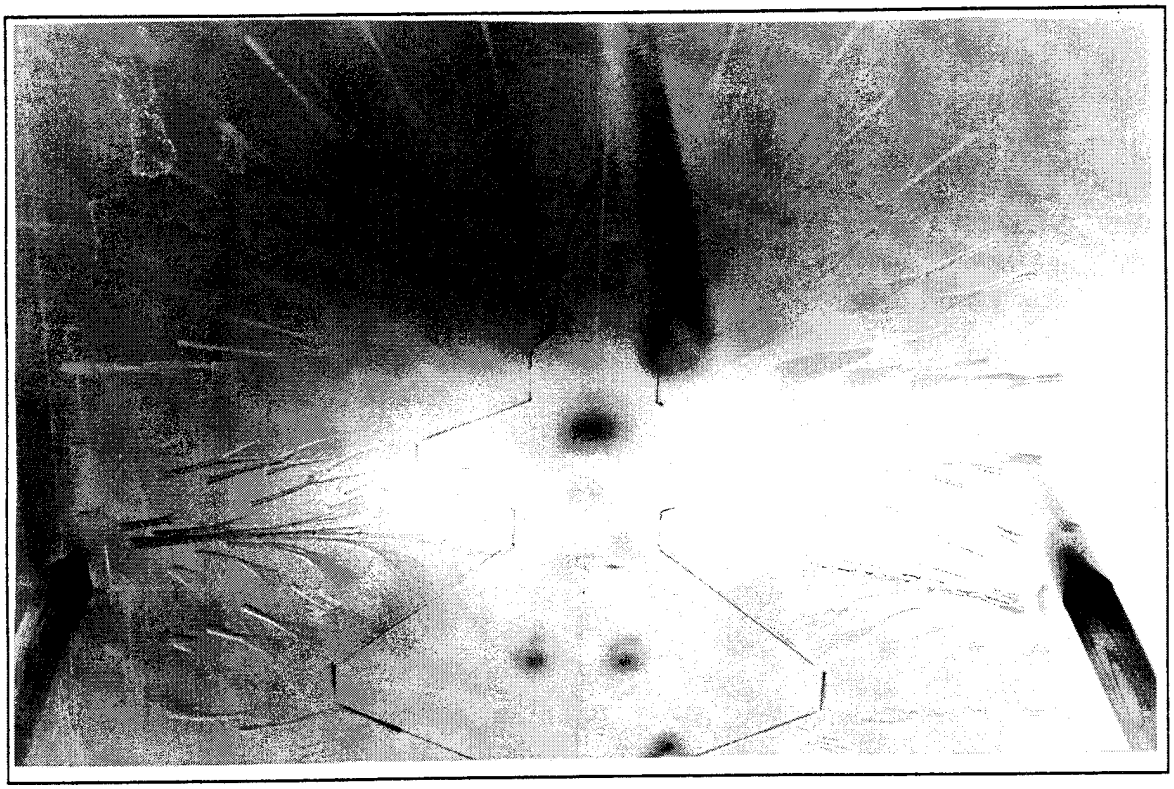

Figure 64 NTR = 1.5, Ground-Plane Height 4.57"

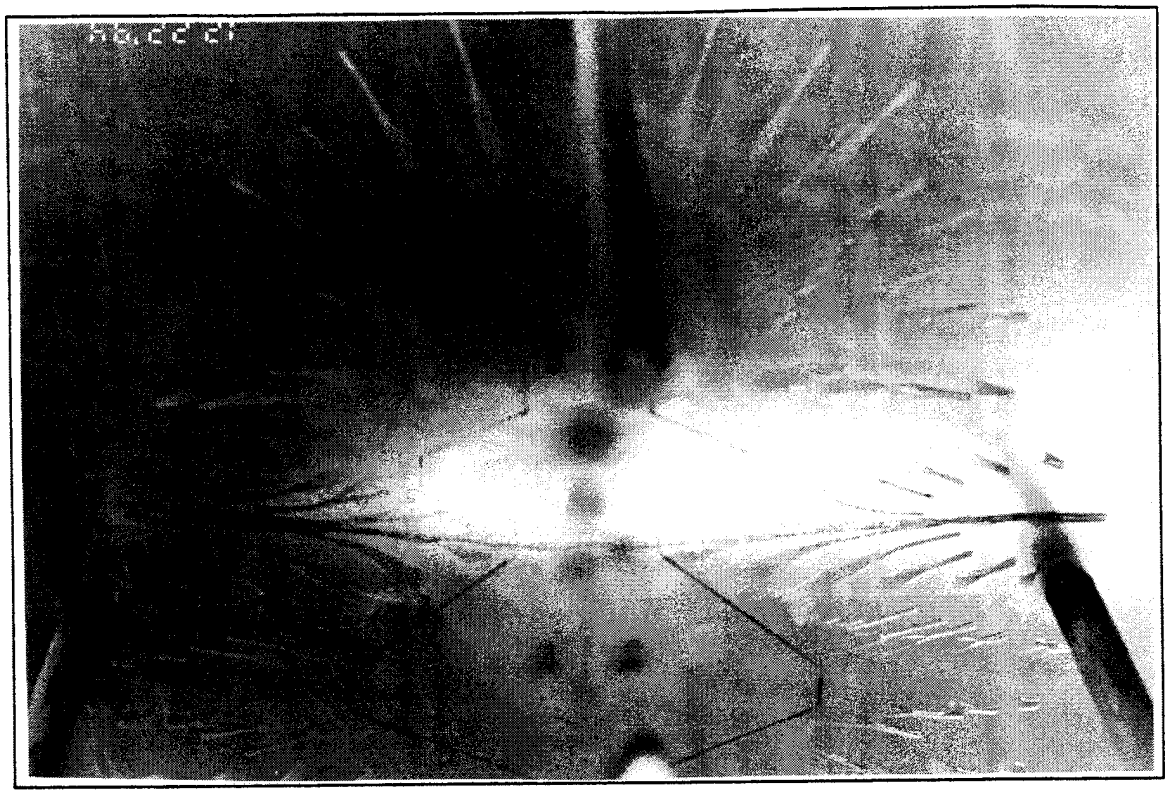

Figure 65 NTR = 1.5, Ground-Plane Height 6.85"

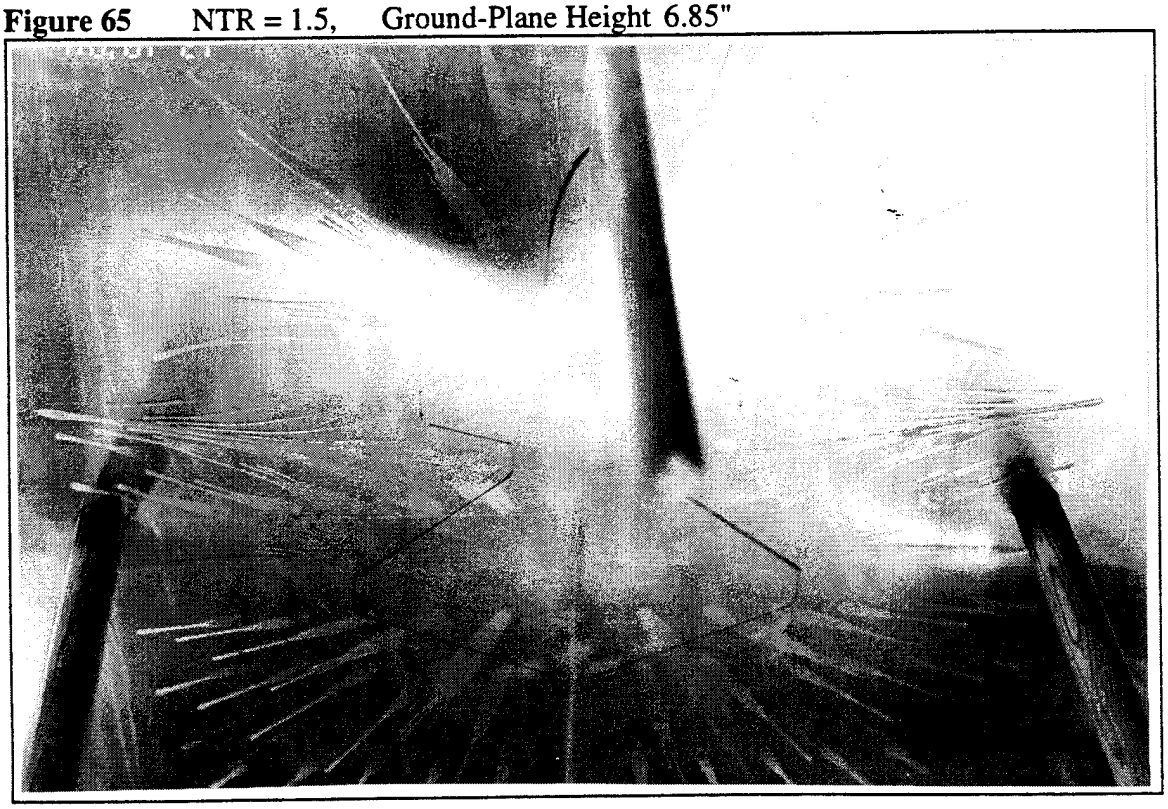

Figure 66 NTR = 1.5, Ground-Plane Height 9.14"

Figure 67 NTR = 1.5, Ground-Plane Height 11.42"

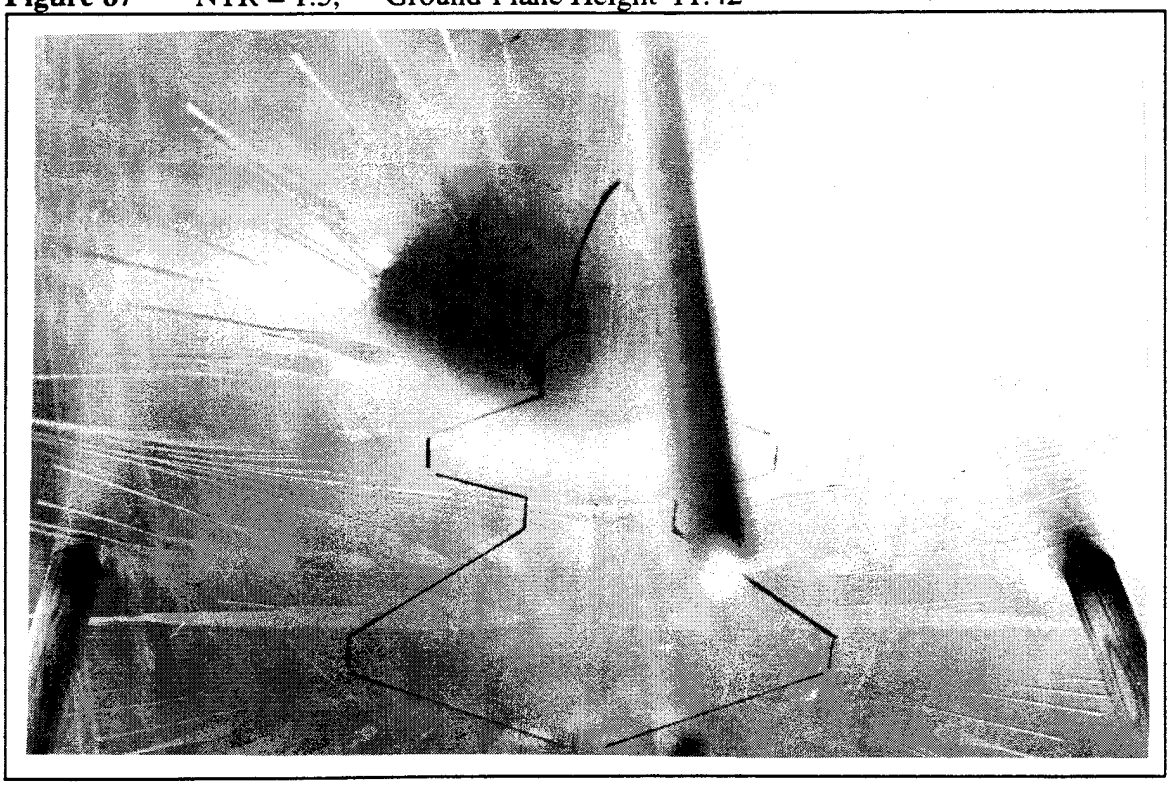

Figure 68 NTR = 1.5, Ground-Plane Height 17.13"

VII. NTR = 4.9 NO WALLS NO STRUTS

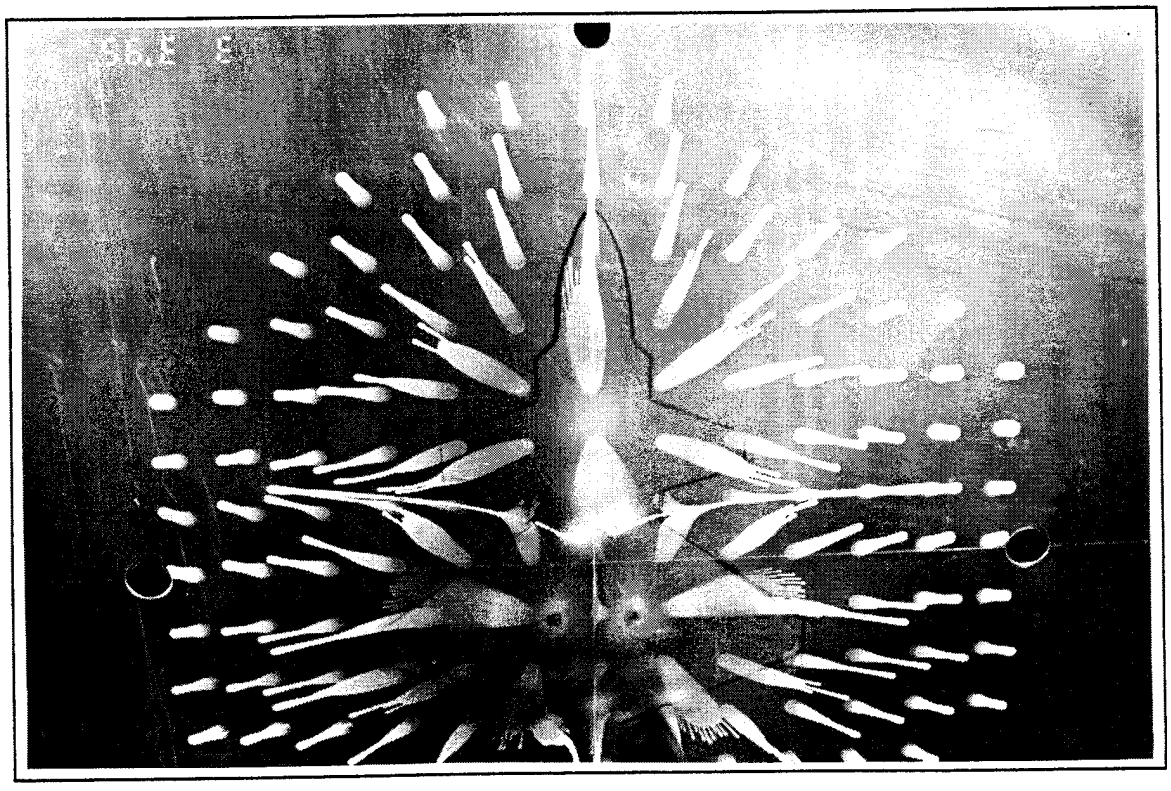

Figure 69 NTR = 4.9, Ground-Plane Height 1.14"

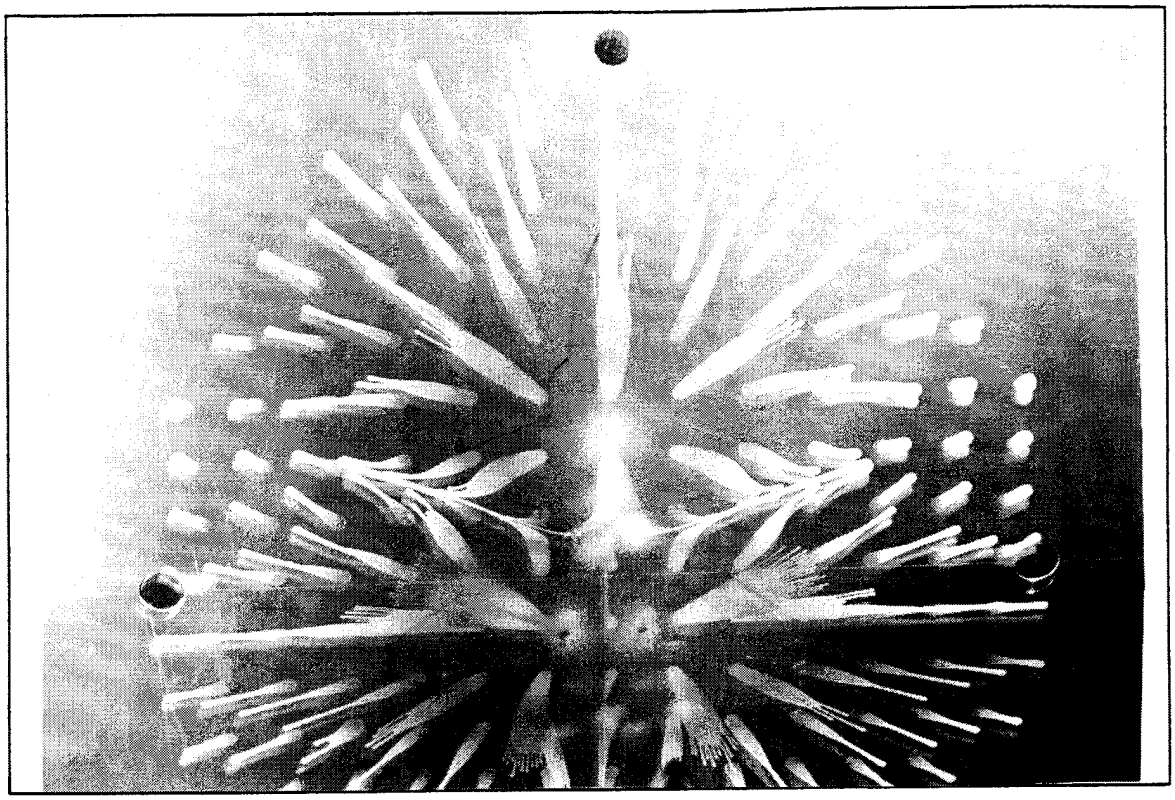

Figure 70 NTR = 4.9, Ground-Plane Height 2.28"

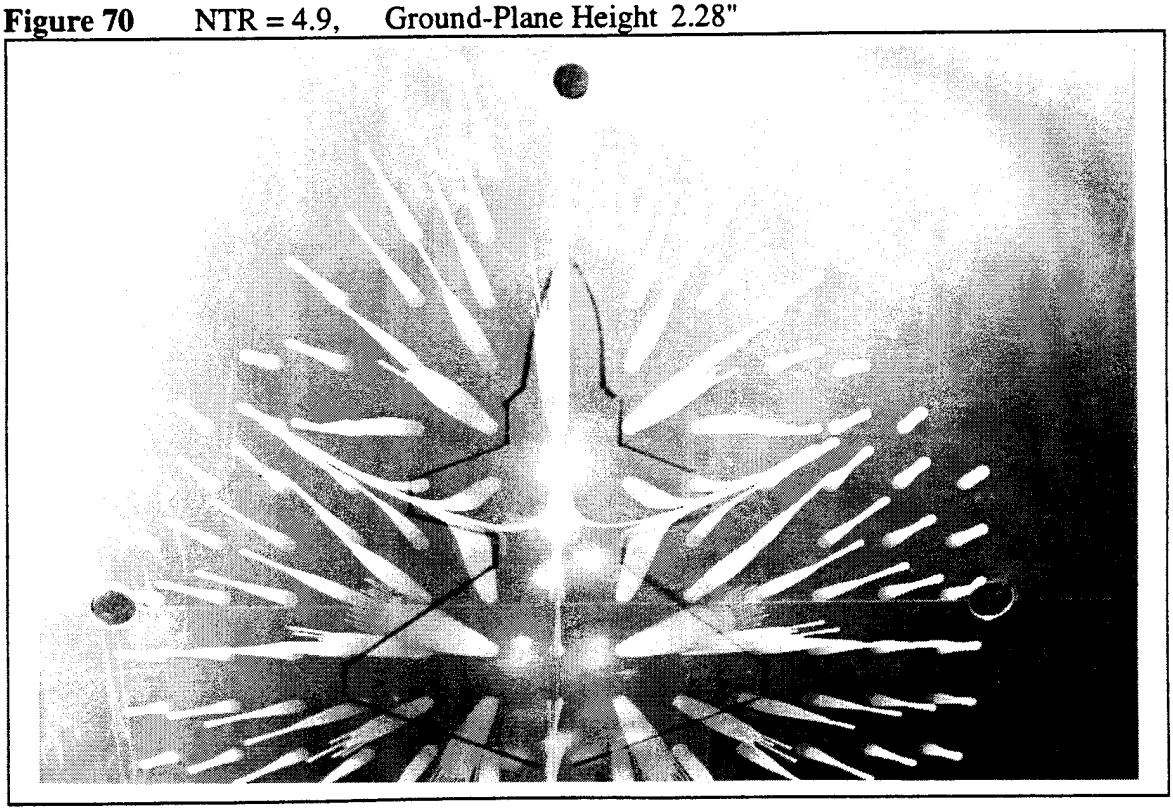

Figure 71 NTR = 4.9, Ground-Plane Height 4.57"

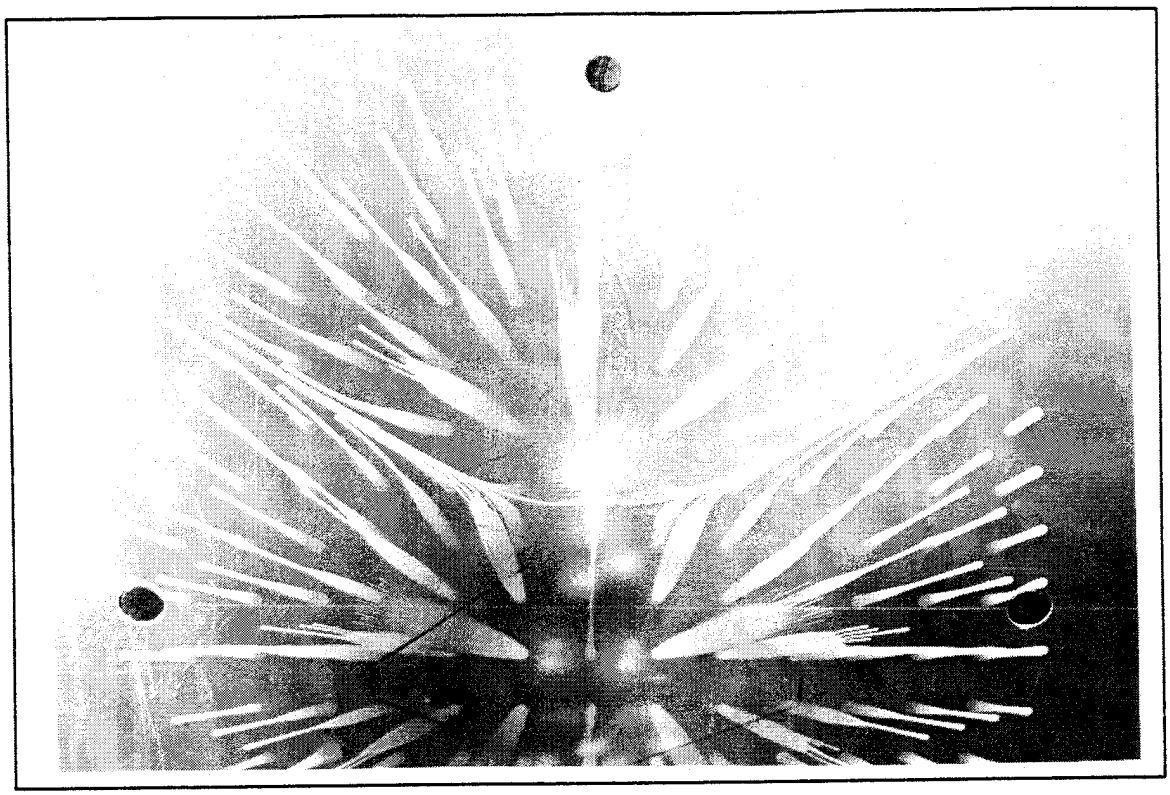

Figure 72 NTR = 4.9, Ground-Plane Height 6.85"

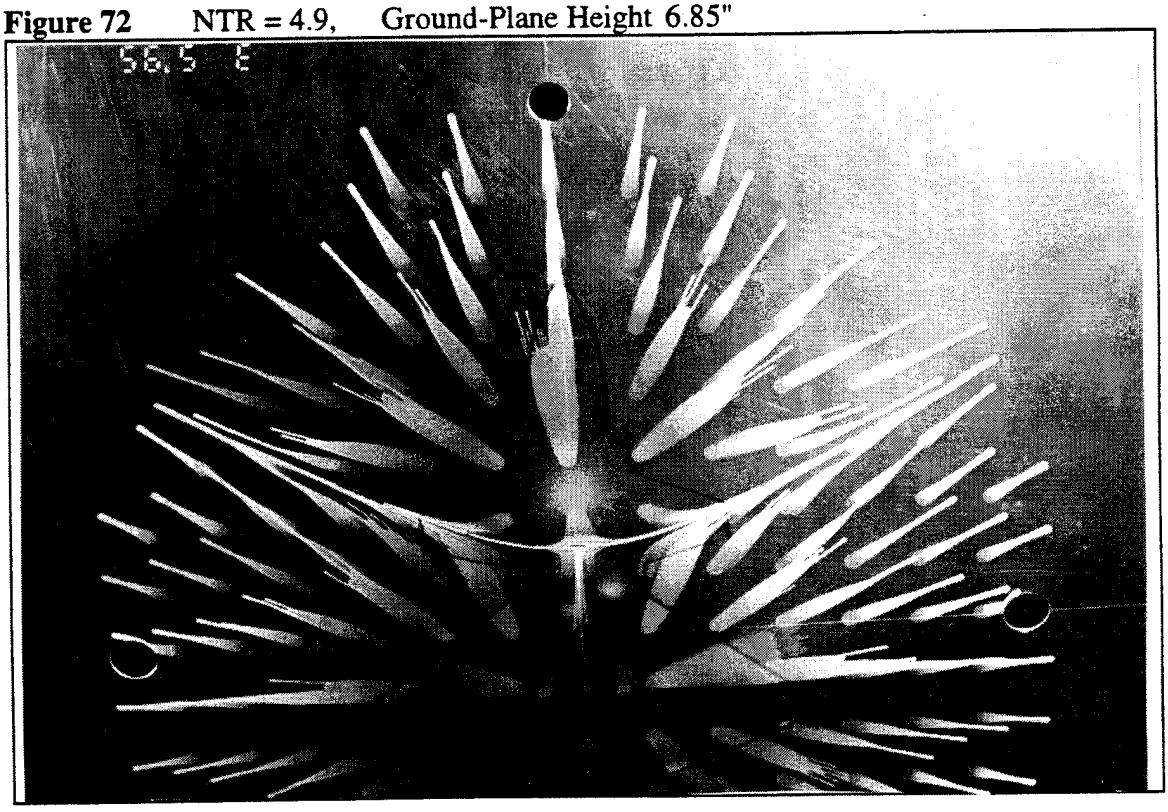

Figure 73 NTR = 4.9, Ground-Plane Height 9.14"

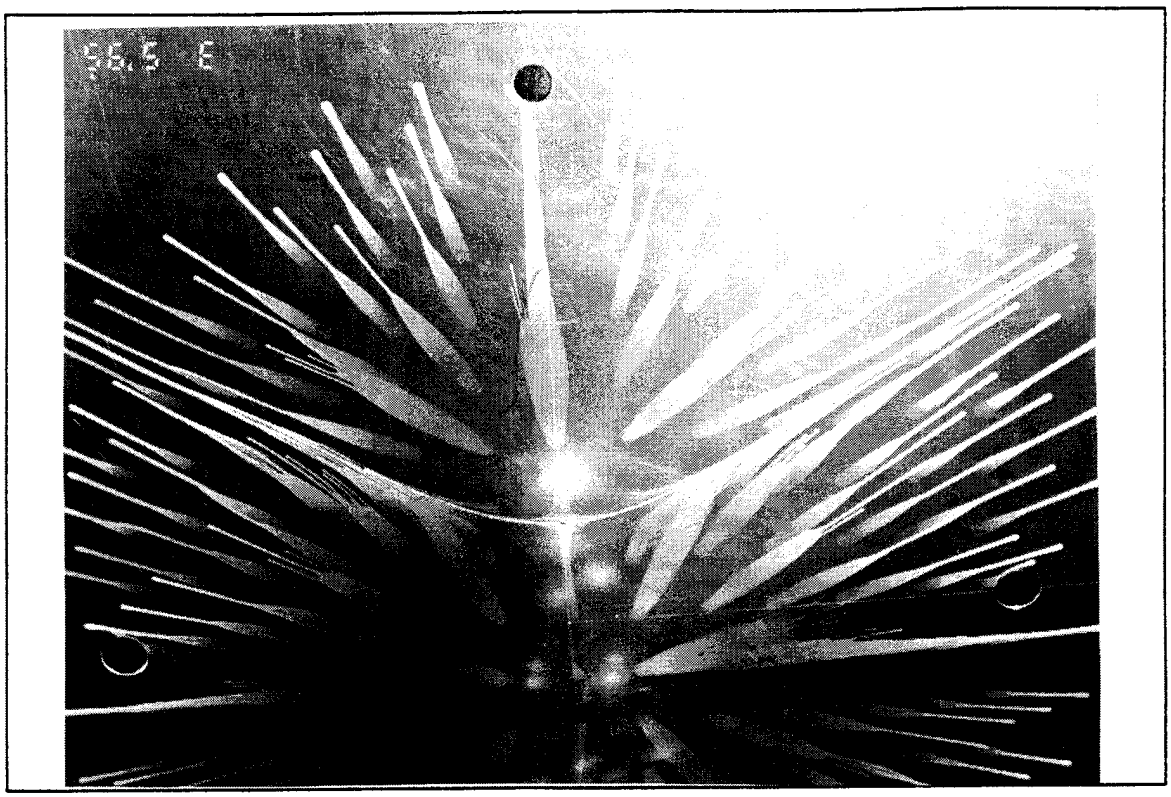

Figure 74 NTR = 4.9, Ground-Plane Height 11.42"

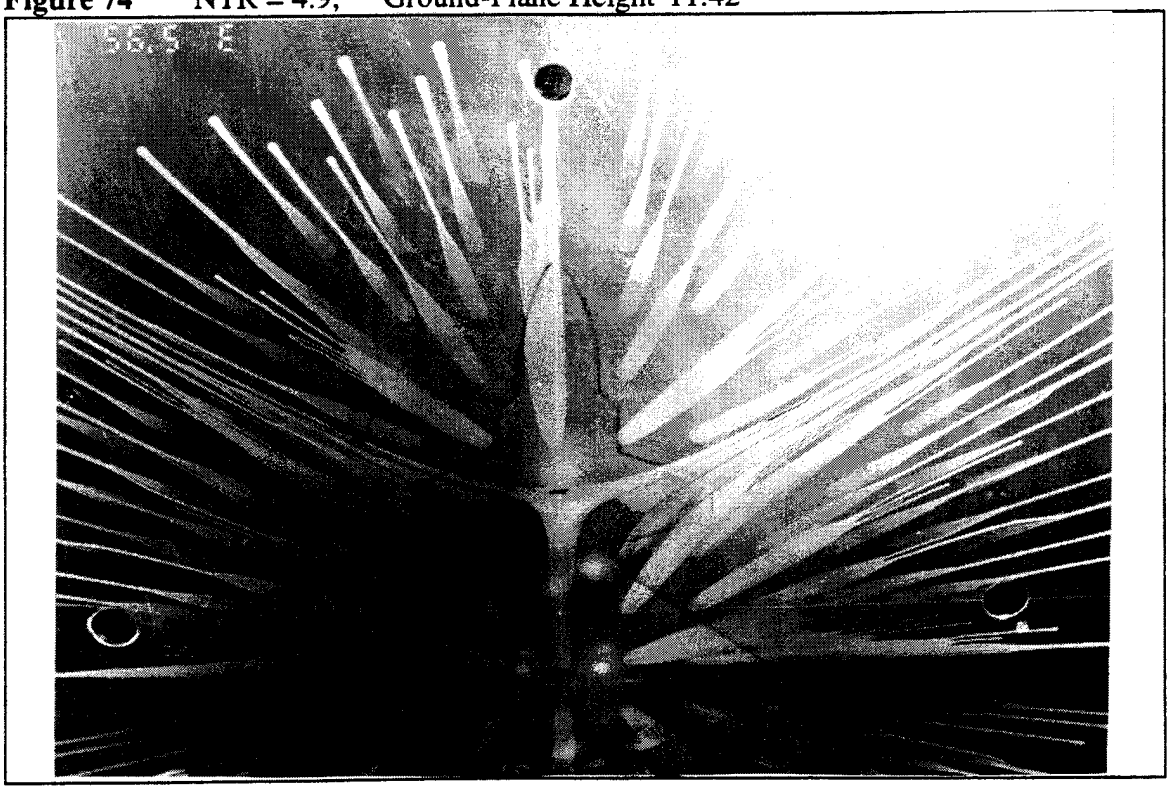

Figure 75 NTR = 4.9, Ground-Plane Height 17.13"

VIII. NTR = 4.9 WALLS STRUTS

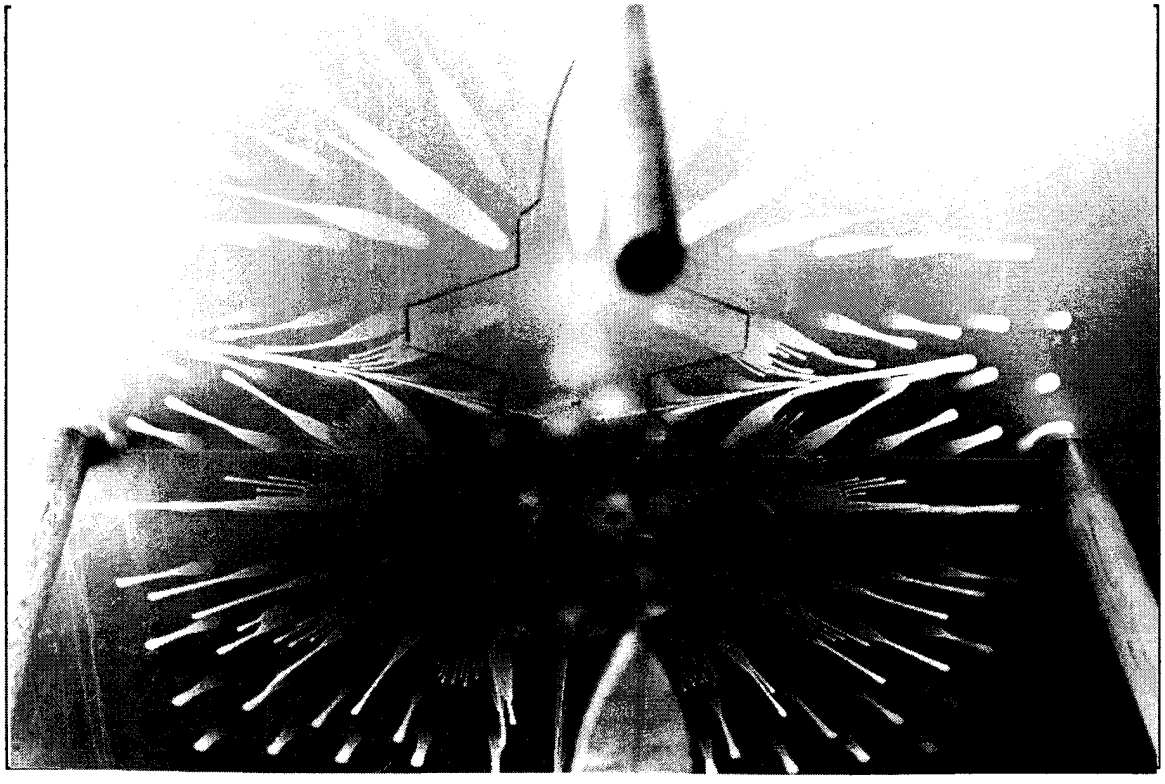

Figure 76 NTR = 4.9, Ground-Plane Height 2.28"

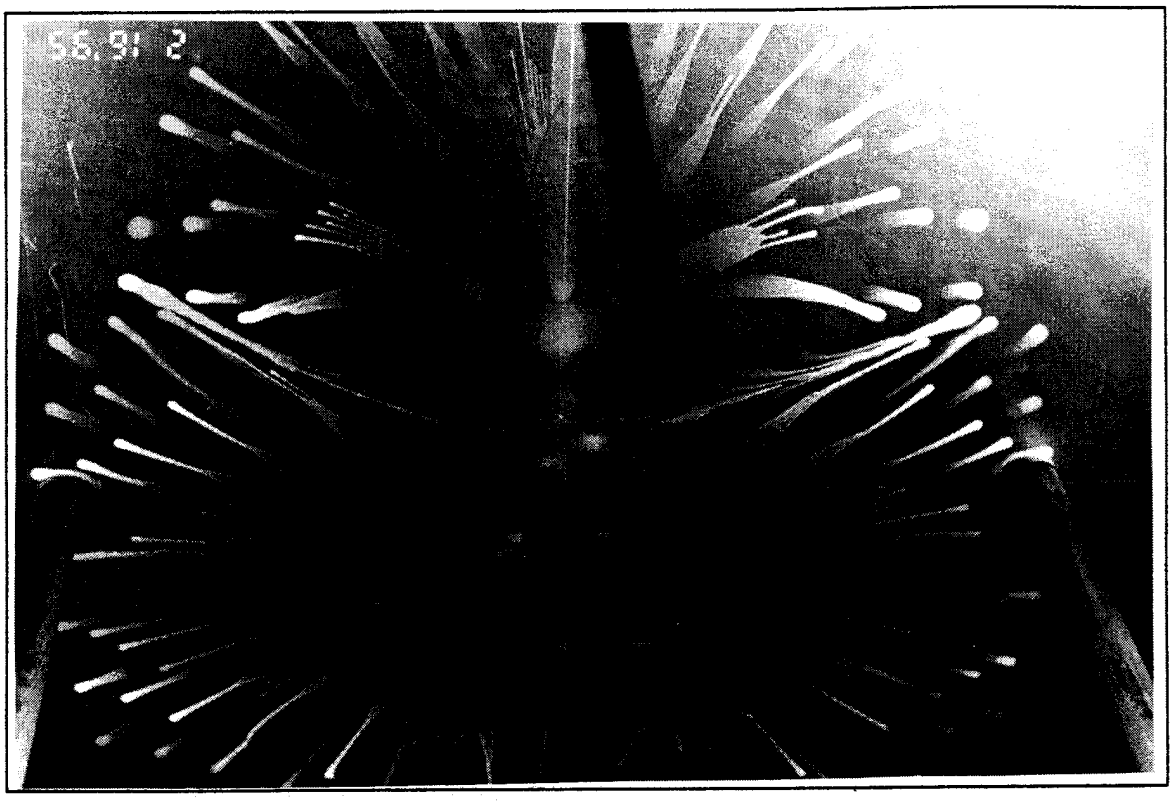

Figure 77 NTR = 4.9, Ground-Plane Height 4.57"

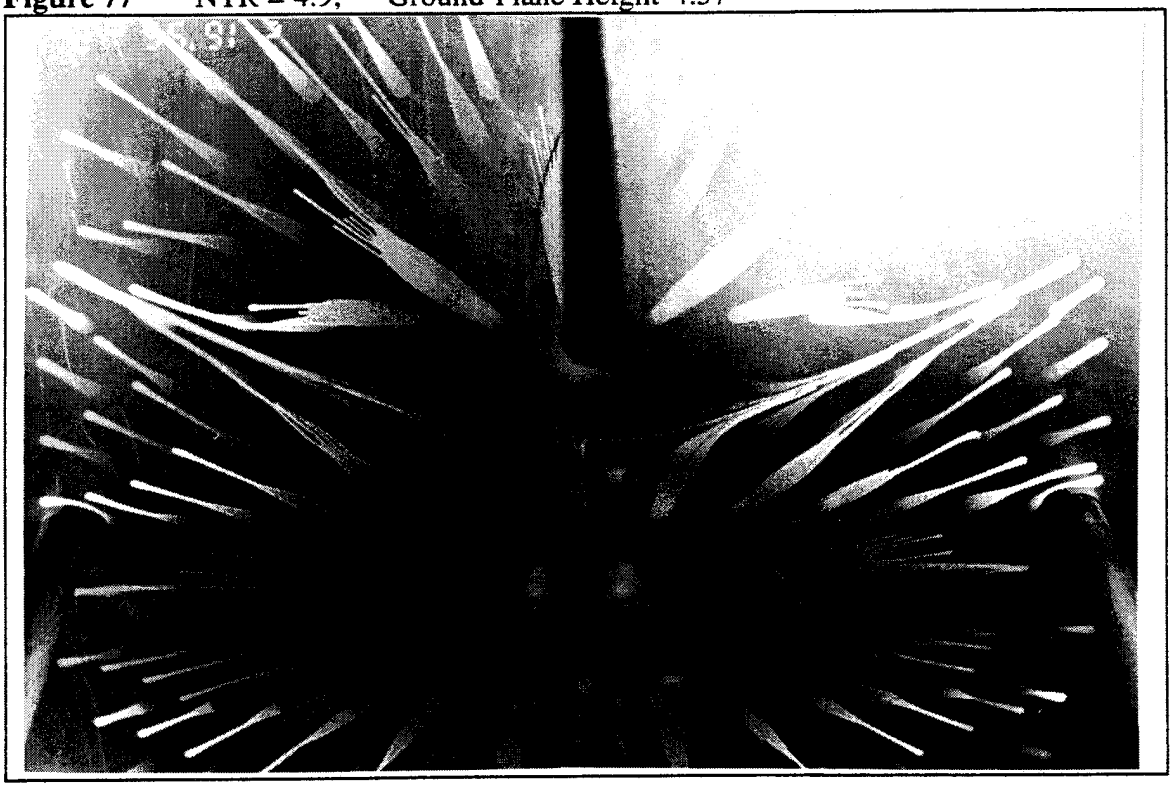

Figure 78 NTR = 4.9, Ground-Plane Height 6.85"

IX. NTR = 4.9 NO WALLS STRUTS

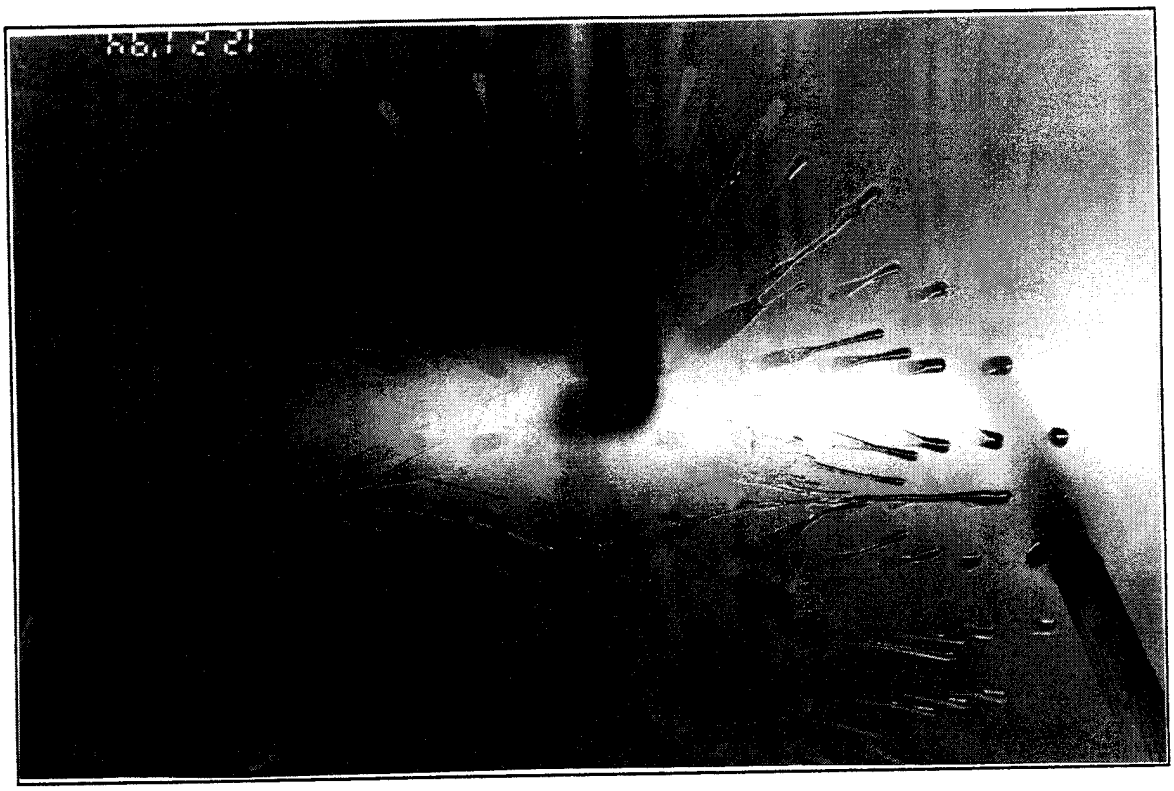

Figure 79 NTR = 4.9, Ground-Plane Height 1.14"

Figure 80 NTR = 4.9, Ground-Plane Height 2.28"

Figure 81 NTR = 4.9, Ground-Plane Height 6.85"

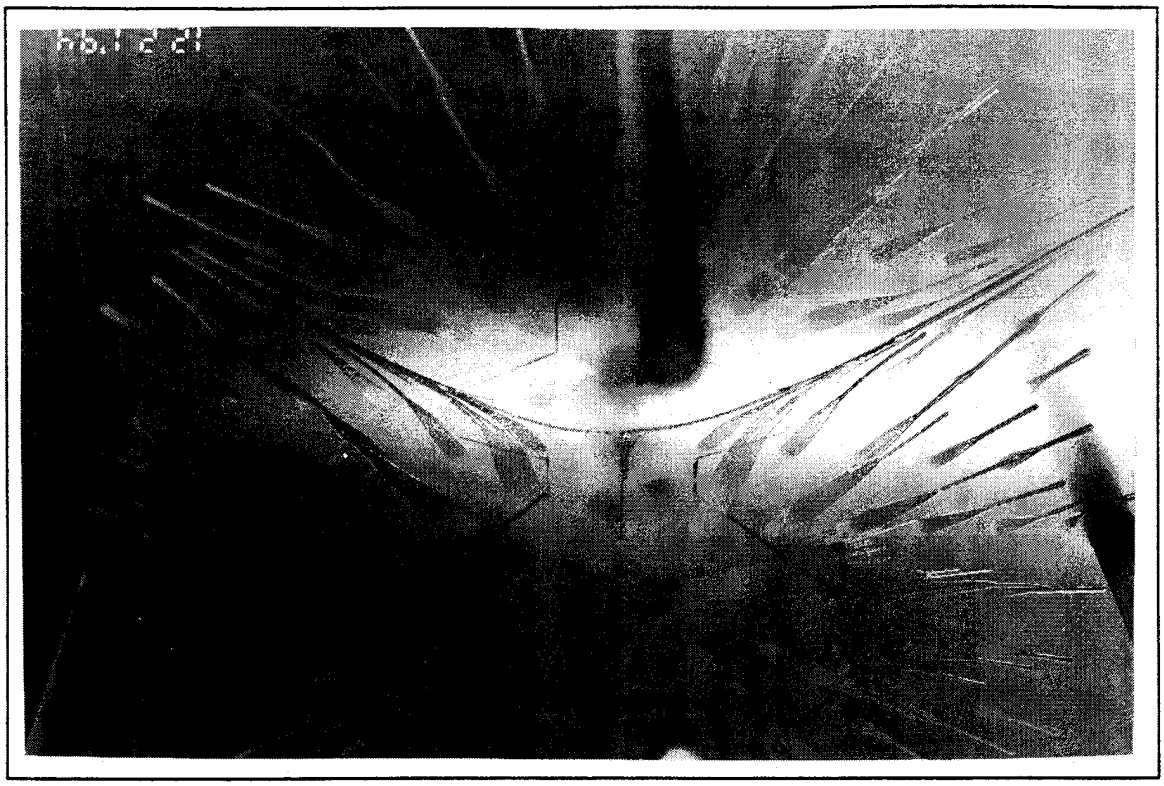

Figure 82 NTR = 4.9, Ground-Plane Height 9.14"

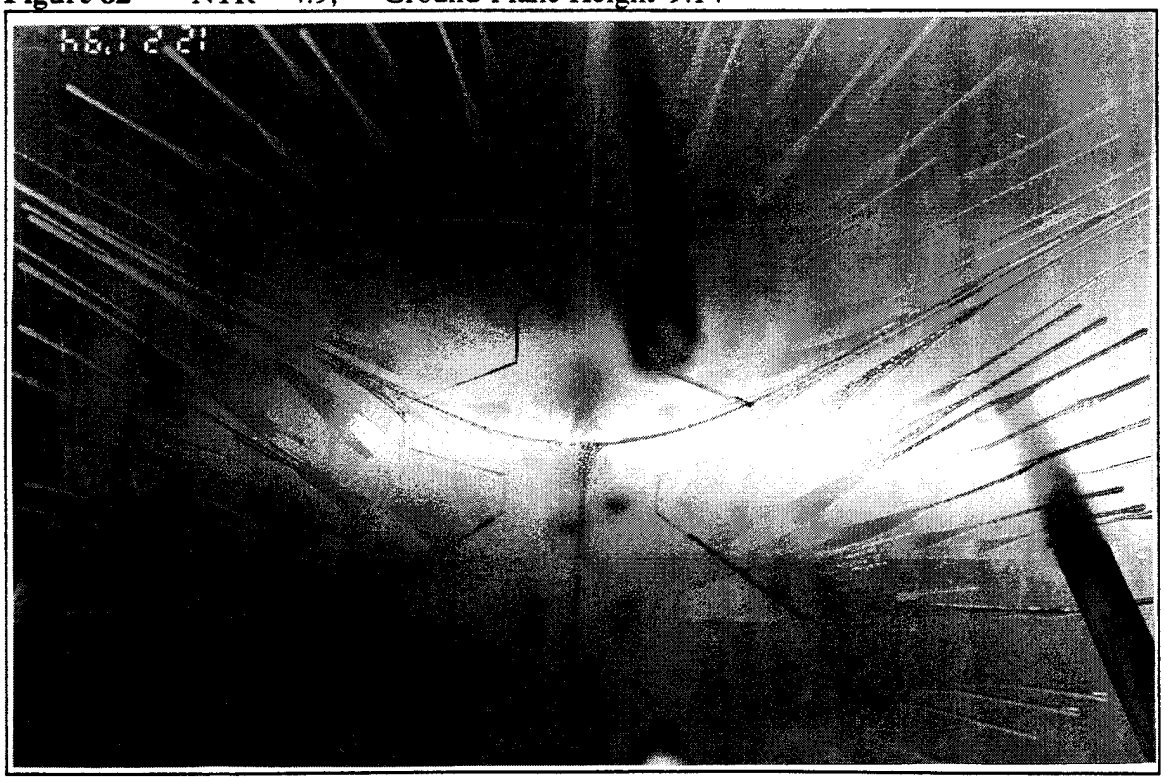

Figure 83 NTR = 4.9, Ground-Plane Height 11.42"

LIST OF REFERENCES

1. Kandebo, S.W., "Lockheed, Pratt Test ASTOVL Concept," *Aviation Week & Space Technology*, v. 141 no. 15, pp.48-51, 06 March 1995

2. Platzer, M.F. and Margason, R.J., "Prediction Methods for Jet V/STOL Propulsion Aerodynamics," *Journal of Aircraft,* vol. 15, no. 2, pp. 69-77, 2 February 1978

3. Winston, M.M., Albang, L.F. and Gentry, G.L., Jr., "*A Simplified Approach for Preliminary Estimation of VTOL Induced Effects in Hover*," paper presented at the Navy Workshop on Prediction Methods for Jet/VSTOL Propulsion Aerodynamics, Washington D.C., 28 July 1975.

4. Dooley, W., "An Experimental Investigation of Jet-Induced Ground Effects and Support Strut Interference on a STOVL Configuration in Hover," Master's Thesis Naval Postgraduate School, Monterey, CA, 1994

5. Margason, R.J., "CALF Thrust and Effective Velocity Ratio," NASA Ames Research Center, 3 May 1994 (Unpublished).

INITIAL DISTRIBUTION LIST

		No. Copies
1.	Defense Technical Information Center Cameron Station Alexandria, VA 22304-6145	2
2.	Library, Code 52 Naval Postgraduate School Monterey, CA 93943-5101	2
3.	Chairman, Code AA/Co Naval Postgraduate School Monterey, CA 93943-5106	1
4.	Professor S.K. Hebbar, Code AA/Hb Naval Postgraduate School Monterey, CA 93943-5106	5
5.	Professor M. F. Platzer, Code AA/Pl Naval Postgraduate School Monterey, CA 93943-5002	3
6.	Michael Kristy 515 E. Lynnwood Ave Arlington Heights, IL 60004	2
7.	Michael J. Harris Aircraft Division Code Air-931 Naval Air Systems Command Washington, D.C. 20361-9320	1
8.	Rich Margason Code FFF, M.S. 247-2 NASA Ames Research Center Moffett Field, CA 94035-1000	1
9.	Larry Olson Chief, Code FFF, M.S. 247-2 NASA Ames Research Center Moffett Field, CA 94035-1000	1

10. Sam Wilson
Manager, STOVL / CALF Project
Code FPP, M.S. 237-2
NASA Ames Research Center
Moffett Field, CA 94035-1000 — 1

11. Doug Wardwell
Aerodynamics Manager, STOVL / CALF Project
Code FPP, M.S. 237-2
NASA Ames Research Center
Moffett Field, CA 94035-1000 — 1

12. Tim Naumowicz
Code FFF, M.S. 247-2
NASA Ames Research Center
Moffett Field, CA 94035-1000 — 1

13. Craig Hange
Code FFF, M.S. 247-2
NASA Ames Research Center
Moffett Field, CA 94035-1000 — 1

14. Tom Arledge
Code FFF, M.S. 247-2
NASA Ames Research Center
Moffett Field, CA 94035-1000 — 1

15. Paul Askins
Test Director, STOVL / CALF Project
Code FFN, M.S. 221-5
NASA Ames Research Center
Moffett Field, CA 94035-1000 — 1

16. Peter Zell
Test Director, STOVL / CALF Project
Code FFN, M.S. 221-5
NASA Ames Research Center
Moffett Field, CA 94035-1000 — 1

17. Gavin Botha
Test Director, STOVL / CALF Project
Code FFN, M.S. 221-5
NASA Ames Research Center
Moffett Field, CA 94035-1000 — 1